Università degli Studi di Milano

Scuola di Dottorato in Scienze Matematiche
Dottorato in Matematica e Statistica per le Scienze Computazionali

Dipartimento di Matematica "Federigo Enriques"

Neuronal Ensemble Modeling and Analysis with Variable Order Markov Models

Relatore:
Dr. Gabriele E. M. Biella

Dottorando:
Antonio Giuliano Zippo
XXIII^o Ciclo

Coordinatore:
Prof. Vincenzo Capasso

Anno Accademico 2009/2010

Contents

List of Figures

To little defenceless creatures

Acknowledgments

Introduction

Neuronal cells (neurons) mainly transmit signals by action potentials or spikes. Neuronal electrical activity is recorded from experimental animals by microelectrodes placed in specific brain areas. These electrochemical fast phenomena occur as all-or-none events and can be analyzed as boolean sequences. Following this approach, several computational analyses reported most variable neuronal behaviors expressed through a large variety of firing patterns [13]. These patterns have been modeled as symbolic strings with a number of different techniques [23, 55]. As a rule, single neurons or neuronal ensembles are manageable as unknown discrete symbol sources $S = \langle \Sigma, P \rangle$ where Σ is the source alphabet and P is the unknown symbol probability distribution.
Within the hierarchy of Markov Models (MMs), Markov Chains and Hidden MMs have been profusely employed to model neuronal recording data [2]. However, due to the highly complex dynamic profiles of single neuron (SN) and neuronal ensemble (NE) firing patterns, those models failed to capture biologically relevant dynamical features. K-Order MMs could overcome these failures, but their time and space computational complexity turned them into unfeasibility. Variable Order MMs (VOMMs) meet with these restrictions confining modeling to the effective symbols of a given sequence up to a D maximum order. Formally a $VOMM$ is characterized by a couple $\langle s, D \rangle$ where $s \in \Sigma^*$ is the training sequence and the returned $\hat{P}$ is an estimation of P from source S. Given an arbitrary finite sequence $s \in \Sigma^*$, delivered by a generic source S, a VOMM builds a structure for S. Once a structure has been captured (or learnt) it may undergo tasks like prediction or compression or, again, analysis [9]. Thus, a lossless compression algorithm originated from a VOMM can perform prediction tasks and every prediction algorithm can perform compression tasks [97].
Statistically Based Compression Algorithms (SBCAs) build a prefix tree to estimate the symbol probability by combining conditional probability of a symbol with a chain rule, given d previous symbols ($d \leq D$). In particular, just on the track of previously discussed issues, I took into consideration three SBCAs: Prediction by Partial Matching (PPM)[30], Context-Tree Weighting (CTW)[137] and Probabilistic Suffix Tree (PST)[98].
Prediction capability of these algorithms can be exploited in at least two ways: i) to draw a similarity function between experiments and ii) to analyze the changes of stationary phase of specific experiment dynamics from SN or NE datasets. The predictive accuracy can be measured by functions like the average log-loss (self-information). The average log-loss function measures the average compression rate of s assuming its $\hat{P}$ distribution and so the $\hat{P}$ prediction accuracy. Once the VOMM is trained with a given sequence source A, the average log-

loss between the obtained VOMM model and another arbitrary sequence source B approximates their similarity measure $\mu(A, B)$. Where the sequences represent whole recording experiments, the VOMMs identify the similarity between different recordings, otherwise, if the sequences represent contiguous recorded experiment subsequences, the VOMMs can detect the switching between stationary phases, through average log-loss peaks. These VOMMs can also measure the information redundancy present in the sequence. This application, as shown in results, is particularly relevant for neurophysiologists and provides significant results when applied to recordings of chronic pain animal models. To confirm, by other estimation paths, the similarity measure between whole recording stages, I chose to introduce a more computationally efficient similarity measure (the Normalized Compression Distance, NCD [10]) based on widely acknowledged faster compressors like `gzip`, `bzip2`, `lzma` and others.
The results obtained with these methods come (i) from Ventrobasal Thalamic Nuclei (VB) and Somatosensory Cortex (SSI) in Chronic Pain Animals (CPAs), (ii) from Primary Visual (V1) and (SSI) in rat Cortices and, finally, (iii) from IL human Thalamus Nuclei in patients suffering from states of disordered consciousness like Persistent Vegetative State (PVS) and Minimum Conscious State (MCS).

Chapter 1

Biological Background

The mammalian brain constitutes one of the most complex objects of the known Universe. The brain is composed by different classes of cells. The cells from brain are substantially of two types: **neuronal cells** and **glial cells**. Although the already impressive number of neurons (10^{11}) in the Central Nervous System, the glial cells outnumber neurons by tenfold. However, neurons play the major role in the brain functioning, yet not forgetting the impressive roles of glia in many neuronal activities. The Nervous System can be grossly divided into 3 parts: the Central Nervous System (CNS) that contains the brain, spinal cord, and the retina. The Peripheral Nervous System (PNS) consists of sensory neurons, clusters of neurons called ganglia, and nerves connecting them to each other and to the CNS. These regions are all interconnected by means of complex neural pathways. Finally, the Enteric Nervous System, a subsystem of the peripheral nervous system, has the capacity, even when severed from the rest of the nervous system through its primary connection by the vagus nerve, to function independently in controlling the gastrointestinal and other systems. This thesis is focused on CNS working mechanisms in normal and pathological conditions and namely the neural substrates of the sensory processes and of consciousness. Here below I present a sketchy survey of the structural and functional substrates of the CNS. In particular are presented the basics of the somatosensory system because it is strictly related to nociception and chronic pain and of the human consciousness because relevant results come from patients with consciousness disorders.

1.1 The Central Nervous System: a survey

The CNS is divided in brain, spinal cord, and retina. Stimuli and signals delivered from the PNS traverse the spinal cord and arrive into the brain. Complex structures receive and elaborate these signals. The central most important region involved in the signals and stimuli processing is the brain. The brain is constituted by clusters of neuronal populations connected by an entangled network of complex connections among neurons. Each neuron may receive signals from up to 10000 other neurons. This obviously assumes that there is no all-to-all connectivity but that selected connections among different neuronal populations are privileged and constitute the structures of the extant brain.

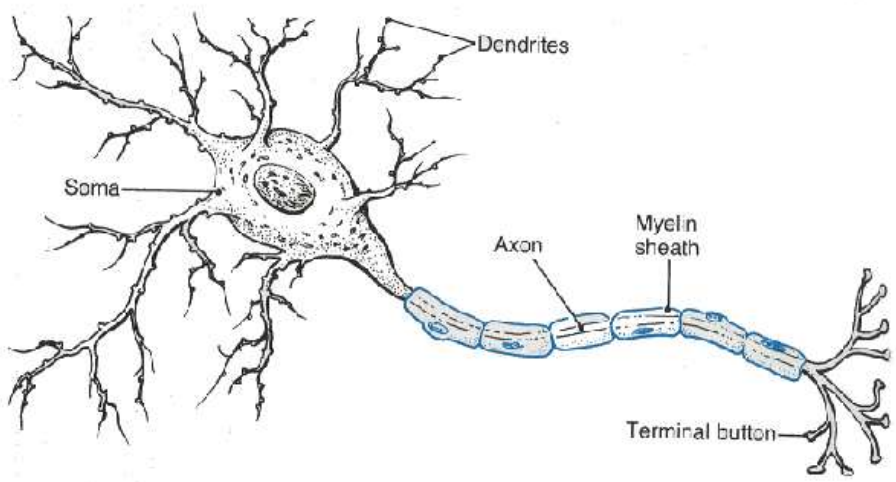

Figure 1.1: A representation of neuron anatomy.

Because the essence of signal processing resides in the single cells, I will now introduce the neuronal physiology.

1.2 The Neurons

Although there are many more glial cells than neurons, the fundamental task of information trasmission and computation is carried out by neurons. However, the glial cells perform several supplementary and support tasks to the neurons.

1.2.1 Elements of Neuronal Anatomy

The neuronal cells can be divided in four parts: the soma, the axon, the synaptic terminals and the dendrities (see Figure 1.1). The dendrities are tree-like structures that represent the main receptive area of the neuron. The soma is the central unit that contains the cellular nucleus and computes the signals trasmitted by dendrites. The major diameter can be as large as 10 to 60μm. The axon is constituted like a filament extending from the exit area of the soma, called hillock, and can be meters long. The axon may be completely nude or covered by one or more layers of myelin sheaths, composed by wrapped myelin cells around the axons. Myelinization dramatically increases the signal conduction up to 120m/s. In fact, the myelin cover inhibits from the ionic exchanges at the membrane level and the signal conduction is transformed from electrochemical to electrotonic. The extension of the myelin sheath is not a continuative coverage at every definite distance it is interrupted (about 1μm gaps), leaving the axonal surface in contact with the extracellular environment (node of Ranvier). These interruptions are strategic being signal amplifiers of electrical signals subject to natural fading along the myelinated axonal branch.

The synapse is a highly complex structure where the signal trasmission between neurons takes place. As a rule, a neuronal axon can establish a number

of synapses with the receiving structures of another neuron (see Figure 1.2). Specifically, the transmission can be established by the branching axon terminals on the dendrities, on the soma or on the axon. The respective synapses are thus called axo-dendritic, axo-axonic and axo-somatic. The axon terminals that constitute synapses present bag-shaped enlargments that contain vesicular bodies filled of neurotransmitters. In these regions (called presynaptic terminals), the vesicle membranes coalesce, by a complex mechanism, with the axon terminal membrane, delivering the substance contained in vesicle. These substances, generally amminoacids or peptides, are called neurotransmitters. On the postsynaptic membrane there is a lot of complex structures called receptors (see Figure 1.3), mainly constituted by proteins, that can receive the molecules delivered by the presynaptic vesicles. The space between the presynaptic and postsynaptic membrane is called synaptic cleft (about 20nm). The reception of a trasmitter by a receptor triggers several fast electrochemical changings that induce the generation of spike signals similar to the presynaptic spike. The ensemble of presynaptic membrane, synaptic cleft, postsynaptic membrane is called synapse.

There exists a large variety of neurotransmitters (and of other substances called neuromodulators) as well as of postsynaptic receptors. This extraordinary multiplicity of transmitters, modulators, receptors allows incredibly flexible signal transmission.

1.2.2 Action Potentials and Signal Transmission

The cell membranes as well as all cellular membranes, present typically a lipid bilayers. Each layer is a flat sheet that forms a continuous barrier around the cell, few nanometer thick and impermeable to most water-soluble polar molecules. Numerous complex proteins cross the membrane and estabilish a functional connection from the inside to the outside of the cell. Some proteins are arranged as channels allowing for the passage of substances (primarily neurotransmitters and ions) across the membrane. These channels can be always open or can present conditional closing mechanisms (called gates) that allow the passage of substance only in particular functional circumstances. Due to extremely sophisticated mechanism, the internal cellular fluid is relative negatively charged in comparison to the extracellular fluid. This stable condition creates potential difference between the intracellular and extracellular fluids. The negative charge can range between $[-80, -55]$mV depending on neuron type. This implies that the electrical potential is negative, in the range $[-60, -80]$mV. In addition, there are several dynamical properties imported by the complex network of the ionic transmembrane channels. In fact, some of these channels are selectively permeable to sodium, potassium, calcium (positively charged) or chlorine (negatively charged) ions. The selective gating is specific for the various ion types. Specifically the sodium ions are much more concentrated outside the cellular membrane, the reverse being true for the potassium ions. The concentration of the calcium ions is regulated on much more robust and complex conditions. Finally, the chlorine ions are more concentrated outside the cell membrane.

In order to understand the signal transmission, the electrical and the chemical potential must be considered. Taking into account that cell inside is strongly negative, positively charged sodium ions, more concentrated outside the membrane, obviously show a tendency to get into the cell both for electrical and

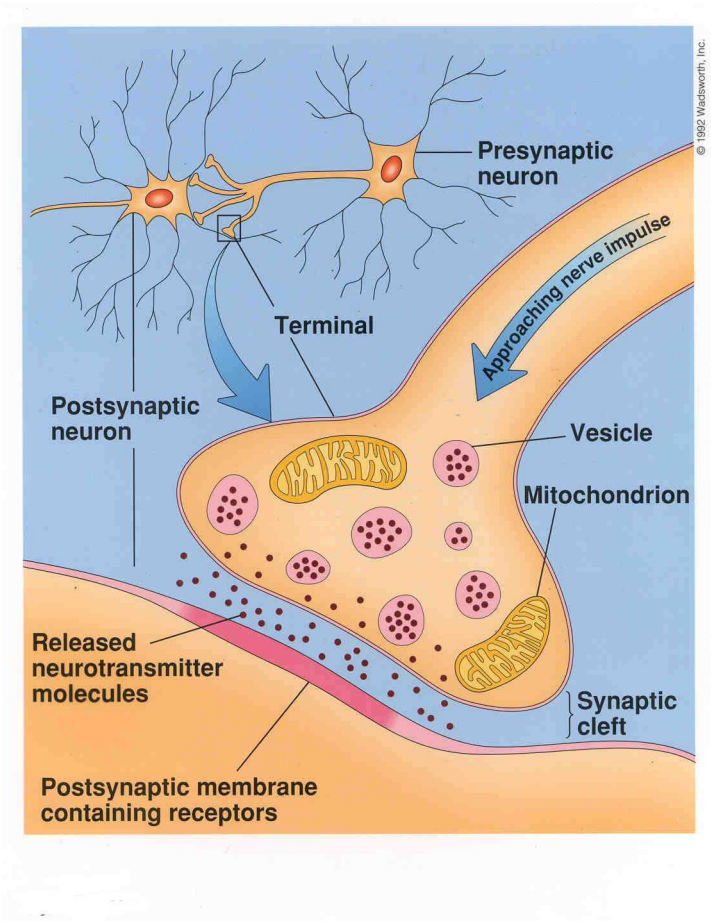

Figure 1.2: A schematic representation of synapse.

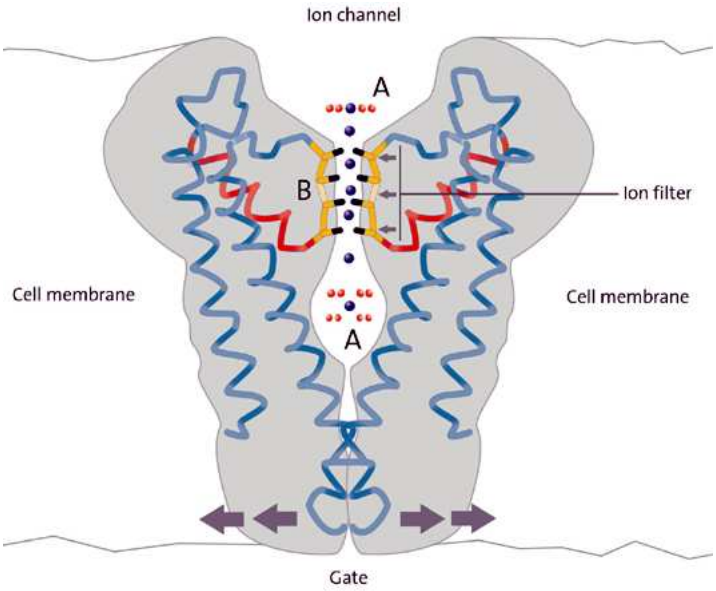

Figure 1.3: A protein that functioning as ion channel.

chemical gradients. The potassium ions, more concentrated inside the cell, are driven by a chemical gradient that pushing them outside, the electrical gradient being, on the converse, holding them inside. Given this picture, it is easy to understand that chlorine ions tend to remain outside the cell by electrical gradient and conversely driven in by chemical gradient. The calcium ions, generally more concentrated (at resting) outside of cell, show sodium-like behaviors.
The stable state of an ionic equilibrium reached by the system shows the resting potential at the negative levels discussed before. The resting potential undergoes continuos fluctuations due to incoming signal to the neuron. Most of this fluctuations are unable to trigger an action potential but simply deviate the potential either towards more positive level (*depolarization*) or towards negative level (*hyperpolarization*). The ion channels may exist with different dynamic properties: either they are gated by complex structures called *receptors* or they are gated by specific potential levels or again they may be stably open allowing for a free ionic passage.
When an input strong enough moves upwardly the potential to a threshold that may be between $[-45, -35]$ all-or-none event takes place and a fastest depolarization is triggered driven by a massive sodium ion entrance into the cell. This massive flux reverses the ionic balance across the membrane bringing the internal milieu to positive values $[+20, +35]$ relative to the external one. This sudden event has 400μs length. At the very peak of depolarization, suddenly, all the sodium channels close under the electrochemical gradient push and a new rush of potassium channel opening takes place. Due to the current internal positivity, the potassium ions tend to rush outside the cell both for chemical and electrical gradient, see Figure 1.4. This potassium outflow has a greater temporal length 500-600μs and tends to restore the original negative resting potential with the outflow of positive charges. The potassium current is so powerful that

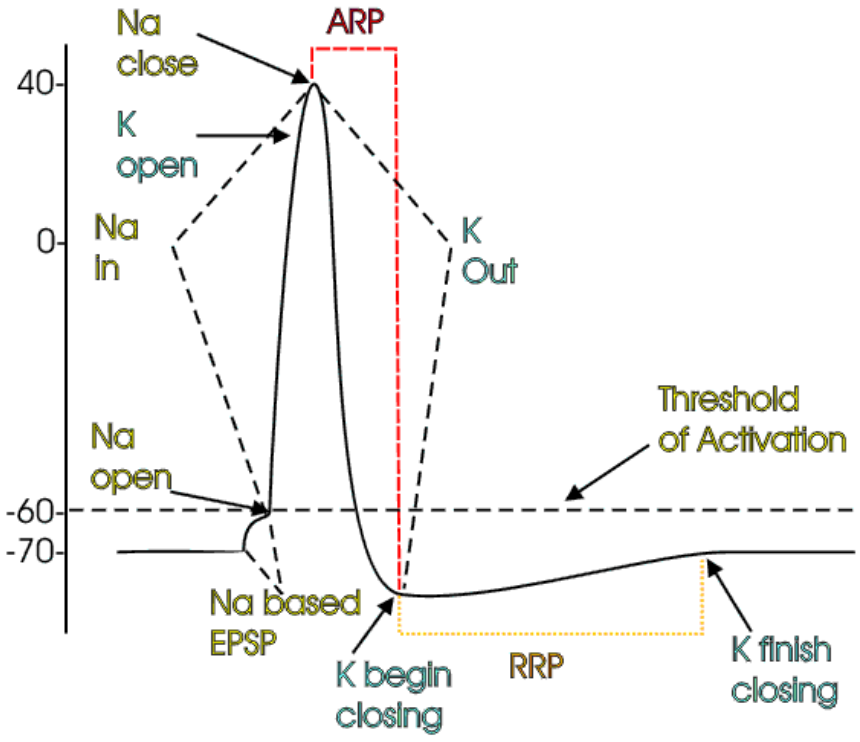

Figure 1.4: The action potential and its ionic current components.

the internal potential is pulled to even more negative ($-80m$V) values before regaining the normal negativity. During this hyperpolarizing period the neuron is unsensitive to further depolarization input (*absolute refractory period*). The short time length between the end of depolarization and the normal resting potential there is a short period where the neuron is again excitable by inputs stronger then the usual ones (*partial refractory period*). This depolarization/hyperpolarization schema shows different behaviours, one of the most important is the unusual activation observed in hyperpolarized states where a calcium current normally inactive at standard resting potential is undergoes a de-inactivation and becomes expressive with a very powerful and long lasting calcium spikes displaying over its crest fast supeimposed sodium spikes producing the typical electrochemical behavior called *burst*.

1.3 The Somatosensory System

The somatosensory system processes the sensory inputs to the body and namely it displays estimating properties for proprioception, touch, temperature, nociception and so on. The somatosensory system is constitued by receptors placed

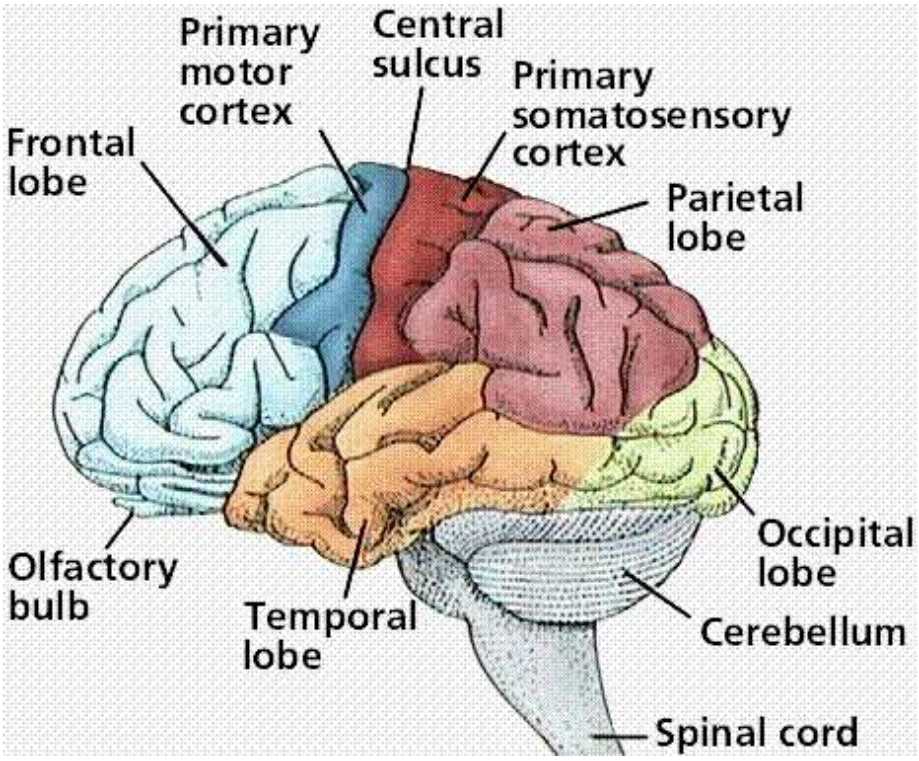

Figure 1.5: Cortical areas of human brain.

in the periphery of the body (the cutaneous district, tendons and muscles, viscera, the special senses), the peripheral sensory neurons and by the central neurons delivering the signals up to the thalamus and to cortices. The sensory information is, by these means, conveyed to the cortex. In the CNS, two brain regions play a crucial role in the sensory information processing: the primary somatosensory cortex located in the postcentral gyrus of the parietal lobe (SS-I), (see Figure 1.5), and the ventrobasal nuclear complex (VB) of the thalamus. These structures, along with their connections, form the so called *Thalamocortical loop*.

1.3.1 A brief introduction to Thalamus Anatomy

The thalami are two paired symmetrical organs and represent the major part of diencephalon. Each of the two thalami is a structure divided in many subsets, histologically distinguishable, called *nuclei* (see Figure 1.6). The nuclear nomenclature respects, in general, the internal thalamus topography. In fact there are the anterior, medial, intralaminar, posterior nuclei, etc. In particular, two important nuclei of VB complex for somatosensory information processing are represented by the ventroposterolater (VPL) nucleus and the ventrolater (VL) nucleus.

All the neurons of the somatosensory thalamus and many neurons of intralaminar and medial thalamus are populated by neurons connected to the cortex: the

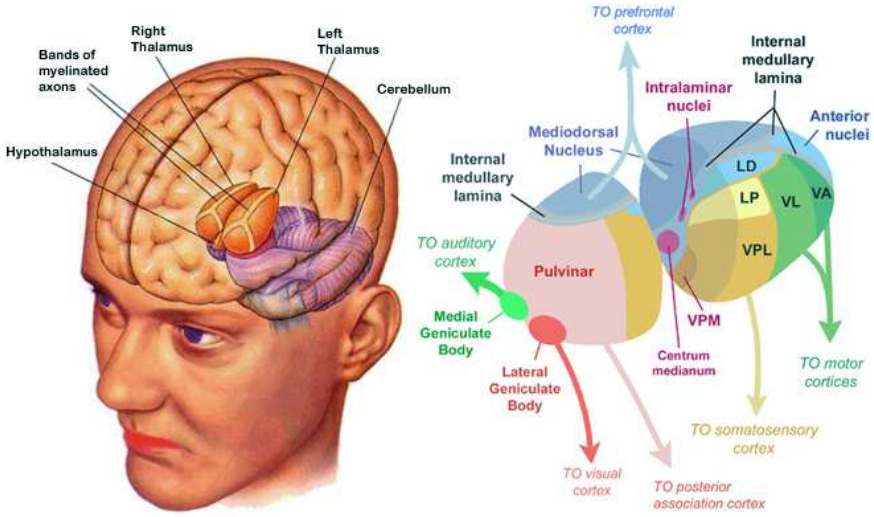

Figure 1.6: Thalamus within the human brain (left). Thalamus nuclei and their cortical projections (right).

thalamocortical (TC) neurons (else thalamic relay neurons) and local inhibitory neurons. These last are present only in the superior mammals. Another crucial nuclear complex involved in the function of thalamocortical loop is the reticular-thalamic (RT) nucleus. While the relay thalamic neurons are excitatory neurons (on the reticular thalamic neurons and on the cortical neurons), the reticular thalamic neurons display strong inhibitions onto the thalamic relay neurons (see subsection below).

1.3.2 A brief introduction to Cortex Anatomy

The cerebral cortex meanly presents a layered structure with variable number of layers and appearances being actually a smooth or a folded structure. These folds help to structure the so called *cerebral circumvolutions* that thanks to their geometrical constractions extend the cortical surface and volume. In mammals there is a gradual evolution related to both cerebral surface and volume (strongly influenced by folds) and to many kinds of neurons. Each of the six layers endorses different functions that can express wholely in the each specific cortical area. For instance, in the sensory cortex, the fourth layer that receives the thalamic output is extremely developed in comparison to its presence in the motor cortex where it expresses a minor role. Conversely, deeper layers (the fifth and sixth) more involved in motor roles are strongly developed in motor cortex.
Cortical neurons represent an heterogeneous population most variegated for structural and functional features. The cortical circuits of signal processing appear to be regular throughout the different mammalian species but show profound differencies. In this work, I will consider only a few types of cortical neurons that actively take part in sensory signal elaborations. Specifically, the fourth layer neurons that receive input from TC cells are called *granular* cells for their granular-like appearing in histological observations. Just on this track

of morphological comparison the fifth and sixth layer neurons because of their similarity with triangular shape are called pyramidal cells. The fifth layer neurons are connected to the TC and RT neurons and with other cortical layers. These connections are predominantly excitatory. Cortical excitatory neurons can perform the following behaviors:

1. *Regular Spiking* (RS). The most diffuse in cortex. They emit a series of low, if necessary increasing, frequence spikes.

2. *Intrinsically Bursting* (IB). They emit first a short burst of spikes then a series of regular spikes.

3. *Chattering* (Ch). They generate a sequence of spike bursts (at 40Hz) spaced out (at 0.1 to 0.8Hz) by resting periods.

Cortical inhibitory neurons can perform the following behaviors:

1. *Fast Spiking* (FS). They emit a series of spikes like RS but with higher frequency.

2. *Low Threshold Spiking* (LTS). They show high frequency regular spikes followed by a fast adapting phase.

1.3.3 The Thalamo-cortico-thalamic loop

Taking into consideration the connection between thalamus and cortex and the diverse neurons in both structures, it is possible to divide the thalamocorticothalamic (TCT) loop dynamics in three mechanisms (see Figure 1.7):

1. The TC cells that receive input from sensory spinal cord pathways trasmit the signals (action potentials) onto the granular cortical layer and onto the reticular thalamus. The former produces an excitatory effect on granular layer. Simultaneously it can be observed an excitement of RT neurons that rapidly induce a negative feedback, i.e. an inhibition on the TC cells that began the stimulation. This system represents the first loop of the whole TCT.

2. In the meantime the granular layer neurons induce an excitement of pyramidal neurons of below layers. These pyramidal neurons excite both the TC neurons of point 1 and the RT neurons. This system represents the second excitatory loop of the whole TCT.

3. Because from the fifth piramidal layer there is an other excitatory pathway onto the RT neurons, these last are reactivated and produce a second inhibitoty input onto the TC cells. This last system is excitatory and inhibitory.

The slight temporal differences among the three mechanisms allow a reached variety of discharging mode with complex rhythms and oscillations. Furthermore the TC neurons present a peculiar behavior that makes more complex the whole scenario. From a dynamical point of view these cells have a bistability, i.e. they can work with two different dynamical states. The choice is determined by intrinsic TCT loop modulations and by external loop input. Specifically

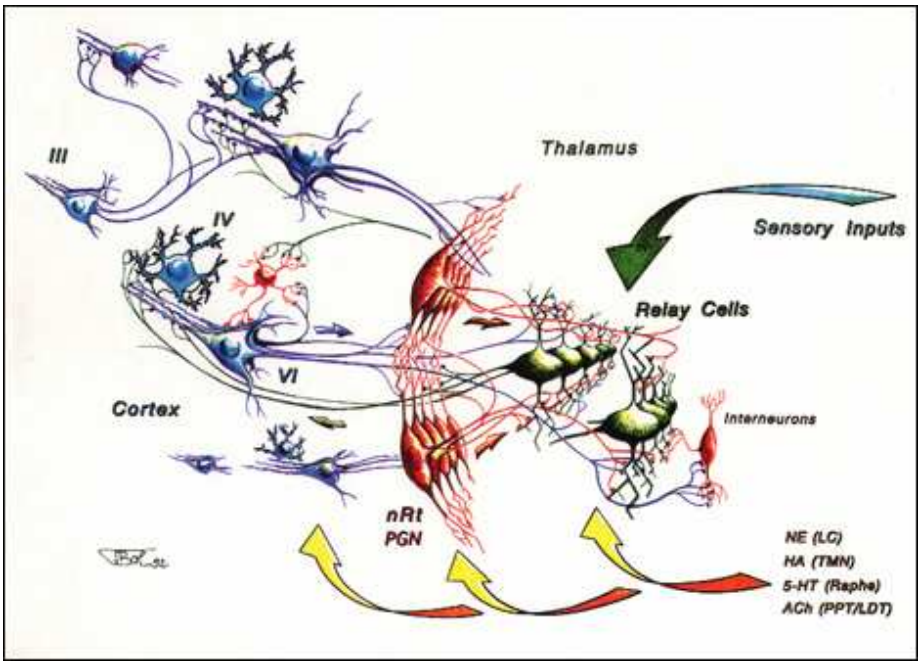

Figure 1.7: Thalamocortical loop. We can observe the involved neurons like TC neurons (relay cells) and granular/pyramidal cortical neurons. The thalamic cells in red are RT neurons.

two different discharge patterns can be observed: the first called *tonic* and the second called *burst*. The former presents a FS-like behaviour with frequency that can exceed frequencies of 300Hz. The latter instead presents short spike patterns (6 to 10 spikes) at very high frequency (approximating 1 kHz). This last behavior is mainly due to the peculiar characteristic of calcium channels of TC neurons. These channels are opened during hyperpolarizations (due to an inhibitory input that brings the potential almost to -90mV) and calcium ions enter into the cells. Thus, the inhibitoty input trigger a generation of a series of very fast consecutive spikes that bring the resting potential to regular values.

1.4 State of Consciousness

The concept of consciousness is massively variegated. The term *consciousness* can be faced from several philosophical and psychological perspectives. From a cognitive neuroscience point of view, the consciousness recalls notions like awareness, wakefulness and attention. In fact, a simple definition of consciousness often state that *consciousness is the ability to be aware of themself and surroundings*. Again, consciousness does allow us to know of our own existence and of the existence of objects and events, inside and outside our organism.
Consciousness has, obviously, a neural counterpart, i.e. neural patterns that involve several brain regions (sometimes this concept is referred as *neural basis of consciousness*). A lot of neuroanatomical and neurophysiological considerations support this brain-mind scenario. For instance, various cell groups in

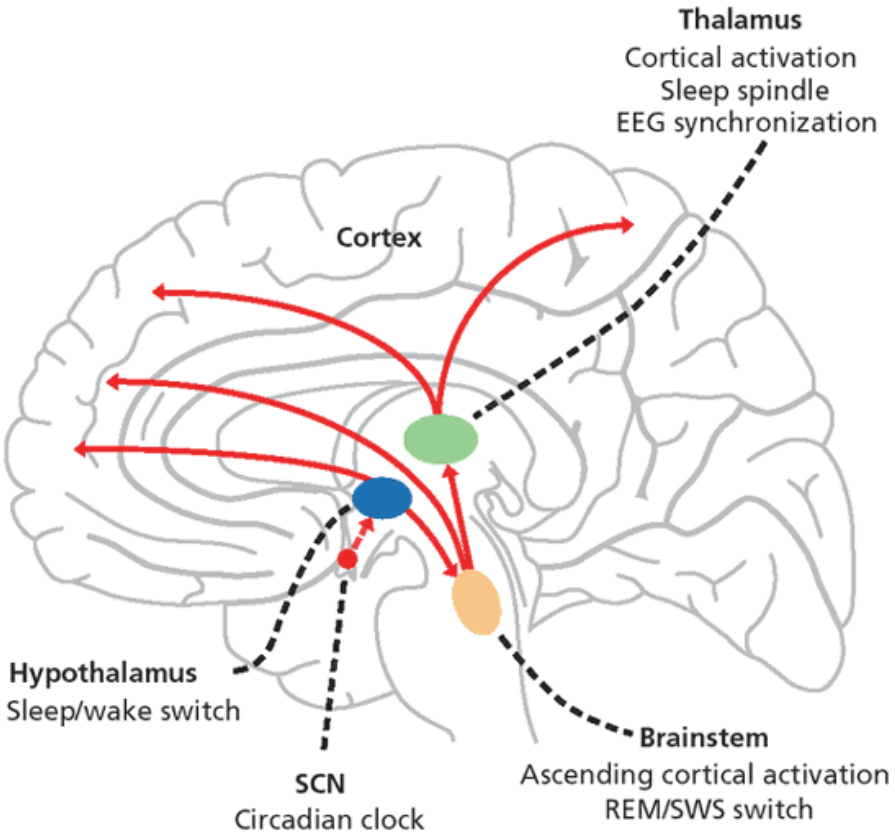

Figure 1.8: The brains ascending reticular activating system (ARAS) is responsible for arousal and substains the wakefulness.

the brainstem modulate wakefulness by ascending projections to the cerebral cortex. Also, there are presumably glutaminergic projections from the classical reticular ponto-mesencephalic nuclei to the intralaminar nuclei of the thalamus, which in turn project to large areas of the cerebral cortex.
As a rule, the brains ascending reticular activating system (ARAS) is considered one of the crucial system involved in the arousal and wakefulness state (see Figure 1.8).
In this work I considered also neuronal recordings from patients with disorders of consciousness.

1.4.1 Human Disorders of Consciousness

Although the ARAS has a redundancy of pathways and neurotransmitters, a severe disrupting into the ARAS caused by trauma and/or injury almost surely involves an alteration of the normal state of consciousness that can be transient or persistent like coma. Not only ARAS's damage should cause coma. Cortex and thalamus injuries but also metabolic and toxic disorder, seizures, infections can produce coma states.

Coma is typically defined as a state of unarousble consciousness. Clinical evidences include failure of eye opening to stimulation, a motor response no better than simple withdrawal type movements and a verbal response no better than simple vocalization of nonword sounds.
In the following subsections I focus on the two particular disorders of consciousness: the Minimally Conscious State (MCS) and the Persistent Vegetative State (PVS).

The Minimally Conscious State

The minimally conscious state is a condition of severely altered consciousness that has been distinguished (only in the last years) from the vegetative state (VS) by the presence of minimal but clearly discernible behavioural evidence of self or environmental awareness. Definite behavioural evidence of self or environmental awareness is demonstrated on clinical examination. There is increasing evidence from neurobehavioural and neuroimaging studies that important differences in clinical presentation, neuropathology and functional outcome exist between MCS and VS. However, no strong neurophysiological differences are been found. The possible emergence of eye-opening signals that the reticular system has regained control over wakefulness, although individuals in VS remain completely unaware of self or environment. In VS, the brainstem also resumes control over vital bodily functions including respiration, heart rate and thermal regulation. Although these functions may still be compromised during VS, life-sustaining interventions such as mechanical ventilation are usually not required. To establish the diagnosis, there must be an evidence of least one clear cut behavioural sign of cognitive processing and the behaviour must be reproduced at least once within the same examination. Because behavioural fluctuation is common during MCS, it is generally necessary to conduct serial examinations before an accurate diagnosis can be made.

The Persistent Vegetative State

The assessment of patients in the vegetative state is extremely complex and depends frequently on subjective interpretations of the observed spontaneous and volitional behaviour. In fact, until recent developments, VS and MCS were not differentiated. In recent years, a number of studies have demonstrated an important role for functional neuroimaging in the identification of residual cognitive function, and even conscious awareness, in some patients fulfilling the clinical criteria for vegetative state. Such studies, when successful, may be particularly useful where there is concern about the accuracy of the diagnosis and the possibility that residual cognitive function has remained undetected. However, use of these techniques in severely brain-injured persons is methodologically complex and requires careful quantitative analysis and interpretation. Patients in the vegetative state are, anyhow, awake but are assumed to be entirely unaware of self and environment. If a vegetative state endure for at least 3-6 month after acute traumatic or non-traumatic brain injury, then the patient is considered in PVS. The *persistency* denotes irreversibility.

Chapter 2

Computational Neuroscience Modelling

Neuroscience is an interdisciplinary field that involves biology, computer science, mathematics, philosophy, etc. Currently, the neuroscience are divided in several branches. Each of these study topics of interest employs different experimental and theoretical techniques. This thesis covers the following neuroscience branches: the systems neuroscience and the computational neuroscience. The former aim is to study the neurophysiology of important neurological systems like motor system, auditory system, somatosensory system, etc. To meet these objectives, the systems neuroscience employs methods that record the neurophysiological activity of neurons or groups of neurons with microelectrodes, two-photon microscopy, functional magnetic resonance imaging, etc. The latter aim is to make models and analyses for the observed data, in order to understand the hidden fundamental functioning mechanisms of neurophysiological and cognitive systems. In the following sections, I introduce crucial features for both approaches involved in this thesis. In our lab we recorded electrical activity of neuronal ensembles in the rat somatosensory system, while in the clinical environment we recorded from human intralaminar thalami by array of microelectrodes. Methods for recording, modeling and analysing are presented in detail in the following sections.

2.1 Multielectrode thalamocortical recordings

Sixty rats (Sprague-Dawley, Charles-River, Calco, LC, Italy) weighting 300-400gm were used. The neuronal electrophysiological recordings were taken from the side contralateral to the treated paw, the EEG recordings from the contralateral side of the skull, ipsilateral to the treated paw. As for the EEG recordings a specially designed electrode asset was used. For the analyses we chose electively the EEG data from the second derivation that was mirrorlike complementary to the contralateral somatosensory primary cortex where the neuronal cortical recordings were obtained. For the electrophysiological recordings, two 3 mm^2 holes were drilled on one side of the skull to gain access to the Ventro-Postero lateral nucleus and to the SS-I cortex. The neuronal recordings were obtained by two matrices of extracellular multiple electrodes framed in 3x3

arrays of single shanks, inter-tip distance 150-200μm, tip impedence 0.5-1MΩ (FHC Inc., ME, USA). Fast thalamic and cortical responses to light stimuli on the sciatic innervation field (the plantar aspect of the left hindlimb) were the anatomo-functional acceptance criteria to start the activity acquisition. In this thesis Single Neuron recordings and Unit recordings are distinguished. These last are meant as the collection of the neuron micropopulation read-out of single shanks of the matrices. For signal amplification and data recordings a 32 channel Cheetah Data Acquisition Hardware was used (Neuralynx, MT, USA) at 32 kHz sampling frequency. Electrophysiological neuronal signals were digitized and recorded with filtering low-high pass bands at 6 kHz and 300 Hz respectively. The EEG data were digitized and recorded with filtering low-high pass bands of 475 Hz-1Hz respectively. Trace visualization was achieved by multitrace electronic oscilloscopes (National Instruments, Milan, Italy). The data stored were analysed off-line both by Matlab and by locally developed softwares. Spike sampling was carried out by an adaptive threshold parametrized on trace noise levels (40mV peak to peak as a mean) with mean signal-to-noise ratio of 4. A histological confirmation of the placement of the electrodes was then obtained on brain coronal sections stained with cresyl-violet after formalin perfusion of the animal at the end of the experiments.
The multiunit recordings were sorted to extract the single cell signals. The spike sorting procedure employed the `Wave_clus` tool [91]. The next step provided discretization of the population spike train into bitstrings where 1 represents a generation of an action potential and 0 the no-spike event, within non-overlapping windows of 1 ms size.

2.1.1 Spike Sorting

The term *spike sorting* indicates the extraction and grouping of spikes into clusters based on a criterium of the similarity of their sampled waveforms. As a matter of fact, in extracellular recording assets, the position of the recording probe (the electrode tip) and the active recordable neurons (within a radius of 150μm or so from the tip) arranged in a kind of lattice, supposedly stable during each recording stage (see Figure 2.1). This assumption, thus, admits that the field of a depolarizing neuron can be steadily acquired throughout a recording session providing self-similar signals. Each neuron may be thus functionally labeled by a specific spike shape and each resulting cluster corresponds to the collection of simil-shaped spikes emitted by one putative single neuron. From now to the rest of work, I call *unit* the activity of a single neuron.

Spike Detection

As a rule, the raw acquired signal is band-pass filtered within the range 300-3000Hz. After this step, an amplitude threshold is applied to detect the spikes from filtered signal. False positive and negative spikes are unavoidable, but good results could be achieved. In a strong-supervised detection system, an expert user sets manually a reasonable threshold. This choice is justified in case of high variable experimental conditions, that are electrode impedences, environmental noise, etc. In most situation, the experimental conditions are quite stable and then the threshold can be set automatically. Several techniques suggest to relate the threshold to the standard deviation of the signal. Finally the spike

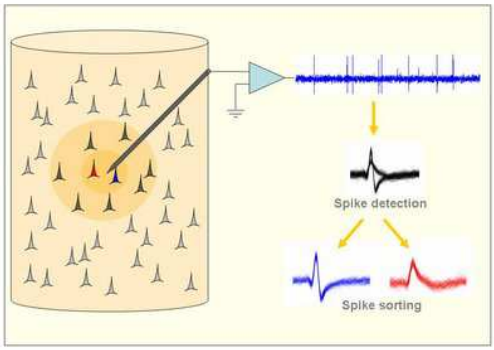

Figure 2.1: An electrode that records the electrical activity within a micro-column. The dark blue circle represents the detectable region that vary with the electrode impedence.

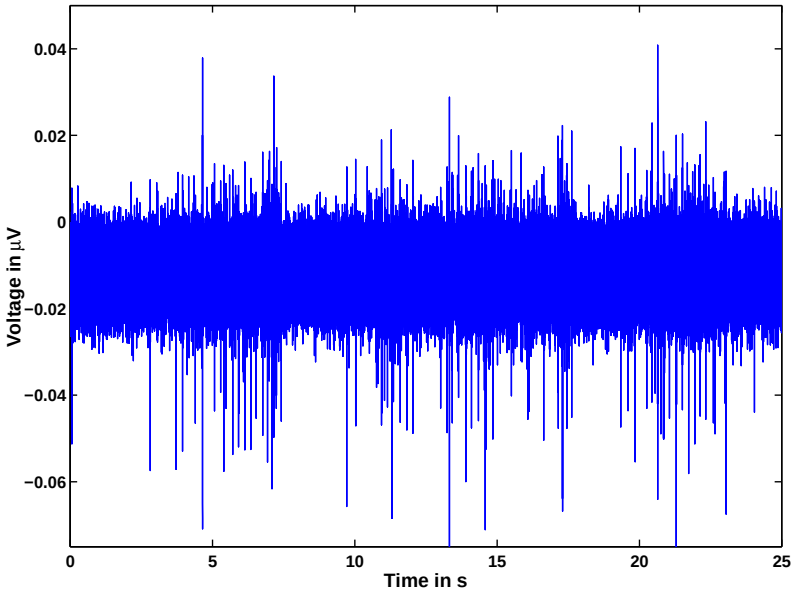

Figure 2.2: An example of the electrical activity recordings with microelectrodes.

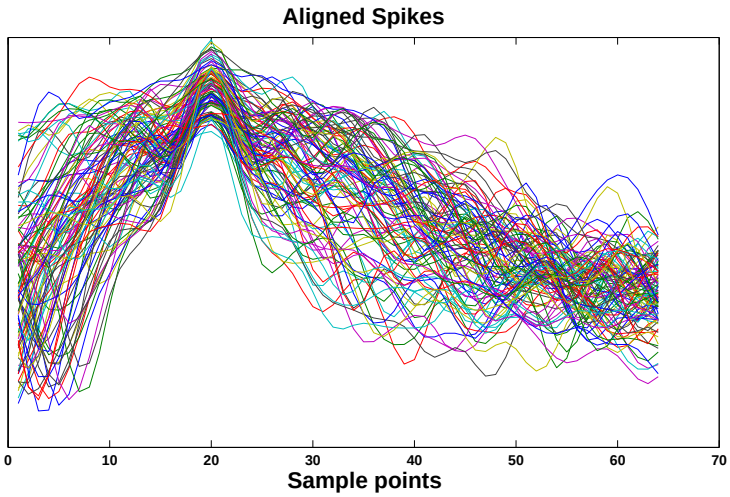

Figure 2.3: 100 spike waveforms each of them with 64 samples

are extracted with a fixed sample size (e.g. 64 samples) and aligned in order to keep the spike peak in the same sample point (see Figure 2.3). The latter stage is called *peak alignment*.

Feature Extraction

The collected spikes belong to one or more neurons. To establish the distance between two spike waveforms is usually useful to reduce the dimensionality of the spike dataset in order to consider the feature that strongly characterize a spike waveform. This stage is called *feature extraction* procedure. The dimensionality reduction must be reduced from a space of dimension m (with m the number of samples per spike) to a lower dimensional space features.
The search for the best discriminating features improves the performance of clustering algorithms and in many cases makes feasible the cluster algorithm computations. For many years, the Principal Component Analysis (PCA) has been employed to extract few principal components that hold most of the signal variances [1]. However, the principal components method with maximal variance does not produce at all times the best separations. In fact, the best separability can be achieved, e.g. by a combination of a high variance principal component with a one with a lower variance. Other newer more successful approaches are based on wavelet analysis to extract features. In fact, recently, wavelet trasform is widely employed to analyze non-stationary and non-periodic signals. The wavelets trasform reconstructs the signal using simple mathematical functions (as base of a vectorial space) that can be translated and scaled in order to recombine the original signal. The wavelet transform can detect time-frequency features that the Fourier transform cannot discriminate [65].

Clustering

The set of collected features, i.e. the detected spikes, needs to be grouped into clusters. The spike membership to a particular group means that the spike has

been generated by the neuron associated with this group. The searching for the best clustering algorithm usually involves theoretical and heuristic assumptions like apriori feature distributions (often Gaussian). One of most used is the Expectation Maximization methods with Gaussian distribution assumption [48]. However, these assumptions bias the results because consider the feature variability perturbed by Gaussian distributed noise. A more recent clustering method, the Super-Paramagnetic Clustering (SPC) [19], not assume any particular distribution of the features. It is characterized by a temperature parameter that in analogy with statistical mechanics, at low temperatures all the data are grouped into a single cluster and at high temperatures the data are split into many clusters with few members each. There is, however, a middle range of temperatures corresponding to the super-paramagnetic regime where the data are split into relatively large size clusters corresponding to the optimal sorting. This method has been applied to spike sorting by Quiroga [91].

Validation

The sorting procedure is, however, a semi-supervised technique. Each steps require the human supervision in order to prevent biological no plausible results, e.g. an unsuitable detection threshold, too many extracted cells with similar wave shapes or otherwise few cells with vary different wave shapes. When this happens the procedure will be repeted changing opportunely the parameters of the previous stages.

2.2 Neural Code

How information is represented in the brain by neurons and neuronal ensembles remains an open and important challenge. Initially, the problem was focused on the mechanisms that relate the single and ensemble neuronal activity with specific stimuli. For instance, in the first experiments on the visual system, the scientists observed the changing of firing patterns before and after a light stimulus. This allowed they hypothesize for the fundamentals of photoreceptor cells functioning principles. In recent studies spontaneous activity brought to the scene for its growing role in neural dynamics. Furthermore, in CNS there are periodic neural collective spontaneous activities involving simultaneously several structures. The outcomes of these coordinated co-activations are called *neural oscillations* or *rhythms* easily recordable by the electroencephalogram (EEG).
In this work I will discuss the theoretical background of spike activity recorded by microelectrodes. Thus I will introduce some preliminary theoretic view point about the information carried by spikes. Spikes can vary notably in duration, amplitude and shape but they are typically treated as identical stereotyped events in neural coding studies. Furthermore, if the brief duration of a spike (about 1ms including rising and falling phases) is left out, a spike sequence, or spike train, can be viewed simply by a series of all-or-none point events in time. The lengths of interspike intervals (ISIs) between two successive spikes in a spike train often vary, apparently randomly and are also largely studied.

2.2.1 Firing rate

One of the first coding scheme proposed, successfully applied during the last 80 years, hypothesize that most information about the stimulus is expressed by neuron firing rate (number of spikes per second). Furthermore, Statistics and Probability model the variation of responses by a given stimulus from trial to trial. For instance, in most sensory systems, the increasing of stimulus intensity corresponds to an increasing of the firing rate increases [8], and to decreases in trial to trial sequence showing a response habituation of neurons.
Considerations taken from behavioral experiments have shown that reaction times are often rather short. For instance, a fly can react to new stimuli and change the flight direction within 30-40ms. This is not long enough a time for spike counting and averaging over some long time windows. The fly responds after that a postsynaptic neuron has received one or two spikes [39] thus a frequency code is not appliable to these response events.
Firing rate is easy to measure experimentally and robust for noise interference. However, characterizing a spike sequence by firing rate, any information possibly encoded in the temporal structure of the spike train is disrupted. Therefore in the last 20 years this encoding scheme has been less intensively studied.

2.2.2 Spiking timing

The study of spike sequences with temporal codes emerges by the limitations of firing rate encoding. In other words spike timing seemingly largely represents the information content of signals. There is no absolute time reference in the CNS, the information is carried either in terms of the relative timing of spikes in a neuronal ensemble or in respect to a spontaneous brain oscillation or again in relation to a stimulus [39]. Thus, methods like correlations become crucial for these studies. A variant of this hypothesis shows that in experiments involving responses to stimuli the time-to-first-spike is only considered [45]. From this point of view, the brain does not have time to evaluate more than one spike from each neuron per processing step, thus, the first spike should contain most of the relevant information. However, using Information Theory approach on several experimental data, various groups have shown that most of the information about a new stimulus is indeed conveyed during the first 20 or 50 milliseconds after the onset of the neuronal response. Thus, even the pure Spike Timing hypothesis does not appear to fullfil the request of a complete coding scheme.

2.2.3 Population coding

In the late 40s, one important concept that D. Hebb brought forward was that a stimulus is encoded by nervous system within ensemble of neurons (he called them *cell assemblies*) that functionally work for the same goal [49]. This idea has been exploit to propose a new kind of coding that assumes that an information is encoded within a population of neurons [140]. Population coding reducts uncertainty due to neuronal variability and it is able to represent a number of different stimulus attributes simultaneously. Population coding is also much faster than rate coding and can reflect changes in the stimulus conditions nearly instantaneously, such that it can solve the previous problem of fly movements. Individual neurons in such a population typically have different but overlapping

selectivities, so that many neurons, but not necessarily all, respond to a given stimulus. This feature can also explain the information redundancy abundantly observed in several experiments regarding on the visual systems. In this work I will just on spiking timing and population coding.

2.2.4 Stationarity issues

Spike trains as well as many others biological sequences are non-stationary. Cells adapt their functioning by several external and internal factors. These adaptations produce metabolic changings. In neurons, the metabolic adjustments could strongly modify the discharge patterns, i.e. the wave shapes, but they also variate the spike patterns. These events are relatively slow. In fact, occur almost in several minutes and hours or more. The stationarity assumption for neuronal firing patterns can hold only within these short time intervals.

2.3 Neuronal analytical Modeling

A biological neuron model is a mathematical description of the neuron features designed to precisely model and predict the generation of action potentials. The variables that describe a neuron are: an input x with some synaptic weight vector w and an activation function ϕ determining output y. This is the basic structure used in artificial neurons, which in an artificial neural network often looks like

$$y_j = \phi\left(\sum_i w_{ij} x_i\right) \tag{2.1}$$

where y_j is the output of the jth neuron, x_i is the ith input neuron signal, w is the synaptic weight, and ϕ is the activation function. Until the late 40s, these models were largely studied despite their scarce biological plausibility.
In the following years, neuron physical analogues have been used instead of abstractions such as "weight" and "transfer function". The input to a neuron is often described by an ion current through the cell membrane that occurs when for instance neurotransmitters cause an activation of ion channels in the cell. The cell itself is bounded by an insulating cell membrane with a concentration of charged ions on either side that determines a capacitance C. Finally, a neuron responds to such a signal with a change in voltage, or an electrical potential energy difference between the cell and its surroundings, which is observed to finally result in a voltage spike called an action potential. This quantity, then, is the quantity of interest and is given by V.

2.3.1 Integrate-and-fire

One of the simplest and earliest models of a biological neuron is certainly the Integrate-and-Fire model. This model sums the input currents and whenever the sum is greater than a fixed threshold it generates an action potential. If the sum does not achieve the threshold, the membrane potential fluctuates near the resting potential values. Formally this can be described as

$$\dot{v} = I + a - bv, \quad \texttt{if} \;\; v \geq v_{threshold}, \;\; \texttt{then} \;\; v = c, \tag{2.2}$$

where $a, b, c, v_{threshold}$ are model parameters and I is the total input current. When the membrane potential v achieves the value $v_{threshold}$ the model emits a spike and then v is set to c, the resting potential.
The model is computationally inexpensive and can be used for large scale network simulations. However it cannot reproduce important behaviors like bursting and adaptation. There exist little more complicated model variants like the Quadratic Integrate-and-Fire model (also known as theta-neuron) with a good biological plausibility.

2.3.2 Hodgkin-Huxley

In 1952 A.L. Hodgkin and A. Huxley, physiologists and biophysicians, studying the axons of giant squid neurons, they developed a quantitative model able to electrophysiological describe the propagation of action potentials within the axon [51]. From a mathematical point of view, the model is a system of four non-linear ordinary differential equations that includes the description of membrane potential, the activation of sodium and potassium currents. The model is computational expensive, in fact, a 1ms simulation requires almost 1200 flops. This condition makes this model computational tractable with simulations of few neuron networks. Formally the model is described as:

$$\begin{aligned} C\frac{dV}{dt} &= I - I_K - I_{Na} - I_L \\ I_K &= g_k(V - E_K) \\ I_{Na} &= g_{Na}(V - E_{Na}) \\ I_L &= g_L(V - E_L) \end{aligned}$$

where $i \in \{L, Na, K\}$ are defined as follow:

$$\begin{aligned} g_i(V,t) &= \hat{g_n}\phi^\alpha\chi^\beta \\ \dot{\phi}(V,t) &= \frac{1}{\tau_\phi}(\phi_\infty - \phi) \\ \dot{\chi}(V,t) &= \frac{1}{\tau_\chi}(\chi_\infty - \chi) \end{aligned}$$

with C the membrane conductance, V the membrane electric potential. I is the total membrane current. I_k and I_{Na} are the potassium and sodium currents. E_i ($i \in \{Na, K, L\}$) is the inverse Nerst's potential. The variable g_K and g_{Na}, functions of time t and voltage V, are the conductance of respectively potassium and sodium channels. L is the *leak channel* that represents the natural ion permeability of membrane. The maximum conductance values for potassium and sodium are respectively $\bar{g}_K$ and $\bar{g}_{Na}$. Finally m, h and n are the gating variables that represent the linear dynamic of sodium and potassium channels. The variable m and n are active for depolarization instead of h that is inactivated

for depolarization. These are defined as follows:

$$\begin{aligned}
\frac{dn}{dt} &= \alpha_n(1-n) - \beta_n n,\ n_\infty = \frac{\alpha_n}{\alpha_n+\beta_n},\ \tau_n = \frac{1}{\alpha_n+\beta_n} \\
\frac{dm}{dt} &= \alpha_m(1-m) - \beta_m m,\ m_\infty = \frac{\alpha_m}{\alpha_m+\beta_m},\ \tau_m = \frac{1}{\alpha_m+\beta_m} \\
\frac{dh}{dt} &= \alpha_h(1-h) - \beta_h h,\ h_\infty = \frac{\alpha_h}{\alpha_h+\beta_h},\ \tau_h = \frac{1}{\alpha_h+\beta_h}
\end{aligned}$$

These parameters have been empirically determined by the authors.

2.3.3 Izhikevich

Proposed by E. Izhikevich in 1999, this model revolutionize the scenario of analytical neuron models. Its most successful features are the contained computational cost and the high-level biological plausibility [55]. In fact this model can describe a large number of neuronal types particularly for thalamus and cortex. The Izhikevich's model was born from a deep study of neurons from a dynamical system point of view. Bifurcation methodologies reduce many biophysically accurate Hodgkin-Huxley neuronal models to a two-dimensional system of ordinary differential equations ([56]) of the form

$$\dot{v} = I + 0.04v^2 + 5v + 140 - u \tag{2.3}$$

$$\dot{u} = a(bv - u) \tag{2.4}$$

with the auxiliary after-spike resetting

$$\texttt{if}\ v \geq +30,\ \texttt{then}\ v = c, u = u + d, \tag{2.5}$$

where v is the membrane potential, u is a recovery variables which accounts for the activation of potassium ionic currents and inactivation of sodium ionic currents, and it provides negative feedback to v. The total input current is represented by I and a, b, c, and d are dimensionless parameters. The part $0.04v^2+5v+140$ represents a fitting of the spike initiation dynamics of a neuron. With the right choice of parameters, i.e. $a = 0.02, b = 0.2, c = -65, d = 6$, the model reproduces a RS neuron or with $a = 0.02, b = 0.2, c = -50, d = 2$ a IB neuron.
I performed several simulations with this model in order to reproduce synthetic spike sequences.

Chapter 3

Mathematical Modeling Methods

A study at the microscopic level involves an observation of neural cells or neurons. In this perspective neurons behave in most various fashions exhibiting action potentials or spikes. The recordings of a neural ensemble can be studied at two *granular* levels. At the microscopic level the dynamic features exhibited are expressed by single neuron (SN) spike trains, i.e., the time series of neuronal action potentials. At the mesoscopic level, the collection of the recorded spike trains is identified in the multitrace recordings by definite time windows (from now called *neuronal ensembles*, NE). I label both data types as *neurophysiological sequences*.

Machine Learning (ML) is an interdisciplinary field (primarly from computer science and mathematics) that studies the ability of computer algorithms to infer new knowledge starting from some observations. The observations are usually called, in diverse scientific fields, *empirical data*. Since the empirical data train the ML algorithm, they are also called *training sets*. Generally, the training set is treated by numerical systems (e.g. decimal, floating-point, binary, etc). Numerous successful ML algorithms require this assumption. In fact, for instance, Support Vector Machine (SVM) algorithms are able to infer a discrimination rule among the observed numerical data. The SVM algorithm works with a quadratic optimization method into an euclidean space.

Whatever the training set is made of text, images, sounds, or anything else, it can be considered as a symbolic sequence. In the training set, viewed as symbolic sequence, the single item represents the state of the set of states that the symbol source (the observable that delivers the observations) can assume. In this perspective the label that tags a system state doesn't assume a particular meaning. A partial order does not hold among the state labels. Learning of features and structures within a symbolic sequence (the training set) is called *sequential data learning*. Lossless compression algorithms perform sequential data learning in order to exploit the extracted structures and regularities to compress the training sequence [105, 59, 60].

In this thesis I combine methods from sequential data learning with neurophysiological sequences.

3.1 Symbol Sources

As a rule, single neuron or neuronal ensembles are manageable as unknown discrete symbol sources $S = \langle \Sigma, P \rangle$ where Σ is the source alphabet and P is the unknown symbol probability distribution.
In a first instance, the evolution of neural activity in time can be modeled by a Bernoulli stochastic process $\{X_t\}_{t \in \mathbb{N}}$, where X_t are Bernoulli random variables with $X_t \in \{0, 1\}$. A Bernoulli stochastic process implies that every X_t is independent and that each variable is characterized by an unknown common parameter p. I am interested to the dynamics that drive the evolution of X_t in order to estabilish potential dynamical features like recurrent behaviours, changing in modes and multiple interactions among neurons. But bernoullian independence implies that the process is memoryless. Thus this simple Bernoulli model fails to capture immediate rules like "is higher probable that a spike (symbol 1) is followed by a 0 (no-spike) than vice versa".
Passing from modeling to analyses perspective, for decades the analyses of these symbolic signals were carried out by elementary functions like correlation, estimated by e.g. Pearson coefficient, that can only measure the linear relation between two neuronal spike trains. This approach points out two problem classes:

1. Pearson correlation coefficient can estabilish (potentially) a linear relation between two spike trains

2. any correlation function is symmetric. In our perspective I could map spike trains in a Potential Field. In this space a similarity function between point couples shows, as a raw, no true symmetry but trivial cases. In other words, where X and Y are two spike trains, it can be easier to achieve X from Y than the reverse.

Mutual information, and other statistical dependence measures like rank correlations, address only the first class. Therefore I must face the task to solve both problems simultaneously. On this track I propose a general framework based on spike train structure learning, a method able to catch linear as well as nonlinear relationships such as recurrent schemes and predictive rules within the given spike train. This would allow us to potentially test the Y-predictability from X. With such an approach, it could be accessible the information *about X-Y relationship direction*. Given an ensemble of spike trains, I try to exploit this general method as consisting of these two stages:

1. **Structure discovery for sequence**. I develop a pattern capturing predictive model for the neurophysiological sequences.

2. **Structure similarity between sequences**. I compute a similarity matrice as a kind of correlation matrix on a sequence collection.

Single neuron sequence structures can quantify the neuronal behavioural redundancy. Redundancy is proportional to the predictability. Historical works show that high level prediction is equivalent to high level compression [97, 9]. In fact, ideal compression (i.e., compression at or very near to the entropy of the sequence) would be achieved if using the past observed symbols then it is possible to predict with probability 1 the next symbols.
Defining neurophysiological sequence similarity indicates the complexity level

(inverse to the amount of shared patterns) of the neuronal ensemble. As for point 1, I will discuss Makov Processes and their related estimation algorithms. For point 2, I present an analysis based on similararity distances through compression algorithms.

3.1.1 Finite Markov Process

Now I try to take into consideration several stochastic models with arising complexity and predictability. The Bernoulli stochastic model assumes the independence of its binary trials. The tossing coin outcomes follow this model. Of course, any next coin toss outcome doesn't depend on the previous one. Biological evidence suggests that action potential generations is strongly dependent on short-term previous history. In this modeling stage, the aim is to capture the time dependence between trials as many as possible. So I leave a Bernoulli process to introduce a more powerful process family able to deal with time dependence between outcomes, the *Markov Models* (MMs).
Given a finite stationary process $\{X_t\}_{t\in\mathbb{N}}$ with values $X_t \in \Sigma$ and $|\Sigma| < \infty$, [1] representing the spike activity of single neuronal cell, if the following condition, called Markov property, holds:

$$P\{X_t = x_t | X_{t-1} = x_{t-1}, \dots X_0 = x_0\} = P\{X_t = x_t | X_{t-1} = x_{t-1}\} \qquad (3.1)$$

then the process $\{X_t\}_{t\in\mathbb{N}}$ is a *Markov process*. In other words, if the stochastic process outcomes depend on by the immediatly past event then the process is *Markovian*. Starting with an initial state $X_0 = x_0$, the events are linked one-by-one and this justify the term *chains*. The concept of Markov Chain completes and expands the classical Markov process. A formal definition of Markov Chain is the following statement:

A Markov Chain is a triplet given by a finite set $\Sigma = \{1, 2, \dots, k\}$ *called states, an initial probability distribution* $\mu : \Sigma \to \mathbb{R}$ *and a stochastic matrix* M *called transition matrix such that* $m_{i,j} \geq 0 \forall i, j \in \Sigma$ *and* $\sum_{j\in\Sigma} m_{i,j} = 1$

In particular, the element $m_{i,j} \in M$ tells us the probabilities to pass from state i to state j. Suppose that the processed spike train consists of a Markov Chain with $\Sigma = \{0, 1\}$. The 2x2 transition matrix M contains the probabilities to pass, e.g., from 0-state to 1-state. Knowing M, after some estimation procedure, I can extract useful informations. In fact, M has a predictive power. In the following example if I observe a 1-state I can conclude, that with probability 0.9, the next state will be 0.

$$M = \begin{bmatrix} 0.8 & 0.2 \\ 0.9 & 0.1 \end{bmatrix} \qquad (3.2)$$

Although the improvement compared to the Bernoulli process, the prediction power of a Markov Chain model for spike trains is very poor. In fact, neurons may exhibit many different and quite regular behavioural patterns of activity like tonic spiking or bursting [8]. The Figure 3.1 represents the typical behaviour of a thalamic neuron (remarking that the timescale is $\tau = 1$ms) represented by the

[1] in our experimental framework $\Sigma = \{0, 1\}$ for spike trains modelling and $\Sigma = \{\sigma_1, \sigma_2, \dots\}$ with $|\Sigma| < \infty$ for neuronal ensembles modelling

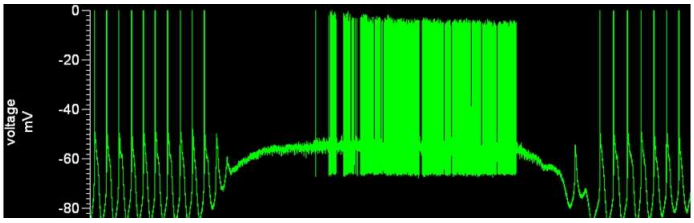

Figure 3.1: A tipical behavioural pattern of a thalamic cell during tonic-bursting phases

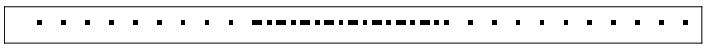

Figure 3.2: The respective symbolic sequence where black cells represent spikes.

sequence $\sigma = 0000100001000010000100001000010000100001000010000100001101011-0101101011010110101101011010110101000010000100001000010000100001000010000100001-000010000100001$, displayed in Figure 3.2. In this case the prediction accuracy is very low because the model is unable to catch any of two important schemes within the sequence σ (the repetitions of "00001" and of "11010"). This is meanly due to the fact that the Markov property holds only for one backward event. The σ sequence will represent in the rest of this section a toy example. If I extend the number of past events that conditions the outcome of the next state, the prediction power of these models arises. This concept leads to the definition of Markov Chains *order* or *length*. Formally

Given a stationary process $\{X_t\}_{t\in\mathbb{N}}$ *with values* $X_t \in \Sigma$ *and* $|\Sigma| < \infty$*, if the condition* $P\{X_t = x_t|X_{t-1} = x_{t-1}, \dots X_0 = x_0\} = P\{X_t = x_t|X_{t-1} = x_{t-1}, \dots, X_{t-k} = x_{t-k}\}$ *is satisfied for some* $0 < k \leq t$*, with* $k, t \in \mathbb{N}$*, then the process is a Markov process of order (or length)* k *(*$k - MM$*).*

The k-MMs are able to construct models that estimate every conditional probabilities $p(\sigma|c_k)$ where σ is the next outcome of the c_k sequence, i.e. the k past events before σ. So if there's some recurrent context that triggers a particular sequence of events this will be detected for some value of k. For example, suppose that a neuron emits a spike after a string pattern $c = 10100001010$. When I construct the k-order Markov model for this neuron, if I choose $k = 11$ then I am sure that, with some estimation procedure, $p(1|10100001010)$ is close to 1.
With $k = 2$ states and a 1-order model, then I have 4 possible transition to estimate. With a 2-order model I have 2^3 possible transition and so on. So, the *dimensionality explosion* takes the upper hand increasing the model length. In the previous example, with a 11-order, I would estimate 2048 possible transitions, but with 7 possible states, the number of transitions would be almost two billion! The general asymptotic combinatorial rule is that the dimension grows as $O(|\Sigma|^k)$. This issue brings the k-order Markov Chain to be unfeasable in most pratical cases. In our experiment, the neurophysiological sequences are usually long 10^6ms and $|\Sigma| = 2$ for spike trains and $|\Sigma| \approx 10^3$ for neuronal ensembles. However, I should remark that, generally, many transitions will never

occur. So, the estimations of the respective probabilities will be close to zero. On one hand, I would choose k as big as possible to increase predictability, on the other hand, I choose k as small as possible to avoid dimensionality explosion and zero-probability issues that bias the estimations.

3.1.2 Variable Order Markov Models

A solution to both problems is represented by Variable Order Markov Models (VOMM, also knows as Variable Length Markov Chains) proposed by Rissanen [96] in 1983. A VOMM outlines the possibility to take in consideration only transition probabilities that effectively appear in an examined sequence. Namely, there exist $p(\sigma|c_k)$ with $k \in \{1, 2, \ldots, K\}$ only for the c_k contexts encountered in the training sequence, where K is the maximum order of temporal dependency allowed. Formally a VOMM is defined as follow

Let $\{X_t\}_{t\in\mathbb{N}}$ be a stationary stochastic process with values $X_t \in \Sigma$, $|\Sigma| < \infty$. Let K be the maximum allowed order with $0 \leq K \leq \infty$ and let $c()$ be the function that establish the order s for any given context $x_i^j = x_i x_{i+1} \ldots x_j$ with $j < i$ and $i, j \in \mathbb{N}$, so that

$$P\{X_t = x_t | X_{t-1} = x_{t-1}, X_{t-2} = x_{t-2}, \ldots\} = P\{X_t = x_t | X_{t-1} = x_{t-1}, \ldots, X_{t-s} = x_{t-s}\}$$

with $s = c(X_{t-K}^{t-1})$. Then $\{X_t\}$ is called the Variable Order Markov Model of order K.

The VOMMs of maximum order K are as powerful as the equivalent all-k-order MMs (all j-order MM with $1 \leq j \leq k$) but employ the minimun amount of space. VOMMs are able to locally optimise memory model usage and could efficiently captures long and short-term temporal dependencies within sequences. In any pratical case, given a context, the c function tell us whenever the context exists in the sequence. This time the toy example can be modelled setting $K = 10$ and constructing, for instance, the following conditional probabilities:

- $p(1|0000) \approx 1$
- $p(0|000010) \approx 1$

and so on for other simple regularities easly detectable.

An example of VOMM

Suppose that we observe the sequence $x_1^T = x_1 \cdot x_2 \cdots x_T = x_1^{11} = \texttt{abracadabra}$ generated by the source $S = \langle \Sigma, P \rangle$ with $\Sigma = \{\texttt{a}, \texttt{b}, \texttt{c}, \texttt{d}, \texttt{r}\}$. Then, we let $K = 2$. To build a VOMM for this sequence, we need to estimate the symbol probability distribution P with $\hat{P}$ through the estimation of conditional probabilities $p(\sigma|s)$ such that $s\sigma$ is a subsequence of x_1^T. Thus, we first extract the contexts of length 1 that trivially are the alphabet symbols and then we proceed with contexts of length 2 that are $s \in \{\texttt{ab}, \texttt{br}, \texttt{ra}, \texttt{ca}, \texttt{ac}, \texttt{ad}, \texttt{da}\}$. Summarizing, seven 2-length contexts plus five 1-length contexts for the VOMM estimation and twentyfive 2-length contexts plus five 1-length contexts for an all-K-order MM estimation.

By definition of VOMM, cases as `ba` are not explicitly estimated and fall into the zero-probability problem that is efficiently solved by VOMM estimation algorithms.
Efficient data structures that help to estimate the conditional probabilities for a given sequence are the Prefix Trees. These data structures store in their nodes every prefix of a given sequence. Recalling the previous toy example, we can build a prefix $|\Sigma|$-ary tree with depth K for sequence $x_1^{11} =$ `abracadabra` that is

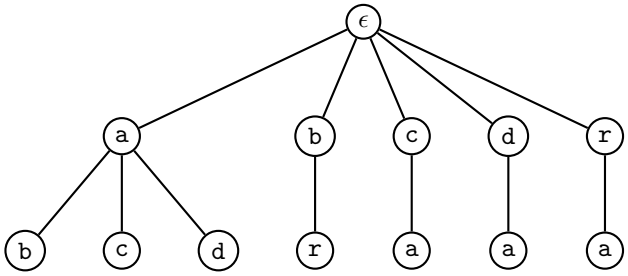

Thus, prefixes of length 1 are stored in the root-to-first-level node paths, prefixes of length 2 are stored in the root-to-second-level node paths and so fourth.

Comparison with Hidden Markov Models

The Hidden Markov Models (HMMs) are MMs with hidden states. A set of observable states is mapped into the set of hidden state with an emission probability distribution. Several HMMs for neurophysiological sequences have been developed. A VOMM overcames several HMMs issues. Although the HMMs can model complex sequences, they may not be suitable to capture longer range sequential dependencies. Furthermore, HMMs suffer from local optima during estimation phase.

3.2 Lossless Compressor Codes

The Kolmogorov complexity (KC) of an object x expressed as a string (or symbol sequence) represents the length of the shortest program, for a universal Turing machine, that outputs the x string. In other words, the Kolmogorov complexity measures the amount of useful knowledge to compute a given object that is the semantic object content. The KC is uncomputable and this can be proved by the reduction from the uncomputability of the Halting Problem. The first important inequality is that:

$$KC(x) \leq |x| + c, \forall x$$

where c is a costant and $|x|$ is the x length.
Some information contents are syntactically accessible, some others not. For instance, considering the digits of the natural constant π, no syntactic information can be extracted. In fact, π (as many other natural constants) passes every randomness test. No structure can be extracted only from their digits. Nevertheless it is quite simple to write a short computer program that outputs the π digits. Thus, only semantic information allows π digits compression.

However many symbolic sequences involved in real-world problems could be syntactically compressed. Moreover, many symbolic schemes are unaccessible by a human observer being the million symbol long recurrences within a string undetectable.
Lossless compression algorithms allow syntactic compression of an object like a binary string. The basic idea is that, given a fixed object, a compression algorithm is able to rewrite the object such that the length of the rewritten version is smaller than the original version length. The reduced object length proves the compression algorithm capacity to describe the object in terms of rules and schemes. Hence the compression algorithm abilities purely act on a syntactic level. In this way compression algorithms impose an upper bound to Kolmogorov complexity. This upper bound is stronger than the previous inequality since:

$$KC(x) \leq C(x) \leq |x| + O(1), \forall x$$

where $C(x)$ is the x compressed version length. The idea that compressor codes could approximate Kolmogorov complexity was first presented in several works [29, 28, 10] that led to the definition of a similarity metric called Normalized Compression Distance and to that of a kernel function based on it. Their results showed successful applications with unsupervised and supervised tasks such as text categorization, protein and music clustering.
Learning of sequential data remains still an open challenge. VOMMs obtain good results in several classification tasks on symbolic data [9]. Lossless Compression Algorithms (LCAs) given a string σ of fixed length n return a coded string ζ with length c with $c \leq n$. In the Lossless family, the compressed string ζ can be univocally decoded in order to reobtain σ. There exist several LCAs. Each of them is based on specific techniques like dictionary, statistics, block-sorting and many others. The basic idea behind every LCA is to find regularities, recurrent patterns within the sequence in order to exploit this information to compress the string. For example, the string 01101101110101101101110101101101011011 is long 36 characters. If I rewrite it in the form *aaabaaabaaaa* will be long only 12 character with the additional information that $a = 011$ and $b = 101$. Any LCA implicitly constructs a VOMM. I selected three types of statistical-based LCAs considered the state-of-art for their compression ratio performances. These are: Context-Tree Weighting (CTW) [137, 138], Prediction by Partial Matching (PPM) [30, 122] and Probabilistic Suffix Tree (PST) [98, 11]. In general, any lossless compression algorithm, even a simple Lempel-Ziv [135, 147], can be used for prediction. Sometimes, less compression ratio but more computational efficient algorithms could be preferred.
Finally, once the conditional probabilities were estimated, the compression algorithm uses an encoding scheme, usually the arithmetic encoding, to generate the compressed code for the string. The first stage of these algorithms can be exploited to compute conditional probabilities of each symbol, for every encountered context shorter than a fixed constant K.

3.2.1 Prediction by Partial Matching

Let $x_1^T = x_1 \dots x_T, x_i \in \Sigma$ be a sequence of symbols and K be the maximum order for context. A PPM algorithm constructs a tree S rooted in node ϵ, the empty word, where each path from root to node represents an existing sequence

prefix[2] s, of x_1^T, with associating occurence counter $N(s\sigma)$, where σ is the last encountered symbol. The depth of S is always $K+1$ except for trivial cases. The algorithm starts with the tree containing the only empty word ϵ and then processes the sequence x_1^T one symbol at time togheter with its context of length K. Given x_i and its prefix x_{i-K}^{i-1}, the algorithm verifies if there exists the x_{i-K}^{i} path within the tree S. If it exists, the counters of each path node will be updated, otherwise a specific tree branch labeled with the missing path node will be created.
The PPM, like any other statistical-based compressor, needs to handle the occurence of zero-probability symbols. In other words, if I ask to compute $p(\sigma|s)$ with $N(s\sigma) = 0$ once the estimation procedure is done (i.e. the tree construction), I can't conclude that $p(\sigma|s) = 0$. This problem resides in both theoretical and pratical aspects. Given a symbol source with an associated probability distribution, it's impossible to compute the source entropy if even only one symbol probability is zero. I neither can pass to an arithmetic encoder a zero probability symbol [31]. PPM estabilishes two mechanisms to overcome the zero-probability problem: *exclusion* and *escape*. With the *escape* process, for each context s of length $k \leq K$, a probability $\hat{P}_k(escape|s)$ for non appearing symbols after context s is assigned. For other non-zero count symbols, the probability $1 - \hat{P}_k(escape|s)$ will be distributed

$$\hat{P}(\sigma|s_{n-K+1}^n) = \begin{cases} \hat{P}_K(\sigma|s_{n-K+1}^n), & \text{if } s_{n-K+1}^n \in x_1^T; \\ \hat{P}_K(escape|s_{n-K+1}^n) \cdot \hat{P}_{K-1}(s|s_{n-K+2}^n), & \text{otherwise.} \end{cases} \quad (3.3)$$

and for the empty context ϵ, $\hat{P}(\sigma|\epsilon) = 1/|\Sigma|$. The exclusion mechanism enhances the escape estimation. The basic consideration is that if a symbol σ with context s with $|s| \leq K$, then σ can be missed from the estimation of $\hat{P}_{|s|}(\cdot|s')$, $\forall s'$ such that s' is a suffix of s. A Smaller alphabet incurs in potentially accurate estimation.
The operative core of the conditional probabilities estimation is defined by the following equations

$$\hat{P}_k(\sigma|s) = \frac{N(s\sigma)}{|\Sigma_s| + \sum_{\sigma' \in \Sigma_s} N(s\sigma')}, \quad (3.4)$$

$$\hat{P}_k(escape|s) = \frac{|\Sigma_s|}{|\Sigma_s| + \sum_{\sigma' \in \Sigma_s} N(s\sigma')} \quad (3.5)$$

with $N(\sigma)$ be the function that counting the σ occurences in x_1^T, $\Sigma_s = \{\sigma : N(s\sigma) > 0\}$ and with $|s| = k$. If n is the length of the sequence and K the maximum order allowed, PPM requires $O(n)$ in computational time and $O(Kn)$ in computational space.

Prediction with PPM

To compute $\hat{P}(\sigma|s)$ I start from the root and traverse the tree according to the longest suffix of s, denoted s', such that $s'\sigma$ corresponds to a complete path from the root to a leaf. Probability estimation uses the above equations 3.3-3.5. If $|s|$ is the length of the sequence to predict, the prediction procedure requires $O(|s|^2)$ in time.

[2] this data structure is usually known as *trie* or *prefix tree*

3.2.2 Context-Tree Weighting

The CTW algorithm is an ensemble method, combining exponentially many VOMMs, where each of such models is estimated by zero-order conditional probability estimators. Without loss of generality I present the binary alphabet ($\Sigma = \{0, 1\}$) version of CTW algorithm that uses the Krichevsky-Trofimov (KT) estimator as zero-order conditional probability estimators [62]. Several extensions to the multialphabet case exist and require a further explanation of technical details. A part of results is obtained using a multi-alphabet CTW version called decomposed CTW that provides a hierarchical decomposition of the multi-value problem into binary ones. For further details see [125].

Tree Source

CTW models the symbol source that generates the training sequence with trees called *tree sources*. A tree source represents a VOMM, that's a full binary tree with depth up to K, each leaf having an associated probability distribution over the binary alphabet. Formally the tree source is a set $S \subseteq \Sigma^{\leq K}$ of suffixes where each node is a path from a leaf to the empty word root ϵ and where each left son edge is labeled by 0 and each right son edge by 1. I denote with $\mathcal{C}_K$ the set of all tree sourced with K-bounded depth. The zero-order distribution of a leaf s is denoted by $p_s(\sigma)$, $\forall \sigma \in \Sigma$.
A K-bounded tree source S induces a probability distribution over Σ^n for each sequence of length n. The probability is inducted by the chain rule:

$$P_S(x_1^T) = \prod_{i=1}^{T} P(x_i | x_{i-K}^{i-1}) \tag{3.6}$$

Denoting by $y_1^m = SUB_s(x_1^T)$ the ordered non-contiguous subsequence of symbols appearing after the contex s in x_1^T and defining $p_s(x_1^T) = \prod_{i=1}^{m} p_s(y_i)$ with $p_s(\epsilon) = 1$ then the Equation 3.6 becomes:

$$P_S(x_1^T) = \prod_{s \in S} p_s(x_1^T) \tag{3.7}$$

The CTW method

The CTW algorithm firstly guesses the topology (the set S) of the best tree source and then estimates the distributions associated with its leaves. As first point, the CTW algorithm assigns to each $s \in S$ (assuming that the best tree topology is known) a KT-estimator $\hat{p}_s$ that estimates p_s considering all the occurrences s in x_1^T and constructing $\hat{p}_s$ by counting and smoothing. In particular if a and b are, respectively, the number of zeros and ones in the sequence q, the KT-estimator is equivalent to

$$\hat{P}_{KT}(0|q) = \frac{a + \frac{1}{2}}{a + b + 1} \tag{3.8}$$

$$\hat{P}_{KT}(1|q) = \frac{b + \frac{1}{2}}{a + b + 1} \tag{3.9}$$

and

$$\hat{P}_{KT}^{s}(x_1^T|q) = \prod_{i=1}^{T} \hat{P}_{KT}(x_i|q_s) \tag{3.10}$$

Pratically the best tree source topology, for a given sequence, is unknown. Thus, the CTW algorithm considers all possible K-bounded topologies in S, i.e the all possible subtrees of the complete binary tree of depth K and then estimates its zero-order (e.g. KT) leaf probabilies. Finally, the CTW mix all predictions in a computationally efficient way, notwithstanding the exponential size of subtrees, and outputs $P_{CTW}(x_1^T)$, remarking that $\sum_\sigma P_{CTW}(x_1^T\sigma) = P_{CTW}(x_1^T)$. The probability $P_{CTW}(x_1^T)$ can thus be considered as

$$P_{CTW}(\sigma|x_1^T) = \frac{P_{CTW}(x_1^T\sigma)}{P_{CTW}(x_1^T)} \tag{3.11}$$

that is the next symbol probability for each $\sigma \in \Sigma$. Furthermore the sequential zero-order estimation for x_1^T is, by the chain rule, again

$$\hat{p}_s(x_1^T) = \prod_{i=1}^{m} \hat{p}_s(y_i|y_1^{i-1}) \tag{3.12}$$

The Algorithms 1 and 2 define the CTW method.

Algorithm 1 Estimation of the tree sources

```
CTW(x_1^T, x_{1-K}^0, K)
for s ∈ Σ^{≤K} do
  compute and store p̂_s(x_1^T)
end for
return P_CTW(x_1^T) = mix(ϵ, x_1^T, x_{1-K}^0)
```

Algorithm 2 Mixing the estimations

```
mix(s, x_1^T, x_{1-K}^0)
if |s| = K then
  return p̂_s(x_1^T)
else
  return (1/2)p̂_s(x_1^T) + (1/2) ∏_{σ∈Σ} mix(σs, x_1^T, x_{1-K}^0)
end if
```

It is notable that the original version of CTW algorithm assigns fixed weights equal to 1/2. Further CTW extensions exploit this step with other assignment policy well known in other fields like *expert advice learning*. The best CTW implementation requires $O(KT)$ in space and time.

Prediction with CTW

Prediction with CTW requires $O(K|s|)$ and it is performed by Algorithm 2.

3.2.3 Probabilistic Suffix Trees

Probabilistic Suffix Trees are variants of probabilistic finite automata. A PST tries to build a K order VOMM using several parameters. In fact, this method is more supervised than CTW and PPM and tipically needs parameter specifications and tunings to deliver sound results. It is simple to implement and

requires low computational space and time.
Given the x_1^T the training sequence, the algorithm builds a suffix tree S in three steps:

1. build the suffix tree S where each node represents contiguous subsequence s of x_1^T with $|s| \leq K$. The tree S contains all the encountered contexts with length up to K. Hence the frequency of s in x_1^T must be larger than a user defined threshold. Thus the maximum likelihood estimator for $\hat{P}(\sigma|s)$ is obtained.

2. grub probability estimations that doesn't satisfy one of the following conditions:

   (a) $\hat{P}(\sigma|s) \geq$ some user defined threshold

   (b) If $s = \sigma_k \sigma_{k-1} \dots \sigma_1$, then its parent node is its longest suffix $s' = \sigma_{k-1} \dots \sigma_1$. Thus

   $$\frac{\hat{P}(\sigma|s)}{\hat{P}(\sigma|s')} \geq r \quad \text{or} \quad \frac{\hat{P}(\sigma|s)}{\hat{P}(\sigma|s')} \leq \frac{1}{r} \tag{3.13}$$

   where r is another user specified parameter.

3. smoothing: if $\hat{P}(\sigma|s) = 0$ then a minimum (user specified) probability is assigned and the resulting distribution re-normalized.

This algorithm requires $O(Kn^2)$ in space and $O(Kn)$ in time.

Prediction with PST

The PST requires $O(K)$ for prediction. It is done visiting the tree starting from root and following the respective branch of symbol context. The reached node contains the estimated conditional probability.

3.3 Estimation Framework

To clarify the proposed estimation of VOMM with the algorithms above, I present the diagram in Figure 3.3. Once the neurophysiological sequence is obtained from an observed source (neuron), the VOMM construction follows these three steps:

1. Split the sequence in two parts: the first sequence will be used as training sequence (q_1^n) and the second as test sequence (x_1^T).

2. Estimate for each LCAs (PST,CTW,PPM) the VOMM obtaining a $\tilde{P}$

3. Select the estimated distribution $\hat{P}$ among the three $\tilde{P}$, the best one that optimize the following problem: $\hat{P} = argmax_{\tilde{P}} \tilde{P}(x_1^T)$.

Thus, this simple procedure selects the estimated model with the highest propability assignment on the test sequence.

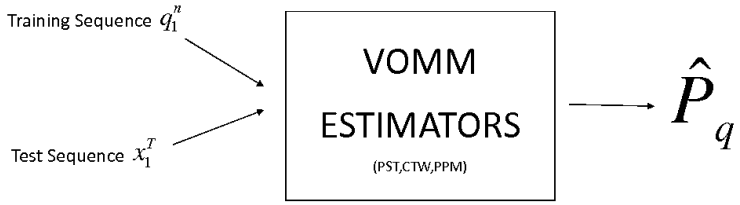

$$\hat{P} = \arg\max_{\tilde{P}} \tilde{P}(x_1^T)$$

Figure 3.3: The estimation framework for VOMM with lossless compression algorithms.

3.4 VOMM's model similarities

Let's set a similarity function μ between two sequences a and b generated by VOMMs X_a and X_b. Once a VOMM for sequence a is built, then I compute the probability that the sequence X_b could be generated by a model. Now I evaluate the possibility to make μ as a metric.
Once I have a set of models Ψ for a set of neurophysiological sequences, the model can be comparable defining a metric μ for every couples of Ψ elements. Let μ be a distance function (or metric) defined as $\mu : \Psi^2 \to \mathbb{R}$ that satisfies $\forall X_a, X_b, X_c \in \Psi$ (the space of VOMMs) the following conditions:

1. $\mu(X_a, X_b) \geq 0$ (non-negativity)
2. $\mu(X_a, X_b) = 0$ iff $x = y$ (identity of indiscernibles)
3. $\mu(X_a, X_b) = \mu(X_b, X_a)$ (simmetry)
4. $\mu(X_a, X_c) \leq \mu(X_a, X_b) + \mu(X_b, X_c)$ (triangle inequality)

Unfortunately our requirements don't match the four conditions alltogether. In fact, as I have previously discussed, I need an asymmetric distance function where the second property doesn't imply $x = y$. This means that it's possible (but very unusual) to find two neurophysiological sequences so stricly coupled to reduced their distance to zero. Even the fourth condition doesn't hold. The mathematical notion of distance function does not match out requirements. Thus, the expected similarity function must respect only the non-negativity condition. However, computational issues arise with this approach. An approach based on the arithmetic encoders is more computationally efficient.

3.4.1 Average Log-Loss

The recorded sequences SN and NE are non-stationary over long time periods, i.e. several minutes [2]. Stationarity is measurable in epochs not exceeding one minute or so. As I introduced in the previous Section, every examined SBCA returns, given a symbolic sequence $s = s_1 s_2 \cdots s_n$, an estimation $\hat{P}$ for P. Suppose that two sequence q_1^T, s_1^n are both observed from source S. The former is the training sequence and the latter is the test sequence. The training sequence builds the VOMM, i.e. the estimated probability distribution $\hat{P}$. The average log-loss uses the test sequence to compute the learning error to evaluate the loss due to employing the distribution $\hat{P}$ instead of P. The average log-loss function is, thus, definied between an estimatated probability distribution $\hat{P}$ and a test sequence as follows

$$l(\hat{P}, s) = -\frac{1}{n}\sum_{i=1}^{n} \log \hat{P}(s_i|s_{i-1}\cdots s_1) \quad (3.14)$$

$$= -\frac{1}{n}\log \prod_{i=1}^{n} \hat{P}(s_i|s_{i-1}\cdots s_1) = -\frac{1}{n}\log \hat{P}(s_1^n) \quad (3.15)$$

and can be employed to estimate similarity between sequences. It is worth to note that minimizing the average log-loss is completely equivalent to maximizing the probability assignment $\hat{P}(s_1^n)$. This fact is very common in the machine learning framework that the best accuracy performance in classification tasks is obtained by minimizing the error over the test set instead of training set that otherwise would bring the classificator to overfitting problem. Given two sources $S^1 = \langle \Sigma, P^1 \rangle$, $S^2 = \langle \Sigma, P^2 \rangle$, their observed sequences s^1 and s^2, a SBCA algorithm (e.g. PPM) and the sequence s^1, the average log-loss returns $\hat{P}^1_{PPM}$. Thus, the similarity function between the two sequences $\mu(s^1, s^2)$ can be defined as

$$\mu(s^1, s^2) = l(\hat{P}^1_{PPM}, s^2) = -\frac{1}{n}\sum_{i=1}^{n} \log \hat{P}^1_{PPM}(s_i^2|s_{i-1}^2 \cdots s_1^2) \quad (3.16)$$

Function μ supplies analyses that involve the study of similarity between experiment runs (SN or NE) and the dynamic of stationary phases within an experiment. These studies on experiment couples allow for quantifying diversity (or similarity) among the whole experimental issue in the database, for instance, PVS vs MCS patients or CPAs vs normal rats.
In spite of the polynomial time complexity of these algorithms, they spend a lot of memory and fail on large datasets (in particular CTW).

3.4.2 Compressor-based similarity function

In the recent years, some similarity functions based on the compressed length have been proposed. The most widespread is certainly the Normalized Compression Distance (NCD). However, several comparisons show that in many real-world problems the accuracy is not significantly differ [105]. This similarity function has been presented in several works by Rudi Cilibrasi and Paul Vitany ([29] ,[28]). The concept behind this function regards the conditional

Kolmogorov complexity that brings to the non-computable distance function called Normalized Information Distance:

$$NID(x,y) = \frac{\min\{K(x|y), K(y|x)\}}{\max\{K(x|y), K(y|x)\}} \tag{3.17}$$

that could be approximated with compression algorithms

$$NCD(x,y) = \frac{C(x \cdot y) - \min\{C(x), C(y)\}}{\max\{C(x), C(y)\}} \tag{3.18}$$

where $C(\cdot)$ function represents the compressed sequence length and $\cdot$ is the sequence concatenation operator. When $NCD(x,y) = 0$ the objects are considered similar otherwise when it is equal to 1 the objects are very dissimilar. However, since the idempotence property can be violated by some compression algorithms[3], it can exceed 1 for little ϵ. This distance was successfully applied to text and music clustering tasks [28]. Although worse performing in compression ratio, widely used Unix compressors (`gzip`, `bzip2`, `lzma`, etc) achieve comparable results in faster ways. Computing the compressed sequence lengths by Unix compressors, I could define the Normalized Compression Distance (NCD) as:

$$NCD(s^1, s^2) = \frac{C(s^1 \cdot s^2) - \min\{C(s^1), C(s^2)\}}{\max\{C(s^1), C(s^2)\}}$$

I remark that the NCD function is a feature-free distance function, i.e. the similarity estimation is not based on some fixed features. On the contrary every other similarity measure is feature-based, i.e. they require detailed knowledge of the problem area in order to measure the similarity/dissimilarity between two objects.
The computational efficiency, in this case, allows for the similarity computation between many paired SN sequences. Given a SN set, I computed the similarity between all the possible pairs. Obtaining a similarity matrix, it's possible to compute L^2 (or Frobenius) matrix norm and to assume this feature as an estimator of NE redundancy.

3.4.3 Stationary Phase Detection

Considering SN sequences it is possible to detect stationary phases and to study dynamical features like *sojourn time* distributions. Detection of stationary phases can be done in two stages: first by splitting the SN sequence in N overlapping windows of fixed length m and overlap size β, where c_t represents the subsequence $s_t \cdot s_{t+1} \cdots s_{t+m}$. Second by finding the time window i, where $\mu(c_t, c_{t+1}) \geq \eta$, for some fixed constant η. The constant β usually belongs to $[\frac{m}{3}, \frac{2m}{3}]$. The constant η can be computed by reference value from the shuffled original sequence. To achieve more robust results it is possible to compute the numerical forward derivative of the average log-loss comparing its value with a geometrically interpretable threshold.
The Figure 3.4 shows an example of this technique capability to highlight the chaotic phase of the Logistic Map within the intermittent region.

[3] when $C(x \cdot x) > C(x)$ instead of $C(x \cdot x) = C(x)$

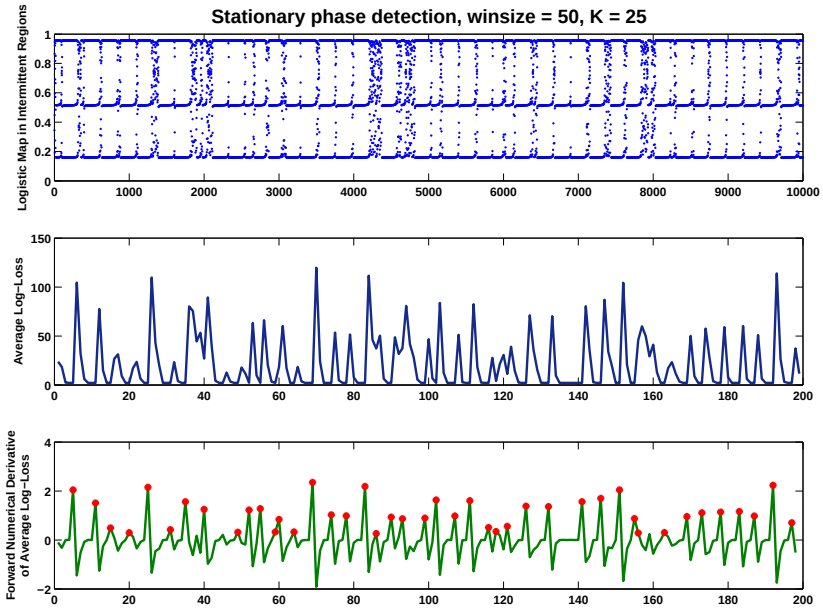

Figure 3.4: In the panel above the Logistic Map within the Intermittent Chaos Region ($\alpha \in [3.8284, 3.8287145]$). In the central panel the average log-loss computed on sliding windows of 500 units at 50 units. In the panel below the peaks of the derivative of average log-loss follow the chaotic region while the periodic phases represent low values of average log-loss.

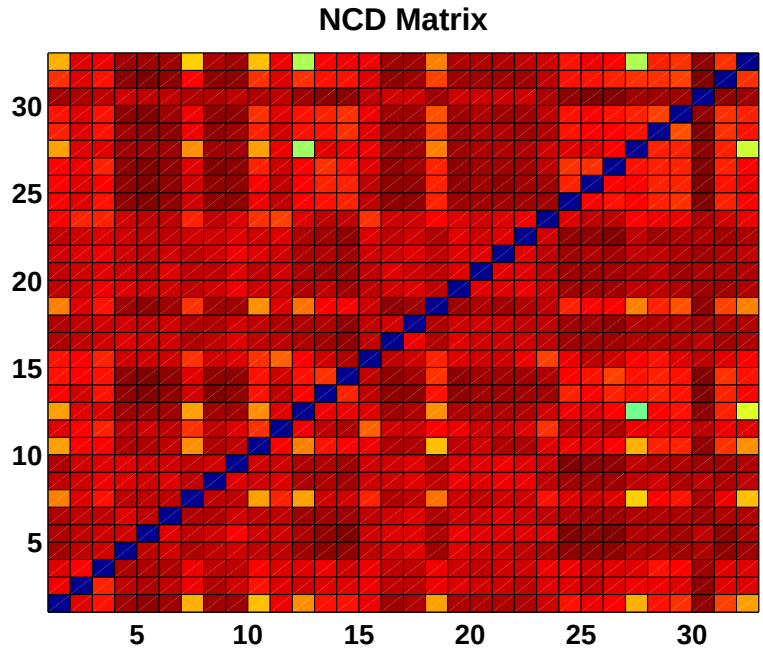

Figure 3.5: An example of NCD matrix from a thalamus of an experimental chronic pain animal model. The recording gathers 33 neurons.

3.5 Neuronal Groups Discovery

Starting from the NCD matrix (see for e.g. Fig 3.5), I considered a functional direct relationship $A \rightarrow B$ between corresponding SNs, computing the set $\Gamma = \{A \rightarrow B | \mu(A, B) \geq \theta\}$. I called this method Neural Group Discovery (NGD). For instance, the NGD procedure computes the graph displayed in Figures 3.6-3.7. A NE functional dependency graph delivers several statistics extraction like the node degree distribution, the connection density and the hub count [21].

3.5.1 Small-World Networks

The NGD method is very closely related to the recent developments in the Small-World Networks theory. The Small-World Networks are graphs (see examples in Figures 3.8 and 3.9) that hold the following properties:

- Scale-Free Topology: the graph topology is very similar in different scale like a finite fractal. This property lies in the node degree distribution that looks like a power-law distribution.
- Clique Presence: in the graph there are several, typically small, complete subgraphs, i.e. subgraphs where each nodes are connected with each one.
- Small Mean Shortest-Path Between Nodes: the communication between two random nodes is very fast.

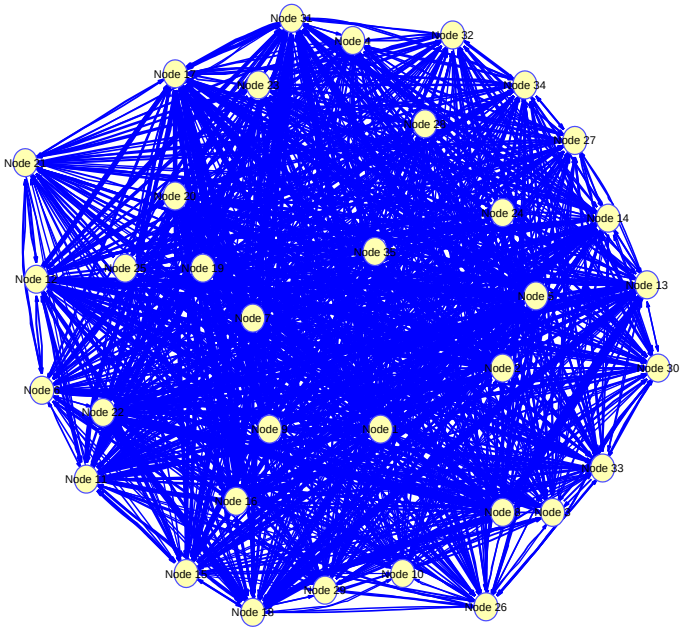

Figure 3.6: An example of NGD procedure computed on the NCD matrix in Fig 3.5 with the 33x33 matrix.

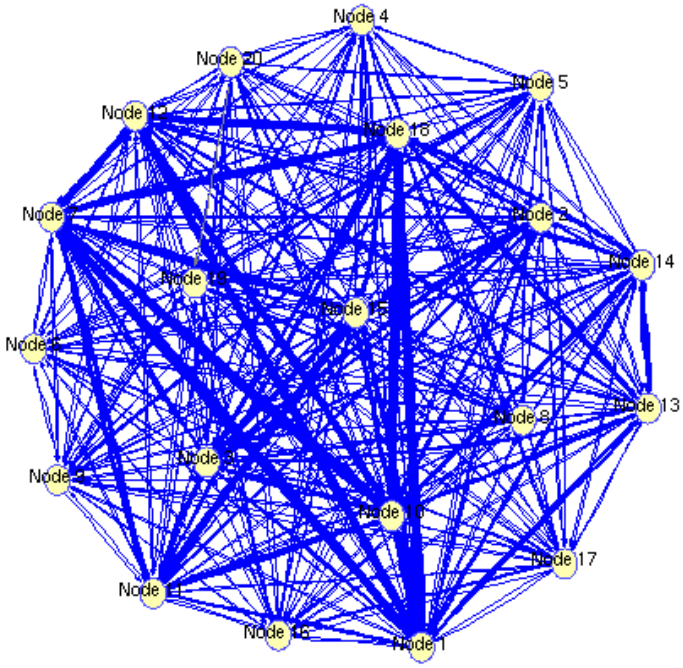

Figure 3.7: An example of NGD procedure computed on the NCD matrix in Fig 3.5. with an extract of 20 cells.

- Hub Nodes Presence: there exist nodes with a high degree.

Robustness emerges from the architecture of these graphs. Simple experiments show that if few edges are randomly deleted in a Small-World Network and in an equivalent random network (same number of nodes and connections) the mean shortest-path between nodes is preserved in the Small-World Network while in the random network the mean length can grow very fast.
Furthermore several results suggest a Small World interpretation (or assumption) of brain networks. From this perspective, some brain network properties hold from microscopic (our subject) to macroscopic point of view (fMRI, PET and other imaging techniques on brain functional areas)[21].

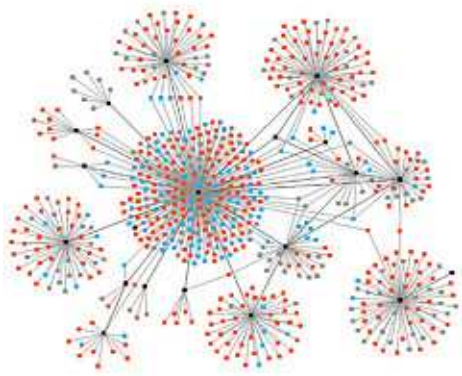

Figure 3.8: An example of small-world network

Figure 3.9: Another example of small-world network

3.6 Graphs, Trees and Statistics

Each of the presented SBCA constructs a VOMM by a tree to estimate the conditional probabilities. The SBCA tree structures can be used to extract features like, for instance, the average tree arity for NE sequences (except for CTW that builds full trees). This endorses special feature of the sequence extracting the *expressiveness* of the recorded neuronal network. Furthermore another VOMM tree feature called High Probability Paths (HPPs) highlights most probable depth-first search paths (according to the highest probability or the probability over a fixed threshold of the children nodes). Using this feature, it is possible to detect neuronal firing modes, such as tonic spiking, intrinsically bursting, etc., nested into SN sequences.

3.7 Modeling Intermittent Chaos

Analyses performed in our lab and several theories on neuronal oscillations show that cortical ongoing activity alternate chaotic and regular behaviors. This evidence suggested to model this peculiar behavior with the intermittent chaos of the logistic map adapting the genetic algorithms by the α value of the logistic parameter. In the following Section I present first, the prepocessing phase of the cortical signals, then I introduce the logistic map and finally the logistic parameter optimization will be shown.

3.7.1 Class Extraction

I define the MxN matrix X. Each element $x_{i,j}$ represents the spike count for the i^{th} unit in the j^{th} time window. I called T the time window duration. Each column $x_{.,j}$ represents the multi unit activity in the j^{th} time window. Whether the temporal sequence $x_{.,j}$ with $j = 1, \ldots, N-k$ and $1 \leq k \ll N$ has regular patterns, then it is possible to predict future activities $x_{.,j+k}$, i.e. $x_{.,j}$ and $x_{.,j+k}$ are correlated in the range of k temporal lags. To make the problem computationally tractable I approximated the sequence $x_{.,j}$, with $j = 1, \ldots, N$ with the symbolic sequence $\{s_j\}$ obtained by clustering the vectors $x_{.,j}$ into a reasonably small number of N_s classes. The procedure is described in details in [115]. In brief I ran the clustering algorithm on the sequence $\{x_{.,j}\}$ for $T = 10\ ms$, $M = 9$. Then I mapped $x_{.,j}$ into the set $C = \{C_1, \ldots, C_{N_s}\}$ obtaining the sequence $\{s_j\}$, $j = 1, \ldots, N$, $s_j \in C$ and $N_s \in \{2, 3, \ldots, 8\}$. I called Activity Class Sequence (ACS) the sequence $\{s_j\}$.

3.7.2 Information Analysis

I assumed that the ACSs were stationary so that $P(s_i = C_n) = P(s_0 = C_n)$ and $P(s_{i+k} = C_n | s_i = C_m) = P(s_k = C_n | s_0 = C_m)$ for $i = 1, \ldots, N-k$ and $n = 1, .., N_s$. I also define $s^0 = \{s_0, \ldots, s_{N-k}\}$ and $s^k = \{s_k, \ldots, s_N\}$. To quantify the temporal autocorrelations I estimated the mutual information between successive states at k lags

$$I(s^0; s^k) = H(s^k) - H(s^k | s^0) \tag{3.19}$$

given the entropy functions

$$H(s^k) = -\sum_{n=1}^{N_s} P(s_i^k = C_n) \log P(s_i^k = C_n) \tag{3.20}$$

$$\begin{aligned} H(s^k|s^0) = \quad & -\sum_{m,n=1}^{N_s} P(s_i^k = C_n, s_i^0 = C_m) \cdot \\ & \cdot \log P(s_i^k = C_n | s_i^0 = C_m) \end{aligned}$$

The estimation of $I(s^0; s^k)$ was corrected by using the quadratic extrapolation [118]. To interpolate $I(s^0; s^k)$ I used the following expression

$$\hat{I}(s^0; s^k) = ae^{-bk} + ce^{-dk} \tag{3.21}$$

I estimated the parameters a, b, c, d through least square optimization by using the Matlab function *lsqcurvefit.m* (The MathWorks, Natick, MA).

3.7.3 Logistic Modeling

To model a class sequence I used the logistic map [79]

$$y_{i+1} = \alpha y_i (1 - y_i) \tag{3.22}$$

and a realization of gaussian white noise ξ distributed as $N(0, \sigma)$. The resulting sequence is

$$z_i = y_{3i} + \xi_{3i} \tag{3.23}$$

and I let α vary in the range $[3.8280, \alpha_c]$ with $\alpha_c = 3.8284271271245$. Because in this region the map exhibits periodic-like cycles of length 3 I built z by extracting one sample every three as shown in equation (3.23). Downsampling preserves chaoticity while in the laminar phase the period changes from 3 to 1. This trick eliminates tiresome long range ripples in autocorrelograms and allows long reiteration of the same class. I divided the z range into N_s intervals so that each interval was associated with a distinct activity state. The size of the interval was adjusted so that the fraction of state occurrence matched the experimental data. I called $I_z(s_0; s_k)$ the temporal autocorrelation function for the z.

3.7.4 Parameter Optimization

Classes tend to reiterate themselves for a while before switching. I called τ_{sw} the distribution of temporal intervals between two successive class switches. Then τ_r and $\hat{\tau}_r$ represent the average residence time within an activity state (i.e. the average over τ_{sw}) estimated, respectively, on the real and on the modeled sequences. I jointly matched $I_z(s_0; s_k)$ with $I(s_0; s_k)$ and $\hat{\tau}_r$ with τ_r by optimizing the parameters (α,σ). For this task I used a genetic algorithm strategy that took as score the average D of the two following distances

$$D_1(\alpha, \sigma) = \frac{\sum_k |I(s_0; s_k) - I_z(s_0; s_k)|}{\sum_k |I(s_0; s_k)|} \tag{3.24}$$

$$D_2(\alpha, \sigma) = \frac{|\tau_r - \hat{\tau}_r|}{\tau_r} \tag{3.25}$$

A candidate solution, constituted by an admissible choice for (α,σ), was defined as a *chromosome*. The algorithm initialization was provided by the random generation of 100 chromosomes that represented the initial offspring. The 5 best chromosomes (lowest D values) constituted the best offspring. The crossover strategy consisted of selecting the 5 worst chromosomes and regenerating them by computing the average of α and σ of random chromosome couples extracted from the 5 best chromosomes. Then an additive random gaussian mutation with zero mean was applied to both parameters in all chromosomes but the best offspring. The stop criteria were either a maximum number of iterations $[200, 1000]$ and a maximum score ($D \geq 10^{-2}$).

Chapter 4

Experiments

To collate a relevant and statistically significant set of electrophysiological recordings is a complex task. Our experiments can be divided in two categories: experiments on cortex and thalamus of rats and experiments on intralaminar thalamus of patients with disorder of consciousness (pdc). Electrophysiological recordings in the rat thalamocortical circuit are introduced in Section 2.1. Technical aspects like anesthesia, preparation and many more require to be also presented.
The experimental animal models used in the labs mimic the originating conditions starting the chronic pain symptomatology. Control animals (CRs) are used to test the results.
The recordings from pdc take part to a project that involves the Pain Neurophysiopathology Labs (National Council of Research, Segrate, Milan, Italy) where I worked out my PhD program, the Department of Neurosurgery (Policlinico San Matteo, Pavia, Italy) and the Institute of Biomedical Technologies (National Council of Research, Segrate, Milan, Italy). The recording were made in five pdc, scheduled to receive Deep Brain Stimulation (DBS) by bilateral implants in intralaminar thalamic nuclei. At present, 3 out of 5 patients have been successfully operated in the period from July 2009 to July 2010.

4.1 Neuropathic Animal models

Peripheral neuropathic pain is a complex syndrome resulting from damage to the peripheral nervous system due to trauma, infection, tumors, immune and methabolic diseases, and other causes. A number of animal models have been reported to simulate human peripheral neuropathic conditions, most of which are based on procedures at or near sciatic nerves. Methods differ in the location and form of injury. We employed three different models for our experiments: the chronic constriction injury model (SC or Bennett [12]), the partial sciatic nerve ligation model (SL or Seltzer [107]) and peripheral inflammatory model (PI) [132].

Animal Preparation

The animals were maintained with regulated 16 hrs light- 8 hrs dark cycles, food and water ad libitum. The rats underwent preliminary barbiturate anesthesia

(50mg/Kg ip) for the surgical experimental preparation. The jugular vein and the trachea were delicately desheated and cannulated to gain, respectively, a drug delivery pathway and the connection to the anaesthesia-ventilation device. The rats were then mounted on a stereotaxic frame and the head was firmly fixed to the frame by usual stereotactical constraints (Narishige, Tokyo, Japan). An electronically regulat ed thermal bed maintained the rat temperature at 37.5 ^{o}C. The scalp was removed and the skull plane was prepared for the placement of both the matrix electrodes and the EEG electrodes. The stereotactical measures were chosen along a stereotactic brain atlas.

Anesthesia

Before the placement of electrodes, the rats were paralyzed by intravenous gallamine thriethiodide (20 mg/kg/h) injection and connected to the respiratory device delivering a gaseous mixture of Isoflurane© (2.5%, 0.4 to 0.8 l/min) and Oxygen (99.9%, 0.15-0.2 l/min) at 1 stroke/s. Curarization was maintained stable throughout the whole experiment by Gallamine thriethiodide refracted injections.

Electroencephalography

The electrodes were fast-implantable/removable skull-surface sliding pins mounted on a fixed support. Five bone embeddings were drilled (to enable a better placement of the 4 recording plus reference EEG electrodes) in fronto-occipital sequence. The stereotactic positions of the EEG derivations were taken using the Bregma as zero point: Frontal cortex Antero-Posterior (AP) +3.0, Medio-Lateral (ML) −2.0; Fronto-Parietal Cortex [Somato-sensory primary Cortex] AP −1, ML −2.5; Mid-Parietal Cortex [Hippocampus] AP −4.3, ML −2.5; Parieto-Occipital AP −10 [Lambda +1], ML −2.0). A conductive EEG paste was placed at each contact to ameliorate the electric coupling. No difference in quality with the traces obtained from classic electroencephalographic recording methods was noticeable.

Surgical Procedure and Stereotaxis

After the removal of the excised bone tiles, the dura mater was delicately removed, under surgical binocular microscope supervision, by the use of eye micro-scissors and forceps.
Each electrode matrix, one for the cortical and the other for the thalamic recordings, was placed into a 3x3 mm^2 hole. The cortical hole (−0.1 to −3 mm AP and 0.1 to 3 mm ML) was drilled over the virtual center of the hind limb cortical projection sensory map (AP +0.3 mm, −2.3 mm; ML −0.1 −3.5) of the SomatoSensory Primary Cortex (SS-I). The cortical matrix was then lowered until layer IV. The thalamic hole was drilled posteriorly (AP −6.0 mm, ML −2.8 mm). The thalamic matrix was then positioned with 25^{o} of postero-anterior slant in order to reach the VL in the VB complex hindlimb projection field at 5200-5500μm. After positioning on the cortical surfaces the matrices were separately advanced in 2μm steps each driven by a separate motor-stepper device (Transvertex, Stockholm, Sweden and Narishige, Tokyo, Japan).

Chronic Constriction Injury Model (SC)

Bennett and Xie reported a rat model of painful peripheral mononeuropathy in 1988 [12]. Along this model the model loosely ties the sciatic nerve (left or right side) with four chromic gut ligatures at the mid-thigh level. SC rats show behavioural signs of spontaneous pain such as mild to moderate autotomy, guarding, excessive licking and limping of ipsilateral hind paw, and avoidance on placing weight on the injured side. Hyperalgesia due to noxious thermal and mechanical stimuli is detectable, as are also cold allodynia and tactile allodynia.

Partial Sciatic Nerve Ligation Model (SL)

In an attempt to simulate causalgia as a result of partial nerve injury in humans, Seltzer and colleagues reported a rat model of neuropathic pain in 1990 [107]. The experimental procedure involves the ligation of the ipsilateral sciatic nerve at the high-thigh level, so that 1/3-1/2 thickness of the sciatic nerve is trapped in the ligature. SL rats exhibit signs of allodynia to von Frey hair stimulation and hyperalgesia to both termal and mechano-noxious stimuli within hours of ligation.

Peripheral Inflammatory Model (PI)

Several studies have used a neuritis model to inflict nerve damage. Freund's adjuvant is injected near the sciatic nerves to cause inflammatory damages. After few hours, allodynia and hyperalgesia are seen instead of thermal hyperalgesia.

4.2 Patients with disorders of consciousness

Extracellular recordings from IL nuclei in coma patients were performed during the surgical session to install a bilateral deep brain stimulators (12h/die, 100Hz, 3mA) [103]. Intrasurgical EEG electrophysiology (three patients GM, MN, SM) consists of two frontal and two occipital electrodes. The neuronal electrophysiology implies recordings by 5 microelectrode channels (FHC, Bowdoinham, ME, USA) with 1 MΩ impedence.
We have recordings the ongoing activity and the neuronal responses during mechano-tactile stimulation or during deep electrical stimulations.

Chapter 5

Implementations

Data collected from electrophysiological recordings are encoded in Neuralynx format (`.Ncs`). These files can be preprocessed using a Matlab routine supplyed by Neuralynx or following the data type specification of the Neuralynx format. In both cases the recorded signal is processed by `Wave_clus` Matlab toolbox for the sorting of spikes. In particluar, I used a modified version of the `Get_spikes_CSC.m` function to perform the spike detection and the `Do_clustering_CSC.m` to clustering the extracted spikes. Thus the original raw signal is converted into a set of temporal binary sequences each of them represents the spike train of a detected neuron.
In this chapter I present some technical aspects concerning the implementation of the methods and the employed programming languages.

5.1 Average Log-Loss Similarity

The average log-loss similarity measure presented in Section 3.4.1 is based on three different VOMM algorithms (PPM, CTW, PST). The PPM and PST algorithms are easy and intuitive to implement. Substantially, they build a single suffix tree and most of their steps are recursive. On the contrary, the implementations of CTW is a very hard task. There exist a couple of open source implementations on the world wide web and one of them is strongly limited by the value that the parameter (K the maximum Markov order allowed) can assume. In 2004 R. Begleiter et al. present a self-contained toolbox written in Java as supporting material of a paper published on the *Journal of Artifical Intelligence Research* that highlights the prediction capabilities of VOMMs based on the state-of-art compression algorithms (PPM, CTW, PST). The toolbox, called `vmm` offers a complete set of Application Program Interface (API) that I used to compute the average log-loss [9].
Modifing original source code, it's been possible to extract tree statistics like HPP and the average tree ariety.
However as I discussed in method Section (see 3), these algorithms are not so fast: notably, the CTW spends large amounts of memory and execution time notwithstanding the numerous implementation tricks to save the memory usage. The Java program execution paradigm based on the bytecode for the Java Virtual Machine delivers worse performances. Finally, in a typical experimental

session, the temporal dependencies expected within a neurophysiological sequence is included into $[50, 500]$ ms. With a 500-bounded source tree, the CTW algorithm, exceeds every computer RAMs.

5.2 NCD Similarity

The computational issues discussed in Section 3.4.1 justify the utilization of less accurate but more computationally efficient Unix compression algorithms like `gzip`, `bzip2`, `lzma`. Furthermore, these implementations are open source and distributed by the General Public License (GPL). Several developed methods work on the NCD matrix that is built computing the NCD similararity between all sequence couples. The NCD matrix computation involves obviously a quadratic number of steps. Therefore the single effective NCD similarity computations must be very fast in practice in order to make the NCD matrix computation feasible. The `vmm` toolbox cannot achieve this requirement.
I therefore developed a computer program in C++ linked with the Unix compression algorithms directly by the source code of the GPL libraries. This allows for optimizing as much as possible the execution time because the compiled binary code doesn't require external library calls (expect for the system calls). In fact, to compute the NCD matrix of 20 minutes experimental sessions with 30-70 recorded neurons, it takes 2-5 minutes and 1.5-2 GB of RAM. A parallel paradigm, for future enhancements, is well-suited to compute the NCD matrix.

5.2.1 NGD routine

To compute the NGD graph (see Section 3.5) I have developed a Matlab function `graphplot` based on the Matlab `biograph` object (Bioinformatics Toolbox). The function `graphplot` requires an adjacent matrix, i.e. the NCD matrix, and automatically displays the edge weights as the thickness of the diplayed graph edges.

Chapter 6

Results

The results obtained with the methods presented in Chapter 3 come (i) from Ventrobasal Thalamic Nuclei (VB) and Somatosensory Cortex (SS-I) in Chronic Pain Animals (CPAs), (ii) from Cortical Ongoing Activity (Primary Visual (V1) and (SSI) in rat Cortices) and, finally, (iii) from IL human Thalamus Nuclei in patients suffering from disordered levels of consciousness like Persistent Vegetative State (PVS) and Minimum Conscious State (MCS). Summarizing:

i Chronic pain (CP) exhibits a large repertory of signs and symptoms. Notwithstanding the large body of studies with different techniques, a core neural construct still remains unidentified. To address the point, animal experiments (20 Control Animals, CR, and 30 Chronic Pain Animals, CPAs, sudivided in three different models) were carried out. Simultaneous electrophysiological extracellular recordings were performed on isoflurane mildly anesthetized rats by two matrix electrodes placed one in the VB complex of the thalamus, the other in the Primary Somatosensory (SS-I) cortex. The aim of the present research was to identify the spiking signatures of CP in the somatosensory Thalamocortical loop. I used diverse techniques ranging from the Normalized Compression Distance (NCD) to the analysis of nonlinear symbolic dynamics are used. CPAs exhibited higher redundancy, estimated by NCD, both in single and multi unit firing patterns. Functional graphs were defined by NCD-based similarity among those patterns. CPAs graphs presented randomlike structures while CR graphs preserved small world properties. From symbolic dynamic analysis, CPAs revealed a reduced number of distinct states. The profound diversities between CR and CPAs suggest a well identifiable neural signature for chronic pain. The main results, coherent across different pain models, are not inferrable from the diverging evidences of imaging techniques. Furthermore these results suggest a potential attribution of CP to a class of neural pathologies called functional connectivity disorders.

ii Cortical Ongoing Activity:

- During the spontaneous activity (SA) of the cortex, peculiar events called *drifts* are distinguishable. Drifts are functional reconfigurations of small population neuron network activity. Drift have primar-

ily been observed in CA3 region of hippocampus [102]. By means of the above report methods (3.4.3) I have been able to extract these phenomena also in primary cortices of rats.

- While a plenty of experiments provided a wide range of results about stimulus evoked activities in primary sensory cortices, the functional role and the dynamics of cortical SA has been by far less largely addressed. From the dynamical perspective, a major open problem is constituted by the evolution of SA, most modeling works tacitly assuming SA activity to be essentially random. The alternative possibility that SA is, at least for a significant part, deterministic, although highly chaotic, did not gain much attention. The problem, by a novel synthetic approach is here below addressed. The first step is the classification of the multi-unit spike patterns into a reasonable number of classes. Through the use of symbolic dynamics the methods described the SA by characterizing their long range correlations and the maximum residence times for a pattern class. The results show that the nonlinear dynamics of a logistic map tuned in the region of Type I Intermittency can be exploited. The methods presented in Section 3.7 applied on recordings taken both from CRs and CPAs found a great variety of behaviors. Some data exhibited complex dynamics. Others were more regular with intermittent-like phases constituted by long reiterations of the same pattern class. By combining a random noisy component with a logistic map, the method could generate class sequences faithfully reproducing the long range correlations and maximum residence times measured on the dataset.
- When a group of neurons emit spikes simultaneously these events are considered synchronized. During microelectrode recordings, absolute synchronies are rarely detected. More frequently, it occurs that groups of spikes may be detected in somewhat large temporal window (20-50 ms). I called, these closly occurring co-activations, Loose Synchronies (LS) in alternative to the previously discussed (absolute synchronies). Using the VOMMs, I studied the predicibility of these events comparing the results with surrogated sequences. Two important facts emerge from this analysis: (i) Ls predictability vary from 10% up to 100% and (ii) the window temporal dependencies ranged in $\{5, \ldots, 15\}$.

iii Disorders of consciousness. Analyzing the SN sequence of IL neurons I found that the bursting states (typical intralaminar neuron behavior) are more lasting in the MCS patient than in PVS patients.

6.1 Chronic Pain

Along its definition in IASP files [75], chronic pain (CP) represents the common perceptual motif accompanying many pathological conditions that exhibit excruciating sensory disorders yet in distinctive modal, magnitude, origin or temporal features [38]. Because of its exceeding complexity, the entangled neural and extra neural substrates generating CP, from the molecular up to the perceptual stage, are, at best, poorly understood, notwithstanding recent important

conceptual advancements [128, 130, 78]. Additionally, at odds with acute pain, CP is not necessarily ignited from the primarily involved body regions that may have been freed by much time now from the pain provoking causes [40]. Whatever these causes, eventually leading to this *dissociation*, a reverberating perception of pain is often the prevalent or sole remnant. The neural counterpart reflecting this complex perceptual state is complementarily composite and often not linearly related to the perceptual signs. For instance, experimental spontaneous pain or allodynia and hyperalgesia are seemingly mirrored, in the neuronal spinal cord, by spontaneous hyperactivity or hyperresponsiveness to related stimuli [47, 113, 88]. Concurrently, strong correlations between spatial patterns of altered brain activity and pain related behavior in rat chronic pain model have also been shown [72]. Comparably, in humans, coherence of activation magnitude with the estimated intensity of pain has been reported in imaging and electrophysiological studies [37, 89, 41]. In contrast, many neuronal recordings and imaging data often showed mutually inconsistent mosaics of brain area activations and inactivations [22, 53]. Thus, neither actual linear intensity coding for having pain is arguable, nor a necessary and sufficient regional arrangement or its potential hierarchy clearly emerge [7, 129]. These questions interlace with general problems of default mode of brain function [92] and on the issuing concepts of functional connectivity and intrinsic hierarchies [126, 111]. All these problems vividly inspire the appraisal of default activity and connectivity in chronic pain [127]. Models of distributed pain representation in the brain, like the Neuromatrix Hypothesis [73] a more recent *integration* theory [5], diversely interpret CP as the result of integrative regional activities active also in resting states. Accompanying anatomical findings showed also reduced gray matter density in CP [3]. These yet well framed backgrounds, however, give no hints on the way the neuronal brain substrates behave in CP. Because it is not the unit activity to be representative of the perceptual complexity of pain, it is however arguable that some feature, a kind of *neural signature*, either in the single neuron or in the network activities may embody markers of spontaneous CP. These results try to clarify some aspects of the problem of neuron dynamics and network behaviours in spontaneous ongoing activity both in control animals (CRs) and in chronic pain animal models (CPAs). Furthermore they try to extend some inference that in CPAs the current spontaneous neuronal dynamics could contain some feature or marker strongly related to the condition itself. Previous results from our lab on spinal cord dorsal horn neurons, simultaneously recorded from superficial and deep laminae, showed that CP induce a disarray of cross-correlations among the two layer neurons [15]. This evidence suggests to explore potential rearrangements in the functional connectivity of the thalamo-cortical axis. To capture and quantify the latent features of those rearrangements, the analyses of ongoing activities in the default mode pose hard challenges, one amongst them the experimental variability due for instance to anesthesia conditions [123, 95].

The set of presented techniques are applied both on single neurons and on small networks. As for single neurons, it is assumed that the neuronal firing patterns may be shared by more cells in the neural ensemble. Each distinct firing pattern may enclose an individual message and distinct firing patterns might be shared by many units. When a number of patterns is shared among units, these would likely convey reduced information because of the message redundancy. The redundancy within a recorded ensemble, is quantified by a measure of similarity

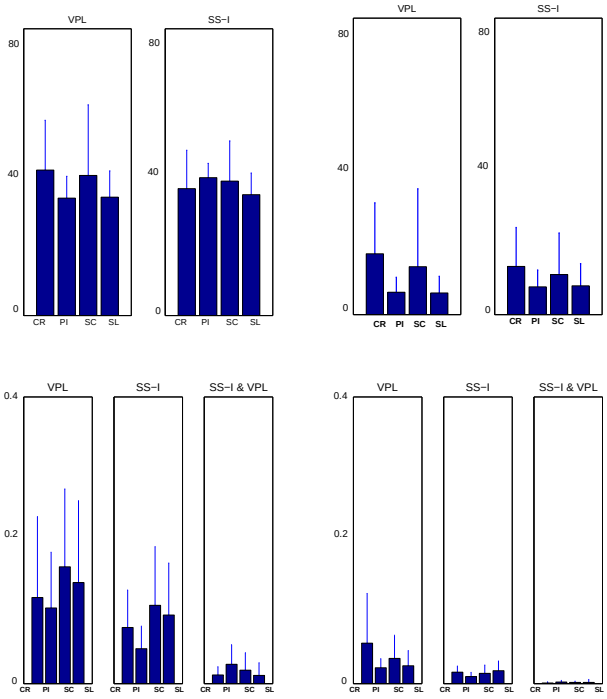

Figure 6.1: Preliminary evidences: Firing rate (above) and Correlation (below) throughout the experimental classes (CR, PI, SC, SL) and the recording sites (VPL and SS-I).

between firing patterns and averaged the results over all possible pattern pairs [10, 28]. CPAs exhibited an increased redundancy that would imply reduced message variety, giving hint for an altered functional connectivity [21]. The neurophysiological and conceptual consequences will be discussed in view of a potential classification of chronic pain in terms of a disconnection syndrome.
To get a preliminary picture of the basic properties of the ongoing activity recordings firing rates and correlations for Units and sorted single cells are estimated (see Figure 6.1). Each recording block lasted 20 minutes and was divided into non-overlapping epochs of 50s. Firing rates were not significantly different between CRs and the CPAs either in thalamus (VPL) or in cortex (SS-I). The correlation coefficients, computed on 10 ms time windows, showed high standard deviations and were about one order magnitude larger in units in comparison with single cells. A comparable intrathalamic or intracortical correlation degree and a collapsed correlation in the VPL-SS-I pair were detected. Again no significant differences were observed between CRs and CPAs. The high variability in firing rate and correlation coefficient was due to major difficulties in keeping the anesthetized animals in comparable conditions. This inter-animal variability, widely acknowledged in the literature [133], exerted major effects on firing rates and correlations on several time scales ranging fron synchrony (1-2ms) to much wider time windows. In spite of careful anesthesia procedures (see 4.1), largely different EEG power spectra were observed 6.2 with bandwidths ranging

from $[0, 4]$ Hz up to $[0, 20]$ Hz. Notwithstanding these drawbacks, isoflurane remains a sound choice as many resting state characteristics, reflective of intrinsic brain organization, are largely preserved at light-mild level of anesthesia like the one used [133].

Anyway, to deal with the above criticalities, subtler techniques less sensitive

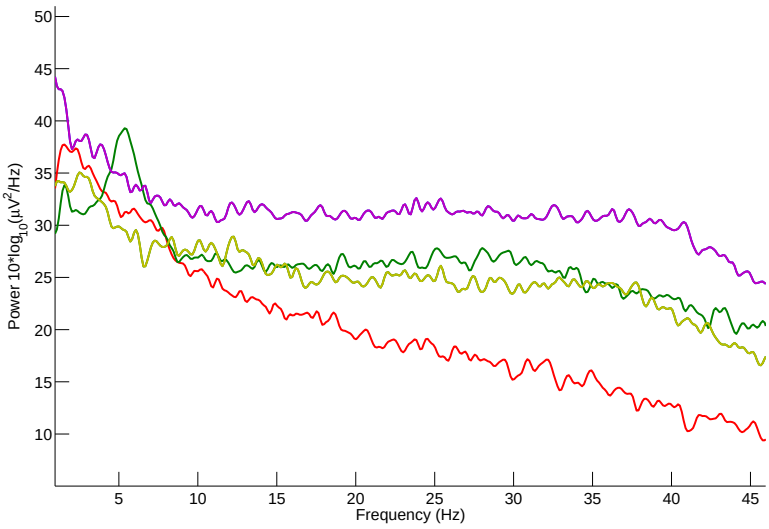

Figure 6.2: EEG power spectra for four different CPAs

to anesthetic states, were required to understand potential markers labelling neural anomalies in CP models. In order to investigate hidden properties like spike train similarities and regular patterns I resorted to the application of the presented techniques.

6.1.1 Single Cell Analyses

I first asked whether the complex activity patterns exhibited by single neurons might be shared by more cells in the neural ensemble. Let's assume that each distinct firing pattern encloses an individual message. Whence shared over many elements, these patterns are likely to convey reduced information because of the message redundancy. To quantify redundancy within a recorded ensemble, a measure of similarity between neurons and averaged the results over all possible pairs are used. Modern compression algorithms capture redundancies in many relevant cases undetected by classical correlation estimates based on 2^{nd} order statistics (e.g. Pearson correlation coefficient).

I therefore chose more sensible methods like NCD (Normalized Compression Distance) that measures symbol sequence similarities. The NCD does not uniquely rely on synchrony and is much less sensitive to altered correlation levels produced by anesthesia. Figure 6.3 displays three raster plots respectively sampled from CR, SL and SC recordings. SC spike trains looks more stereotyped (or redundant) than CR spike trains, these last being more similar to SL. Thus,

as expected, the NCD norms of CR and SL were 20.8% and 5.7% larger than SC. The norm computed on Pearson Standard Correlation coefficient matrix, enables to discriminate only between CR and SC (30%), missing the CR vs SL divergence (0.3% only). I computed the NCD data norms and the results for

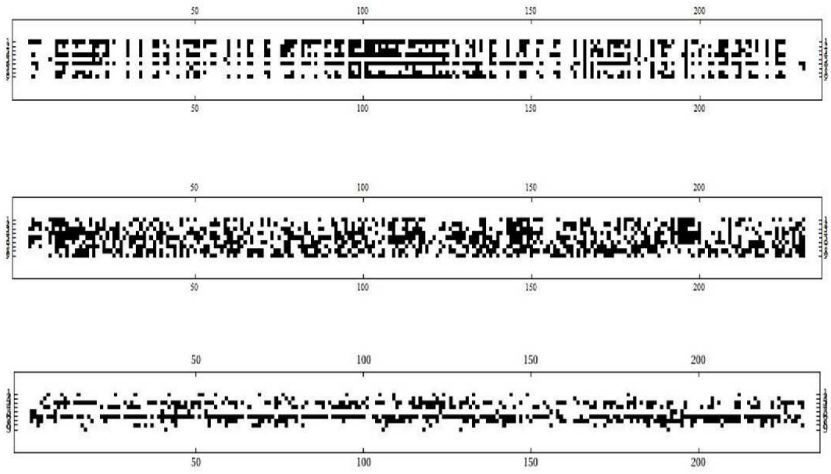

Figure 6.3: Raster plots from (respectively) SC, CR and SL animals.

the whole data set are drew in Fig. 6.4A. In the x and y axes are respectively reported the values for cortical and thalamic neurons. I found that CR and PI exhibited the highest complexity both in VPL and in SS-I although with different magnitudes. The straight line determines the classification of experiments through a supervised learning algorithm, the Support Vector Machine (SVM) with linear kernel (see Methods). The separation between CR and the SC and SL models was significant while there was no separability between CR and PI. The angular coefficient of the separating line is 2/5. Since the inverse tangent of 2/5 is 21.8° it can concluded that VPL accounted for approximately 75% of the whole discrimination.
I then summed-up thalamus and cortex NCD-matrix norms showing an increase of the overall similarity level (i.e. pattern redundancy) in CPAs (Fig. 6.5).
I used Functional Graph Statistics to compute the Node Degree Distribution. Representative functional graphs for the different models are reported in Fig. 6.8. I found, as reported in Fig. 6.9, that CR had a power-law distribution with a heavy tail, SC and SL had a Gaussian-like distribution and PI had a complex binomial-like behavior. This result supports the view of a disrupted functional connectivity altering the CR Small World properties [21, 134], with a label common to CPAs. More in details, CR showed a largest number of cells with low (1-3) and a minor contingent with high (12-16) outgoing connection degrees. PI, SC and SR showed a standard deviation reduction around an intermediate

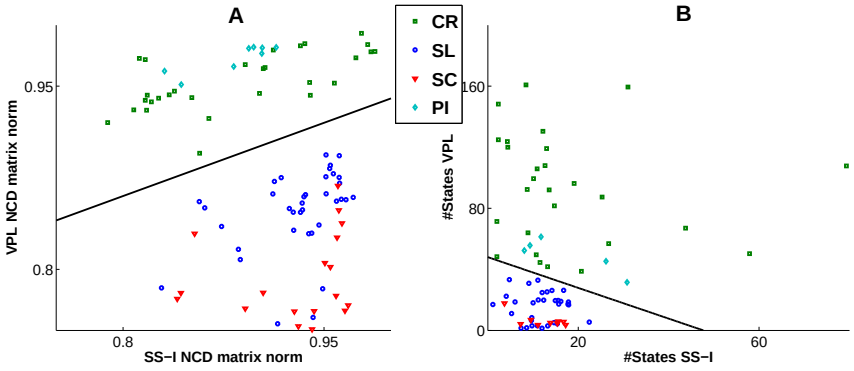

Figure 6.4: (A) NCD Matrix Norms for CR and CPAs experiments. The x- and y-are respectively reported the values of the cortex and the thalamus NCD matrix norm. The straight line represents the classification of experiments through a Support Vector Machine with linear kernel. Different labels reported for each models. (B) Number of distinct Network states on cortex and thalamus axis. Straight line as for (A).

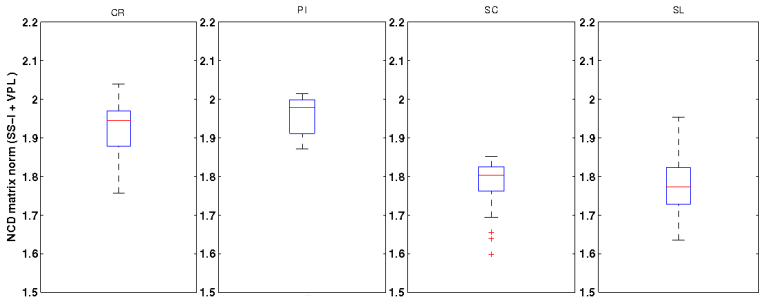

Figure 6.5: NCD matrix norm distribution summed from thalamus and cortex

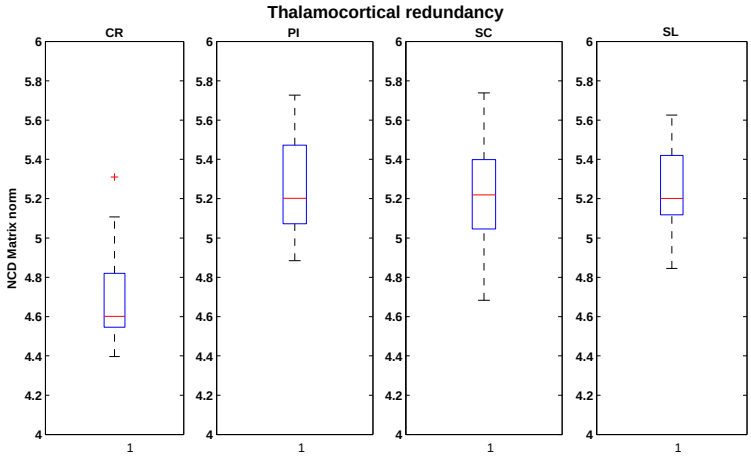

Figure 6.6: Estimated thalamocortical redundancy within the four experimental classes.

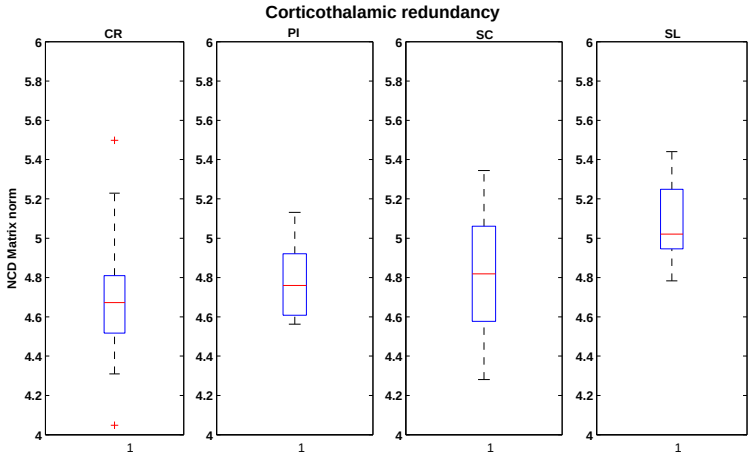

Figure 6.7: Estimated corticothalamic redundancy within the four experimental classes.

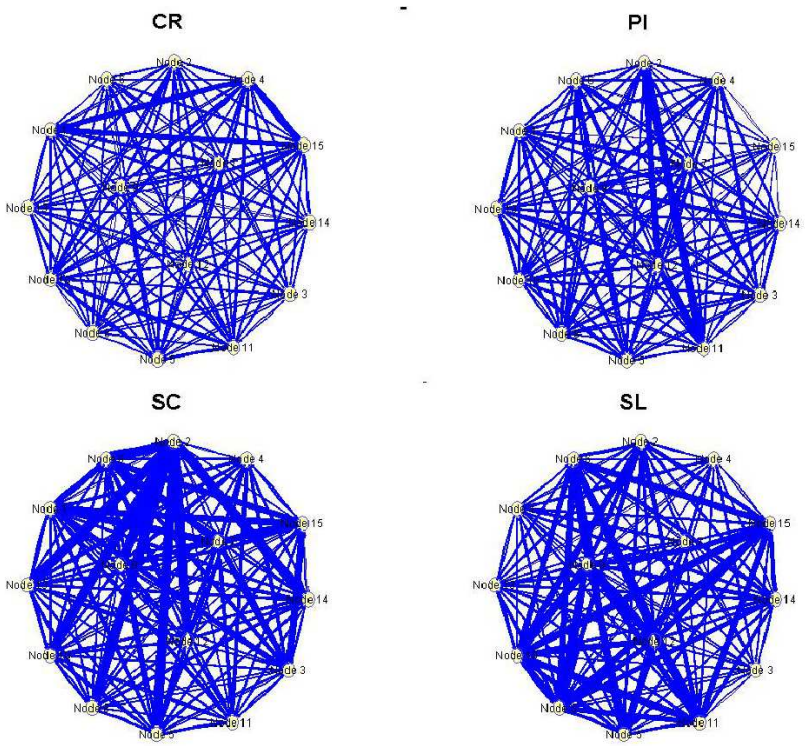

Figure 6.8: Samples of Functional Graphs, respectively from CR, PI, SL and SC.

range (8-12). In addition, analyzing the node distribution tails, where the hub nodes lay, CR graphs display a higher number of hub neurons than PI, SC and SL.

6.1.2 Multiunit Analyses

I estimated the number of distinct network activity configurations. Each configuration are called Multi Unit Spike Pattern (MUSP). MUSPs were constructed over the spiking rasters of the recorded neuronal ensembles. A MUSP is a vector where each single value represents the spike count of a unit in a time window of width T. Because of the stereotyped activity exhibited by single neurons in CP conditions, I investigated if, at higher level of observation, also the variability expressed by small networks, captured by MUSPs, was affected in CP. I first set $T = 1$ms and counted the number of distinct MUSPs in each recording. I found that CR and PI expressed a more ample repertory of distinct MUSPs (Fig. 6.4B). Following the previously adopted SVM separation method, I obtained that the cortex accounted for 45% and thalamus for 55% on the separation line.

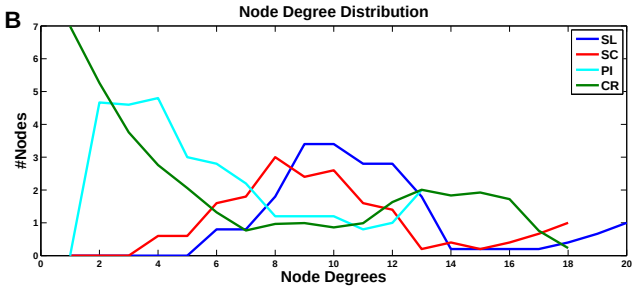

Figure 6.9: The mean node degree distributions computed on the whole experimental dataset.

6.1.3 Discussion

One of the most impressive features of chronic pain is the wide-distributed origin of its causal agents. A chronic or persistent pain can be originated by traumatic events, degenerative diseases, oncologic pathologies, inflammation, hypoxia or peripheral neuropathies [75]. Though all of these pathological conditions have diverse physical, biochemical, neural and metabolic *cores*, the common perceptual label is seemingly that of pain. At most, in the neuropsychological context there's a most wide semantic refinement of sensory, affective, qualitative or synaesthesic features accompanied, for instance, by metaphoric (like burning, gnawing, stabbing) or temporally defined (persistent, wax-and-waning) terms [90]. Despite the semantic variations, the basic issue is indeed dominated by a seemingly routinary pain perception.
The results show that SC and SL chronic pain models increase redundancy in single unit spiking patterns, decrease the number of distinct network states (or Multiunit Spike Patterns, MUSPs), constrain and regularize the network dynamics and trigger redistributions of activity within the local networks. PI models, not yet established as CP states, exhibit neural features laying in between the CR and the CPAs models. This suggests that any model has somewhat a clear expression and that all the models together, and each by itself, create dynamical conditions rarely or never visited by the system in normal conditions. Each pain model appears to replicate, preferably keeping on a thalamocortical (TC) loop district. The different neural pictures contrast with the gross perceptual homogeneity assessed during behavioral tests [14]. This mismatch suggests that potentially diverse agents may convey comparable percepts. The choice of the TC loop is far to be complete in comparison to the whole network in spontaneous ongoing activity, as obvious, but it spots on the main axis of most sensory processes. In addition it focuses a crucial engine of the pain neuromatrix [73]. The importance of the TC loop is further supported in the literature by most different experimental and clinical approaches [57, 109] showing, for instance, that important features of dysrhythmic thalamocortical dynamics can account for several pathological states from psychosis to neurogenic pain [68]. The analysis provides quantitative indices to sketch an objective description of the network connectivity and its derangements, avoiding ambiguities based on controverse clinical experimental appraisals. No electrophysiological study at the neuronal level has been made in long lasting spontaneous brain recordings in models of CP.

In CP models, most elementary labels of the spontaneous neuronal activity like increased anomalous discharge frequency [113], sustained wind-up, activity dependent plasticity disorders and receptor potentiation have been profusely described and exhibited stereotyped neuronal classes in the spinal cord [36, 73, 120, 101, 34]. The preliminary results, instead, no significant difference was recognized in terms of firing rates and of correlation coefficients in the TC loop, in the intrathalamic or the intracortical circuits.
The main analyses explored the active configurations of spiking neurons in spontaneous activity patterns of single cells and small populations. The single cell firing patterns were not unique or specific for a particular neuron but were also consistently replayed by other cells, indicating a certain degree of redundancy. TC dysrhytmia in neurogenic pain exhibited increased coherence within the theta-beta EEG bands [68], a higher spectral power over the frequency range of 2-25 Hz and a shifted dominant peak towards lower frequencies [100]. These results are reasonably consistent with the redundancy in single cell patterns and in the number of distinct MUSPs that was previously observed. These functional anomalies, out of the CPAs seem largely independent from the background EEG spectral composition and, allegedly, from the anesthesia level. In fact, the MUSP variability was observable in the presence of widely different EEG patterns. Many works showed how brain functional networks are charachterized by Small World properties. These properties represent a kind of label related to normal and activated states or to pathological states [21]. I extended a previous approach on neuronal firing connectivity [142] to define functional relationships between neurons, relying on the assumption that similar firing patterns are the result of significant functional relationships. In experiments, the functional graph degree distribution highlighted a substantial rearrangement of the distribution of outward node degrees in the functional graphs. In fact, CPAs had strongly random functional graphs, in comparison to the standard Small World graph encountered in CR animals. Matching results reported in psychiatric and degenerative disorders suggested that functional disconnection might provide a unifying conceptual substrate [24]. Disconnection in the present context does not mean an anatomical disengagement of fibres but altered functional graph architectures. The current knowledge is insufficient to identify a minimal neural correlate for pain perception. The extension and the amount of the TC connection disorders would represent a part of the neural features of chronic pain representing a fragment of a minimal neural configuration for pain.
A contiguity or a parallelism (if not a dependence) may be thus hypothesized between some neural and perceptual states. In fact, in CPAs I measured a substantial redundancy both in the repertory of distinct firing patterns and in their temporal evolution. The redundancy increase may be interpreted either as an emphasis of the relevant core of the message (e.g. pain, per se) or as a loss of system plasticity (at the neuronal and at the network level) compromising the local information flow. Because of the scarcely evolutionary relevance of a chronic pain [139], the positive hypothesis of message repetition seems unlikely. The alternative hypothesis of a pathological sequence of events related to property loss appears therefore preferable. Rich array of neuronal configurations of CR animals can be explained by a major adaptability or plasticity, lost in CPAs, on the simultaneous converging inputs. These results may also explain data in the literature showing that cortical or subcortical stimulations effectively reduce the perception of intractable pains [66, 67, 63]. The delivery

of a timed input could in fact rearrange the disordered networks returning some level of plasticity. Furthermore, chronic pain represents a stereotyped condition corresponding to representations of different neural events and conditions. Further electrophysiological investigations are needed to explore the complex dynamics of neural activity in CP as the very substrate of perceptual events. From a clinical point of view, they may open new potential therapeutical paths based on opportunely tuned stimulations of specific brain areas associated or not with pharmacological approaches.

6.2 Cortical Ongoing Activity

The brain is spontaneously active even in the absence of external input. This ongoing background activity impacts on neural information processing. Most neuroscience studies have focused on brain responses to task or stimulus. However, the brain is very active even in the absence of explicit input or output. Research on spontaneous activity led to the hypothesis that specific brain regions constitute a network supporting a default mode of brain functioning [42]. Spontaneous activity might be informative regarding the current mental state of the person (e.g. wakefulness, alertness) and is often used in sleep research. Certain types of oscillatory activity, such as alpha waves, are part of spontaneous activity.
The following results investigated the nature of the spontaneous activity in rat primary cortices. Primarily, the presence of drifts (activity reconfigurations within neuronal ensembles) is studied. Then I asked whether their presence is linked to other cortical events such as motif repetitions with neuronal synchronizations [54] or intermittent chaotical behaviors [136]. For the former question, I studied the predicibility of high-order events of collective synchrony within a neuronal ensemble from cortical spontaneous activity in rats. For the latter question, I built a model based on the intermittent chaos of the logistic map in specific parameter range using evolutionary strategies (i.e., genetic algorithms). The existence of such models, able to reproduce some cortical events, enlighted important aspects about the intrinsic mechanisms of cortices.

6.2.1 Drifts

A further result came from the study of specific NE activations, captured from ongoing recordings (drifts) [54, 102] observed in primary cortices, for the first time in our lab. In these findings, we suggest that the network states are metastable, rather than multistable, and might be governed by local attractor-like dynamics. Drifts behave like transient co-activations of NEs spread over the populations identified by the recording electrodes. Drift-like patterns had been already observed in different experimental conditions in other cortical structures like the hippocampus, a region involved in complex tasks like learning and memory. In particular, I investigated their presence in primary V1 and SS-I cortices. Studying the evolution of the average log-loss in inter-stage NE sequences from those cortical areas, I found the stationary phase changes (e.g., see Figures 6.10-6.11) correlated with the occurrence of drift phenomena recognized with the NGD procedure that shows significant differences in the functional graphs just before or after a drift occurrence (see Figures 6.12-6.13). The method

works automatically, evaluating the distance between the NCD matrix of candidate windows (i.e., that potentially contain drifts). In fact, in the perspective of an attractor-like dynamic, the attractor changes produce an alteration of the predicibility (measured via the average log-loss) in contiguous time window. The method I developed is more direct and efficient than the synfire chain-based methods [54]. As presented in Section 3.4.3,

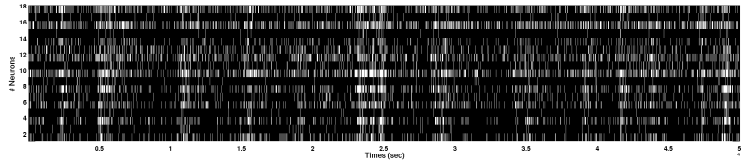

Figure 6.10: Stationarity analysis of NE sequence with eighteen neurons for 50 seconds. In the raster plot of the NE sequence the white cells represent spikes.

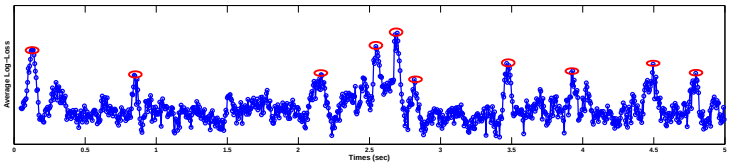

Figure 6.11: The average log-loss computed on overlapping windows on NE sequence in Figure 6.10. High predicibility regions (i.e., low values of average log-loss) correspond to weak synchrony of the ensemble. Note the peaks evidenced by red ellipses.

In the work of Ikegaya et al. [54], the network reconfigurations are considered as spatial rearrangements of activity. These collective events are detected computing the covariance (and other basical statistical techniques) of spike activities in short temporal windows. This approach requires a supercomputer because its computational cost, while the average log-loss method can run on desktop PC and requires only few minutes to detect a significative changing of stationary phase and to check whether a drift took place. Moreover, drifts are detected from a high level perspective. In fact, the NGD procedure computes the functional graph of NE so that the results are based on significant activity features according to the method used in [102] that employs the principal component analysis of NE activity.

6.2.2 Intermittent Chaos in Spontaneous Cortical Activity

Until now the vast majority of experimental works on sensory processing has been focused on evoked activity. In the last decades the development of intracellular and multi-unit extracellular recordings allowed experimenters to characterize the neuronal receptive fields in primary sensory cortices of the diverse sensory systems [94, 84]. In these areas spontaneously arising action potentials account for a substantial fraction of the overall firing activity, their functional

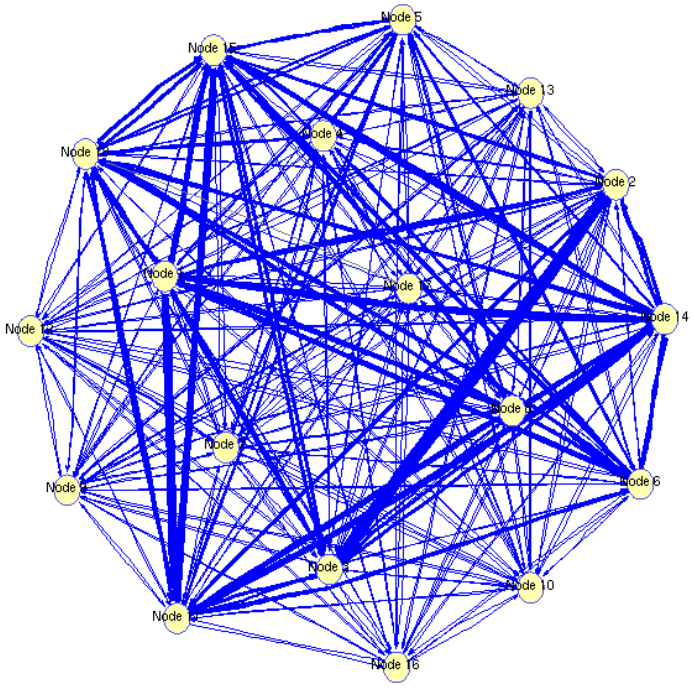

Figure 6.12: The Neural Group Discovery procedures applied to the SN sequences at the window before the first drift.

significance is not understood. Although the ongoing activity in primary cortices has been poorly addressed several works in the sensory spinal cord described significant changes of both ongoing and evoked activities. In particular, beyond the activity changes in the discharge profiles of single neurons, correlations between neurons in superficial and deep laminae collapsed in chronic pain models [15]. Because in chronic pain spontaneous activity perturbations occur along with receptive field modifications [77], spontaneous activity is likely to interfere with sensory processing.
Neural activity is sparse and, probably under the action of energy saver mechanisms [17], only a fraction of cells are significantly activated at the same time. Within local assemblies, neurons arrange highly connected networks and provide a vast array of collective behaviors, the onset and fading of specific activity states among the most relevant. It has been suggested that such configurations could occasionally evolve in non-random fashion and follow regular dynamics [32, 71]. The intertwined nature of random and deterministic dynamics driving the configurations poses an implicit question of their respective contributions to the overall event. Separating the random from the deterministic could shed some light on the self-organizing behavior of cortical neuron assemblies. The interplay between ordered and random drive is critical, the first allowing for faithful representations and propagation of inner states, the second for the assembly activity to evolve and adapt. From non-linear analysis it is well known that a number of systems on the edge of chaos exhibit an intermittent regime

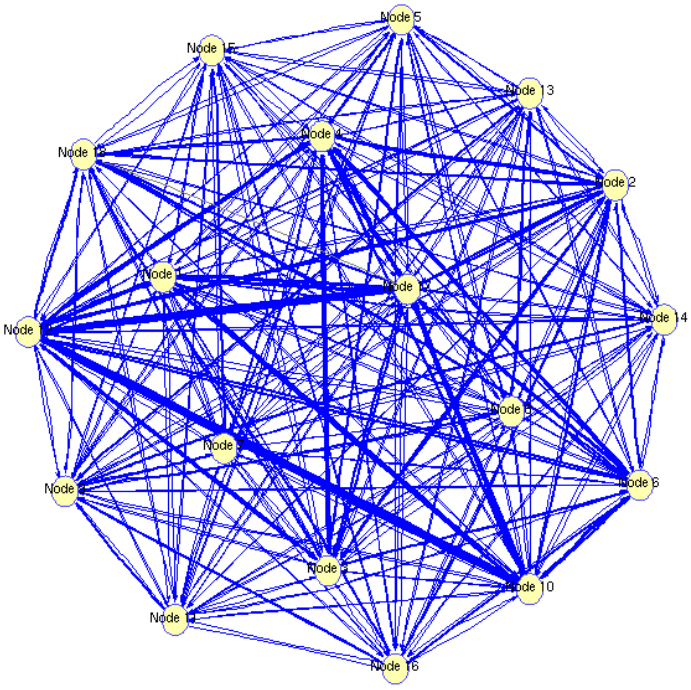

Figure 6.13: The Neural Group Discovery procedures applied to the SN sequences at the windows just after the first drift. Notwithstanding the same neurons involved, the similarity weights distribution is very different.

where relatively regular phases interleave with highly chaotic and unpredictable bursts [87]. Even a simple mono-dimensional, time-discrete system such as the logistic map can express two diverse intermittent behaviors defined as Type I intermittency and crisis-induced intermittency [79]. I tried to apply the previous strategy to data collected from multi-unit extracellular recordings of SS-I cortex. Earlier results showed that, in the same brain region, the residence time in an activity state is longer than expected by chance [115]. Other authors obtained matching outcomes in the hippocampal CA3 layer [102]. Together, these evidences could indicate the presence of intermittent regular behavior. This results show, as first, that the evolution of cell assembly dynamics is significantly constrained by long-range correlation. It is been found that the decay of temporal autocorrelations, quantified by Shannon Information, can be described by the sum of a slow and a fast exponential function, accounting for fast and slow decays respectively at short and long delays. Then the logistic maps to generate symbolic sequences are used, each symbol being associated with a distinct activity state of a cell assembly. Setting the logistic parameter in the neighboring of Type I intermittency the results show a variety of long range correlation profiles. Although the main result exhibits that it is possible to classify and model the experimentally extracted long range correlations between activity states by exploiting the Type I intermittency of a logistic map. In this stage, no spike sorting procedure was applied so that more than one cell could be present in a

single unit. Given standard impedance value (1 $M\Omega$) and the relatively large electrode spacing (150 μm) no spike occurrence was detected by more than one electrode. The resulting picture was constituted by 9 neuron clusters. Only recordings where all nine electrodes revealed a substantial presence of spikes were selected for analyses. Further details are provided in [115]. For a multi-unit recording of spontaneous activity the number of all possible activity states grows exponentially with the number of cells and quickly goes out of control. Accordingly I preprocessed our data by a clustering algorithm in order to identify a reasonable number of activity classes (see 3). In Figure 6.14(B,C) it's reported the result of a clustering (data obtained from an SL animal). Note how chaotic phases interleave with more regular ACSs chunks constituted by long repetitions of the same activity class. Compare the clustering sequence of Figure 6.14(B) with a randomly permuted version in Figure 6.14(C): the intermittent behavior disappeared in the latter and the same chaotic regime was maintained along the sequence. I first described, on the whole dataset of 94 recordings, the dynamics of multi-unit activity by estimating the temporal autocorrelation of the activity class sequences (ACSs) and fitting it with a sum of exponentials (6.2.2). Then the four representative recordings are selected and I modeled the ACSs by combining a logistic map and a random noise. The real and modeled ACSs are compared by estimating the temporal autocorrelation (6.2.2) and the average residence time (6.2.2). The optimal values for α and σ were estimated by using a genetic algorithm. The $I(s_0; s_k)$ and τ_r are called respectively the temporal autocorrelations and the average residence time for activity classes. The scoring function of the algorithm took into account both the distance between the autocorrelation functions, $I(s_0; s_k)$ and $\hat{I}(s_0; s_k)$, and the distance between average residence times, τ_r and $\hat{\tau}_r$. The distances and the overall scores are reported in Table in 6.2.2. For further details see the Section 3.7.

	SL1	SL2	CR1	CR2
D1	0.2011	0.3387	0.7171	0.2845
D2	0.0455	0.0306	0.0124	0.1170
Score	0.1233	0.1847	0.3647	0.2007

Long range correlations of cell assemblies

To quantify the temporal correlations among successive activity classes I computed the Shannon Information $I(s_0; s_k)$ for each lag $k \in \{1, 2, \ldots, 100\}$. The time window duration in which I sampled each state was set at 10 ms and I recorded blocks of 50 s in order to obtain ACSs of 5000 elements. I fitted $I(s_0; s_k)$ with a weighted sum of exponential functions following the expression (3). A representative case in Figure 6.15(A,B) is draw. The first exponential accounted for the fast initial decay at low k values while the second explained the slower decreasing trend at higher k values. In 6.15(C) is reported the distribution of the coefficients a and c. The fast time constant b is larger than the slow time constant c and a is 73% larger than c. The latter result indicates that the fast exponential function had a larger weight in the fitting.

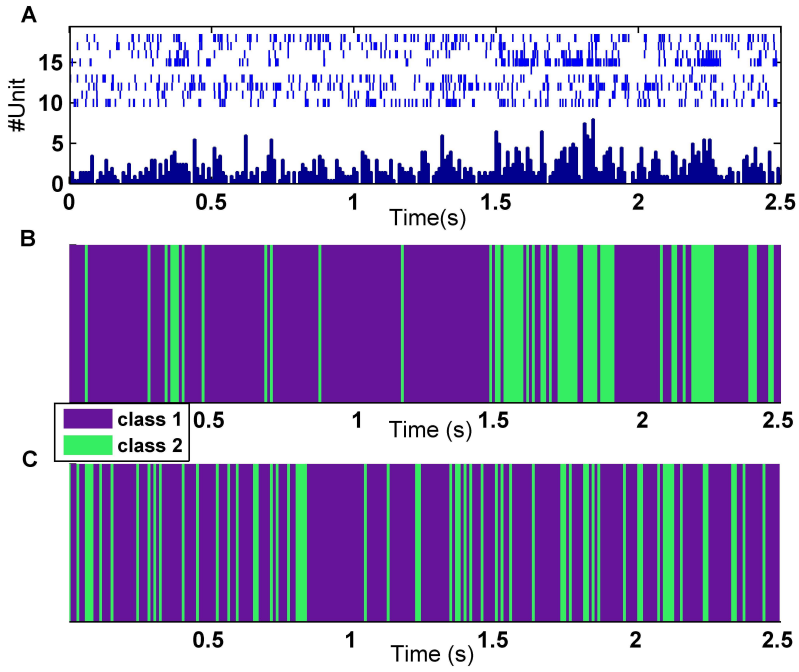

Figure 6.14: Classification of multi-unit activity. A) Sample activity of 5 s duration extracted from a 50 s recording from SL1. The cumulative spike count in 10 ms bins is drawn at the bottom. B) ACS obtained from the data. C) Randomly permuted ACS.

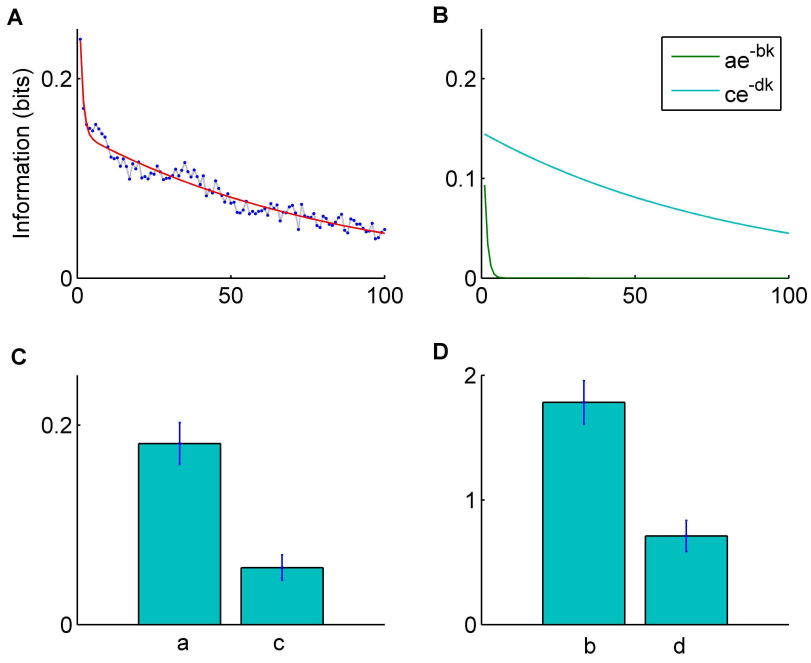

Figure 6.15: Interpolation of $I(s_0; s_k)$ for SL1. A) Model fitting for the estimated $I(s_0; s_k)$. B) The two exponential functions summed to obtain the fitting function. C) Average and standard error for coefficients a and c. D) Average and standard error for coefficients b and d.

Model fitting for the temporal autocorrelation

I investigated the possibility of using a subsequence z of the logistic map with additive noise (see Equations 3.21,3.22) to generate ACSs that matched the temporal autocorrelation $I(s_0; s_k)$ measured on the data. By setting α in a periodic region, $I_z(s_0; s_k)$ approached a constant whose value was determined by the noise level σ (Figure 6.16A,B). Conversely, when I selected an α value associated with a highly chaotic regime, $I_z(s_0; s_k)$ was negligible or null for any positive k (Figure 6.16C,D). It was interesting to find an α range for which the behavior of $I_z(s_0; s_k)$ landed in between these extremes. I selected the region just before α_c value at which the saddle-node bifurcation occurs. In this region a regular behavior was interrupted by chaotic bursts and the average duration of an inter-burst interval for the logistic sequence y scales as $(\alpha_c - \alpha)^{-1/2}$ [87]. Because after a burst the state of z became unpredictable from the pre-burst states, the duration of laminar phases constituted the critical parameter that shaped the temporal autocorrelation $I_z(s_0; s_k)$. For α approaching α_c I could obtain $I_z(s_0; s_k)$ with an arbitrarily slow decay. While the shape of $I_z(s_0; s_k)$ was mainly determined by α, the parameter σ accounted for the stochastic component that affected the gain of $I_z(s_0; s_k)$ and the class predictability within the laminar phases as in Figure 6.16E,F. In Figure 6.17 I report the results from 4 recordings (2 on SL models, Figure 6.17(A,B) and 2 on CR, Figure 6.17(C,D). The former recordings exhibited significantly larger $I_z(s_0; s_k)$ for the whole range $k \in \{1, \ldots, 100\}$ (blu lines). The z sequences that it's been generated could fit the data reasonably well in all cases (red lines). For comparison I also draw the temporal autocorrelation estimated with a Markov Chain (Figure 6.17, green lines). The much faster autocorrelation decay iss inappropriate to model long range constraints on ACSs. The percentage distances (D1) between $I(s_0; s_k)$ and $\hat{I}(s_0; s_k)$ are reported in the first row of Table in 6.2.2.

Model fitting for the residence times

Previously it's been observed from Figure 6.14 the significant occurrence of regular phases constituted of reiteration of the same class. The duration of laminar phases for the logistic map increases, as approached with these methods, the critical parameter value α_c. It is shown that the largest residence time corresponds to the inverse of the distance between Lorenz lines in the low frequency region of the power spectrum [110]. I found a similar behavior for the subsequence z (Figure 6.18A,C), discernible even $\sigma > 0$ and the sequence is corrupted by a moderated level of noise ($\sigma = 0.3$), slightly larger than the one it's used to model the ACSs. To compare real and modeled ACSs the distribution of τ_{sw} representing the intervals between two successive class switches are estimated. I found on the modeled ACSs that the maximum residence time was highly variable across different realizations associated with the same parameters (α, σ), even for ACSs extending up to 200000 iterations. Instead I selected the average residence time τ_r that was far more stable. I normalized τ_r with τ_r^* by applying the following formula:

$$\tau_r^{norm} = \frac{\tau_r - \tau_r^*}{\tau_r^*} \tag{6.1}$$

where τ_r^* is the average value computed on the randomly permuted class sequence. All data exhibited positive τ_r^{norm} values, indicating that residence times

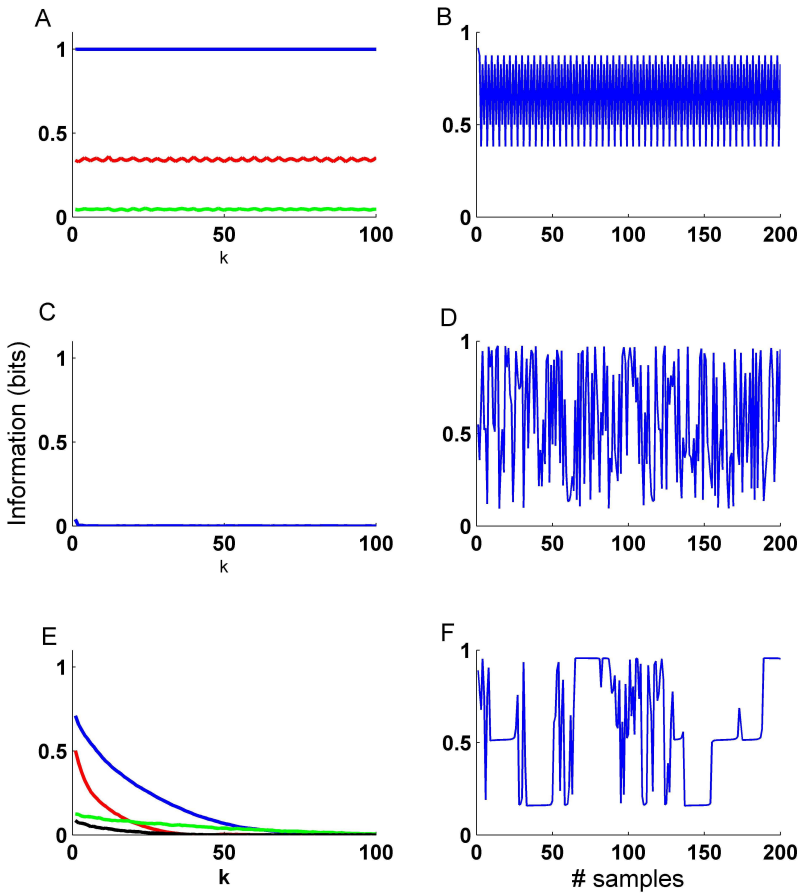

Figure 6.16: Tuning the parameters α and σ within the Type I intermittency region. A) Autocorrelation $I_z(s_0; s_k)$ computed for $\alpha = 3.5$ and $\sigma = \{0, 0.15, 0.3\}$ (respectively blue, red and green line). B) Sample of 200 iterations from z sequence ($\alpha = 3.5$, $\sigma = 0$) C) Autocorrelation $I_z(s_0; s_k)$ computed for $\alpha = 3.9$ and $\sigma = 0$. D) Sample of 200 iterations from z sequence ($\alpha = 3.9$, $\sigma = 0$). E) Autocorrelation $I_z(s_0; s_k)$ computed for $\alpha = 3.82842$ (blue and green lines for $\sigma = 0$ and $\sigma = 0.3$) and for $\alpha = 3.82835$ (red and black lines for $\sigma = 0$ and $\sigma = 0.3$). F) Sample of 200 iterations from z sequence ($\alpha = 3.82835$, $\sigma = 0$)

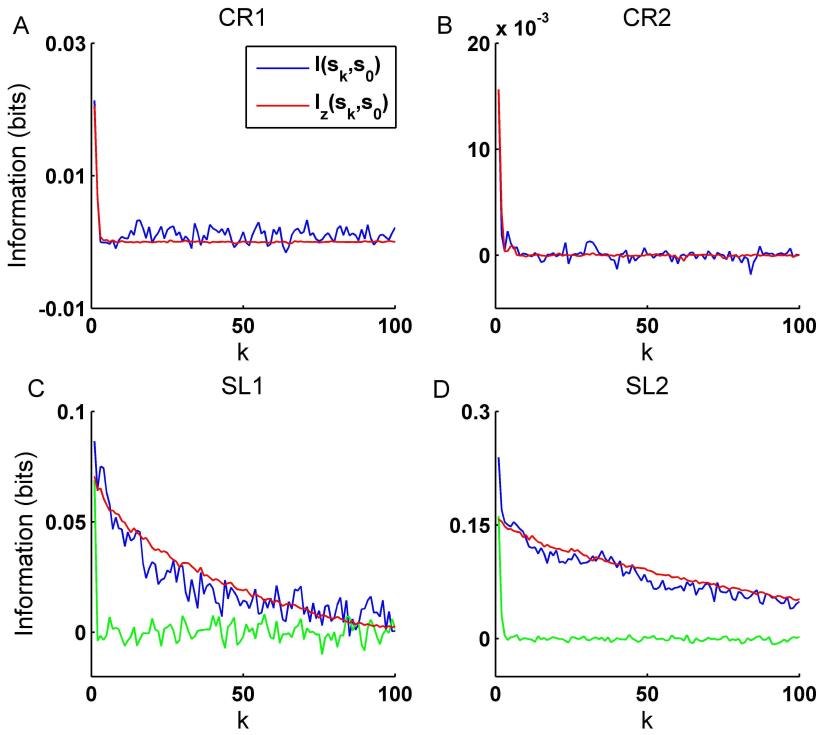

Figure 6.17: Temporal autocorrelation $I(s_0; s_k)$ and $I_z(s_0; s_k)$ estimated on the data (blue lines) and on the modeled ACSs (red lines) for CR1,CR2,SL1,SL2 (respectively A,B,C,D). Green lines in C,D indicates autocorrelations for markov chain models estimated on the data.

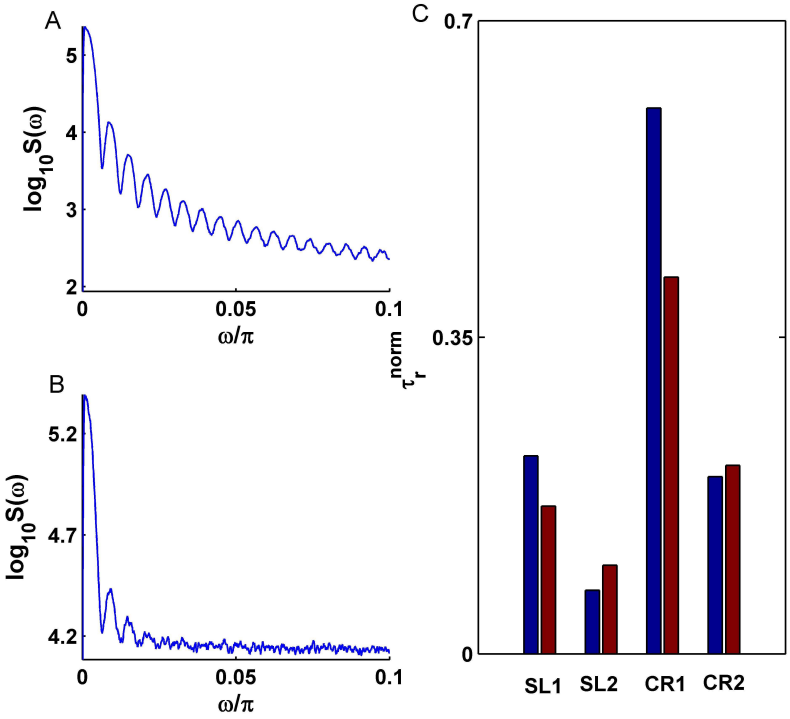

Figure 6.18: Model fitting evaluation for residence times. A) The inverse of the peak distance in the frequency spectrum indicates a well defined maximum residence time for a z sequence ($\alpha = 3.82824$,$\sigma = 0$). B) The peaks emerge even in presence of noise ($\sigma = 0.3$) C) Residence coefficient τ_r^{norm} from data (blu bars) and modeled ACSs (red bars)

are on average longer than expected by chance (Figure 6.18B, blue bars). The modeled ACS expressed the same property and the τ_r^{norm} values are proportional to the ones measured on the data (Figure 6.18B, red bars). The fractional distance (D2) between τ_r and $\hat{\tau}_r$ are reported in the second row of Table in 6.2.2.

Discussion

These results concern the spontaneous population dynamics of cortical ensembles. I first applied a recently developed approach to classify multi-unit activity states [115] and then I studied the population activity through the analysis of the associated activity class sequence (ACS). The results show that ACSs exhibited intermittent behavior characterized by regular phases composed of long reiteration of the same activity class and by highly chaotic bursts.
Long range temporal autocorrelation on ACSs are estimated by using the Shannon Information. Autocorrelation decayed monotonically at increasing delays and is well fitted by the sum of a fast and a slow exponential function. Logistic map tunes at the edge of Type I intermittency the ACSs obtained from the data. The temporal autocorrelation of the sequences generated by the map, after opportune parameter optimization, matched the ones estimated on the data. To confirm the intuition that long range correlations in the experimental ACSs were accounted by class reiteration I estimated the relation between residence time in a class for the data and for the logistic map-based model.
At the present, this is the first time a partially deterministic modeling of cortical dynamics is tempted, previous approaches being entirely stochastic [43, 2]. Type I intermittency of the logistic map was used in biological science to model heart rate variability and blood flow in arteries [145, 83] while, in computational linguistics, tuned at the Feigenbaum point, the map was used to simulate language-like processes [35]. This modeling is supported by previous results where it is showed that activity class tend to reiterate themselves more than expected by chance. Sasaki and coworkers reported that CA3 ensembles undergo metastable states with long residence times [102]. *In vivo*, by recording from spinal cord neurons, the Lévy index appeared able to discriminate between modalities of different noxious stimuli both in normal and injured animals [16]. Other authors found, *in vitro*, that the temporal sequence of network activation exhibits long range correlation and scale-invariant Levy distributions [106].
The utility of this approach is dual. From one hand the association with the logistic parameter α and a random component σ can provide a useful classification of the ongoing dynamics. As it showed such dynamics are highly variable both in normal and pathological conditions. From the other would provide a useful tool for simulating biologically plausible background activity in computational models of neural coding.

6.2.3 Predictability of Higher order Synchrony

The previous results show how the cerebral cortex exhibits highly complex dynamic regimes during spontaneous activity. A plethora of parameters were tried to capture this complexity focusing on different features. One of the most relevant, showed by the spontaneously running cortical networks, is represented by synchronies. While the instantaneous higher order interactions (that incorpo-

rate also higher order synchronies) have been well described by weak pairwise correlations [104], their temporal dynamics has not yet been thoroughly analyzed. A previous work shows that multiunit firing activity exhibits intermittent chaotic behavior [117]. I therefore focused on predictability of higher order loose synchronies (LSs), i.e. firing events jointly occurring within 30-50ms temporal windows. I analyzed extracellular simultaneous multiple recordings of spontaneously active SS-I cortex.
I first developed a statistical method based on a hypothesis test combined to a data clustering to extract and classify synchronous and non-synchronous events. The resulting symbolic sequence represents the multiunit spiking activity where some symbols are associated with LSs and others with non-synchronous events. I approximated the Kolmogorov complexity of these sequences within fixed length sliding windows by the compressed sequence length (CSL) computed with a set of Unix compressors (zip, gzip, bzip2) [10]. On comparing the real sequences (RS) with surrogate sequences obtained through random permutations, I found long strings of significantly low CLS regions in comparison with the surrogated sequences (SS) (Figure 6.19A). The rate of LS occurrences showed high positive correlation with CLS values. LS predictability was analyzed with Variable Order Markov Model techniques estimating both short and long range sequence dependencies [9]. I found that the LSs in RS were 10 to 100% more predictable than LSs in SS and that only the last 5 to 15 symbols were relevant for prediction (Figure 6.19B). Unexpectedly, the rate of correct LS predictions wasn't significantly correlated with CLS. Finally, the rate of LS prediction and the rate of LS occurrence resulted positively correlated. These results deliver important cues on the events leading to the occurrence of LS. The high predictability variability suggests that the cortical LSs may potentially endorse diverse tasks merged in the shared functional state of spontaneous activity [146].

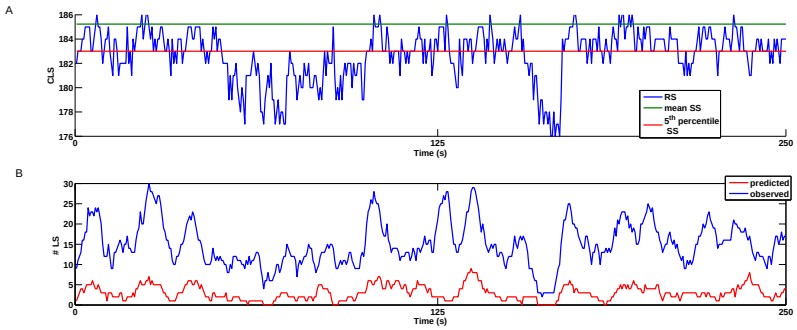

Figure 6.19: Complexity and Predictability of a NE cortical sequence compared with a surrogated one. Above the blue line represents the CLS of the RS, the green line represents the mean of 100 surrogated sequences. Below the number of predicted and observed LS respectively in red and blue.

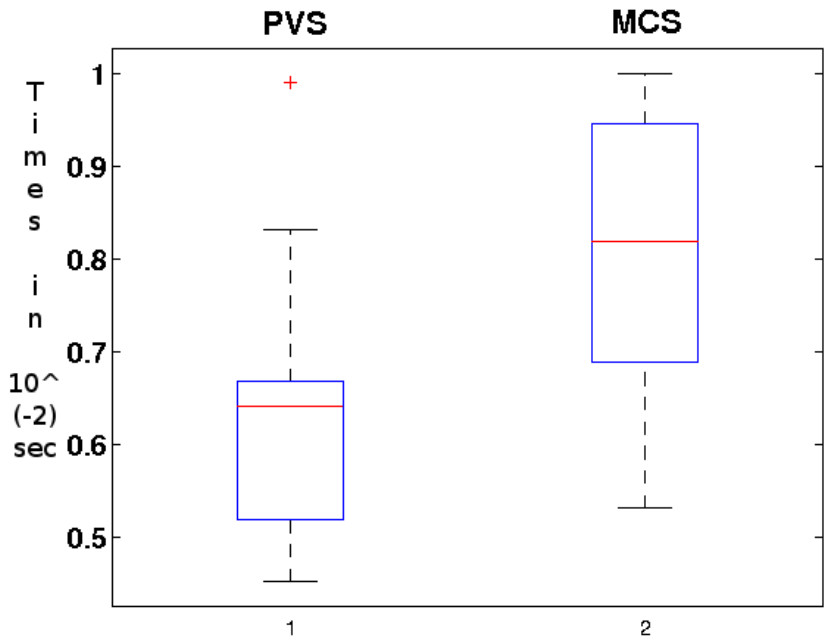

Figure 6.20: Box-Whisker plot of the distribution of the sojourn time in bursting phase of neurons extracted from PVS patients (left) and from MCS patient (right).

6.3 Human Disorders of Consciousness

Finally, preliminary result came from the study of SN sequences from IL neurons in human patients suffering from PVS and MCS. The analysis focussed on the sojourn time in the stationary phases of the sequences. As from the preliminary results, PVS bursting states are less frequent than MCS phase changes. In MCS the burst-stationary sojourn times are more lasting than in PVS, see Figure 6.20. These results can be obtained by two strategies: detecting the stationary phase and then selecting the bursting-like one and again computing the sojourn time distribution or roughly by computing the HPP (see Section 3.6) of the sequence with some VOMM algorithm and comparing the possible bursting paths probability. Burst and tonic are the two most commonly observed firing modes.

Along recent studies the concept of consciousness may be divided into two main worlds: the "core consciousness" that provides the subject the sense of self and of being placed in a specific location and the "extended consciousness" that allows the organism for a sense of self in her/his existence in a before and a past. The first is strongly biological and is not dependent on memory, language and so on. The other is an extremely complex event involving memory, language and, contrarily to the former, evolves in time and is subjected to changes. When core consciousness is impaired also the extended consciousness is deranged. The

problem of disorders of consciousness features extremely complex clinical aspects that involve heavily both sides of the world, apart from their related philosophical contexts. Where, until few years ago the disorders of consciousness were mistankenly interpreted for most of diagnoses, recent developments of the discipline have favoured a strong ameliorment of the diagnostic criteria. Terms like Minimal Conscious state (MCS) and Persistent Vegetative state (PVS) and their differences are now more commonly well identified by specialists. While deep irreversible coma states are characterised by an irreversible stage of disordered consciousness, MCS, and PVS in a minor degree, are potentially subject to changes up to the restitution to a form of true voluntary interactions with the external world. Notwithstanding the tremendous complexity of the networks subserving all the neural dynamics of consciousness, some crucial points seem well evidenced: the axis from the dorsal pontine nuclei to the intralaminar/medial thalamus and to many of the cortices seems a necessary circuit. Many patients with disorders of consciousness show severely damaged brains. Those patients with minor damages or with damages not compromising current vital functions may be enrolled in clinical trials devoted to the placement of chronic electrostimulators in a crucial region of the above circuit and namely into the intralaminar thalamic nuclei. Many other places are also considerable. In the experience of our group the choice of the thalamic intralaminar nuclei is based on the very central topographic and functional role of these nuclei in the circuit. The stimulation of these nuclei is programmed in the view of obtaining diffuse cortical re-activations (or activations) in order to reinstate a positive response of the cortico-thalamic pathway. This reactivation would enable or facilitate a restart of the thalamo-cortico-thalamic loop, thought to be one of the very engines and at the base of all the consciousness phenomena. The obtained results about the sojourn time of the bursting mode is widespreadly held as a forced information transfer mode, this outcome assumes a potentially crucial importance as a likely predictive marker to identify at the neural level the very stage of consciousness and supposedly a reference for the clinical outcome after the placement of stimulatory electrodes [103].

Chapter 7

Conclusions

This work explores the capabilities of recent sequential prediction methods with data from neurophysiological recordings. Several authors investigated the possibility to analyze neurophysiological recordings with methods coming from Coding and Information Theory. In particular, Blanc et al, used Lempel-Ziv complexity to estimate neural correlations [18] and Christen et al, tried to define a distance between spike trains based on Lempel-Ziv complexity [26]. Another important work emphasized again the Lempel-Ziv complexity in the analysis of biomedical signals [52]. Finally, London et al, measured the synaptic information efficacy with a technique based on the context-tree weighting algorithm [70]. No one of these methods define a general methodology for neurophysiopathological recording analyses. In this thesis I studied and used the Variable Order Hidden Markov Models (VOMMs) as tools to model SN or NE sequences in order to understand some basics of the spontaneous activity dynamics. Notwithstanding the positive results of the application, able to extract important features of the spontaneous activity like for instance fine dynamics of phase shiftings, VOMMs are sensitive to single symbol missings or mistakes due to misclassifications inherited from spike detection procedures, thus failing the capture of crucial patterns. In this view the adoption of more robust and efficient algorithms would lead to definitely better estimations of the real neural model.
The central result, concerning chronic pain, highlights the efficacy of my methods to discover latent features within the spontaneous activity. Furthermore, the dynamics of several cortical spontaneous activity phenomena have been explored suggesting important hypotheses. Finally, although the results of the disorders of consciousness are obviously preliminar, due to the sample paucity, they methods have been still able to adapt in this difficult contexts. The sequential data learning is in constant evolution. Spiking temporal sequences are far from being mere addition of spiking events on a temporal line but enclose complex dynamical features like the multiple input sources coming to a single cell. The single neuron spike trains (SN) and the multiunit spike trains (NE) appear as symbolic sequences with most variable behaviors (or firing patterns). Preliminary works done in our lab [146, 115] showed that these complex dynamic profiles are jointly represented in the single neuron discharge profile. As it emerges clearly from the above chapters, a multiregime is a profile displaying several dynamic behaviors as, for instance, alternating laminar and chaotic cycles. One important sign of a phase shifting to another phase is the appearance

of a specific marker sequence of single neuron or neuronal population events. This indicates the presence of a weak schematic structure within the symbolic sequence. The dynamics of the neural structures either of single neurons or of neuronal networks displayed extremely complex features that were only seemingly open to immediate analytical approaches like the study of frequency of discharge or the evaluation of the time lags interleaved among the electrical events (or spikes). Thus, subtler and subtler methods are requested to try to understand the complex message delivered into the spike trains of neurons both as individual activities and as the response to most diverse inputs.
In this context some preliminary seminal works have considered the problem of input coding in the central somatosensory networks. The tactile sensory system has been investigated at thalamocortical level in rat whisker system [82, 33, 84]. Rats typically exhibit a complex exploratory behaviour in order to acquire through actively driven exploratory acts the most relevant features from the external environment. In these papers, several features have been analysed, focussing on coding localization, frequency, amplitude and orientation of whisker deflections. As it emerged, in front of the peculiar diversity in neuronal responses to different features, it has been evidenced that the time of occurrence of the very first spikes represents the most common coding mechanism [86, 6, 85].
These important results show the fast and strong mechanism of coding of sensory stimuli that are however merged into the complex thread of the spontaneous or ongoing activity. Because of the pervasive influences that spontaneous activity may inject into the response repertoire of sensory system it appears an important step to explore the relationships that continuously regulate this intersection between the two dynamic regimes (spontaneous and evoked activities). Indeed, the spontaneous activity is not necessarily synchronized with the time of stimuli onset and imports variability in the neuronal responses. Furthermore it is ubiquitous at the thalamic and cortical level and thus, the neuronal coding scheme has to cope with this variability source. The strategies used by neuronal coding, still a matter of speculation, oblige therefore in order to understand them, an appropriate description of spontaneous activity dynamics. Because, to date, scant attention has been paid to this aspect, my work tries to add some new knowledge about spontaneous activity.
Several controversial aspects still need to be clarified, e.g. the impact of correlations on the population coding. In fact, although the pairwise correlation impact seems neither to add nor to substract a substantial information amount[81], the impact of spatiotemporal higher order correlations still needs further investigation. From this perspective, the intermittent occurrence of long range correlations, that I identified in normal and more frequently in neuropathic rats (at the best of my knowledge this is the first report of such phenomenon), could have a significant impact on the amount of trasmitted information [117].

7.1 Future developments

Very recent works (2010) showed stronger than VOMM based methods like the Variable Order Hidden Markov Models (VOHMMs). The VOHMMs are Hidden Markov Models that allow temporal high order dependencies between hidden states. The application of these methods to SN and NE could identify and ex-

tract schemes nested into the temporal sequences even perturbed by gaps. The technique peculiarities rely on a variable gap sequence mining method to extract frequent patterns with different lengths and gaps between elements. Then it uses these mined sequences to build a VOHMM that explicitly models the gaps. These last implicitly model the order of the VOHMM and explicitly the duration of each state [144]. This algorithm, named by the acronym VOGUE (Variable Order and Gapped HMM for Unstructured Elements) extracts, in addition to the previous actions, the distribution of gap symbols for each mining pattern. These distributions allow for recognizing the nature of these gaps. I hypothesize, with the support of these results [117], that crucial symbols are scattered within an intermittent (laminar-chaotic) behavior within the sequence. A further advantage is represented by the existance of a work about the parallelization of these algorithms in shared-memory computing environments [143]. Recent developments on General Purpose Graphical Processing Units permit to achieve complex computational data mining tasks. In particular, parallel versions of sequence mining algorithms can be developed by NVIDIA Compute Unified Device Architecture (CUDA) framework. It is possible to extract a functional relationship between the SN and NE sequences defining a similarity measure between VOHMMs. The set of all the direct extracted relationships constitute a direct graph that expresses the functional dependencies of the recorded neural assembly. The Neural Group Discovery (NGD) algorithm, presented in previous works [116], achieve such a goal. This strategy, however, misses the temporal evolution of clusters and the statistics computed over the graph.
Possible developments of this project have the aim to achieve a sound and consecutive temporal snapshot, built by NGD algorithm, of the connectionist perspective evidencing the subtlest fluctuations into the cluster temporal developments. Similar works, strictly related to Small-World Networks and Graph Theory, showed functional connectivity redistributions among cerebral areas in several nervous system disorders [21]. Thus, the extension of these techniques in the temporal dimension could supply further results and confirmations to even clinically relevant problems.

This thesis faced the problem of the neuronal ongoing activity. One of the most intriguing problems in the current neurophysiological debate, in fact, is the understanding of the neural activity in absence of any stimulus. The problems related to the spontaneous activity are associated to exceedingly numerous cognitive, sensorial and perceptive tasks taking simultaneously place in the brain. In fact, the whole story of neurophysiology until now has evolved on the basis of stimulus induced responses visual, auditory or somatosensory. The spontaneous activity studied with electroencephalography and imaging techniques in human subjects has recently evidenced a disparate and flexible background in spontaneously running recording stages, pointing out surprising and richest functional landscapes of a state once thought to express only flat dynamics. The problem increases observing ongoing activity patterns during pathological states of the nervous system. Namely, the study of the neuronal spontaneous activity from neurosurgical patients can be done either in conscious waking patients or in patients with disorders of consciousness. In both cases, the spontaneous activity assumes a special importance in that it delivers the hallmarks of the multiple tasks simultaneously carried out in the recorded networks. More specifically, in studies on the neural states of patients with disorders of consciousness, the

evaluation of the spontaneous neuronal activity by microelectrode recordings into the cerebral cortex and into regions of the brain called intralaminar thalami could deliver crucial issues for diagnosis and prognosis on the outcome of the interventions devoted to the placement of neurostimulators.
Experiments on animals are devoted to further study crucial dynamic signatures of the thalamic and cortical physiology and pathophysiology. The thalamus and the cortex are the two crucial components of the reverberating circuit TCT. The TCT loop represents the fundamental pillar enclosing most of the sensory processes and acting as the neural background of consciousness processes. The overall functional picture of the TCT has been partially clarified in a plethora of studies that, notwithstanding great achievements, still misses completeness. In this perspective the analysis with the defined similarity measure defined above, would assume a fundamental importance for achieving a better knowledge of sensory processes both in normal animals and in neuropathological models as in chronic pain animals.

Bibliography

[1] Abeles M, Goldstein JM, Multispike train analysis. *Proceedings of the IEEE* 65:762-773 (1977).

[2] Abeles M, Bergman H, Gat I, Meilijson I, Seidemann E, Tishby N, Vaadia E, Cortical Activity Flips Among Quasi-Stationary States, *Proceedings of National Academy of Science USA*, 92:8616-8620 (1995).

[3] Apkarian AV et al, Chronic Back Pain Is Associated with Decreased Prefrontal and Thalamic Gray Matter Density, *The Journal of Neuroscience*, 24:10410-10415 (2004).

[4] Apkarian AV, Bushnell MC, Treede RD, Zubieta JK, Human brain mechanisms of pain perception and regulation in health and disease, *European Journal of Pain*, 9:463-484 (2005).

[5] Apkarian AV, Baliki M-N, Geha P-Y, Towards a theory of chronic pain, *Progress in Neurobiology*, 87:81-97 (2009).

[6] Bale MR, Petersen RS, Transformation in the neural code for whisker deflection direction along the lemniscal pathway, *Journal of Neurophysiology*, 102:2771-2780 (2009).

[7] Baliki MN, Geha PY, Apkarian AV, Spontaneous pain and brain activity in neuropathic pain: functional MRI and pharmacologic functional MRI studies, *Current Pain and Headache Reports*, 11:171-177 (2007).

[8] Bear MF, Connors B, Paradiso M, Neuroscience: Exploring the Brain, *Lippincott Williams and Wilkins*, (2006).

[9] Begleiter R, El-Yaniv R, Yona G, On Prediction Using Variable Order Markov Models, *Journal of Artificial Intelligence Research*, 22:385-421 (2004).

[10] Bennett CH, Gacs P, Ming L, Vitanyi MB, Zurek WH, Information Distance, *IEEE Transactions Information Theory* 44:1407-1423 (1998).

[11] Bejerano G, Yona G, Variations on probabilistic suffix trees - a new tool for statistical modeling and prediction of protein families, *Bioinformatics*, 17:23-43 (2001).

[12] Bennett GJ, Xie YK, A peripheral mononeuropathy in rat that produces disorders of pain sensation like those seen in man, *Pain*, 33:87-107 (1988).

[13] Benucci A, Verschure PFM, König P, Existence of high-order correlations in cortical activity, *Physical Review E*, 68:041905 (2003).

[14] Biella GEM, Sotgiu ML, Evidence that inhibitory mechanisms mask inappropriate somatotopic connections in the spinal cord of normal rat, *Journal of Neurophysiology*, 74:495-505 (1995).

[15] Biella GEM, Riva L, Sotgiu ML, Interaction between neurons in different laminae of the dorsal horn of the spinal cord. A correlation study in normal and neuropathic rats, *European Journal of Neuroscience*, 9(5):1017-1025 (1997).

[16] Biella GEM, Salvadori G, Sotgiu ML, Multifractal analysis of wide dynamic range neuron discharge profiles in normal rats and in rats with sciatic nerve constriction, *Somatosensory & Motor Research*, 16(2):89-102 (1999).

[17] Biella GE, Trevisan S, Giardini ME, Probing for local activity-related modulation of the infrared backscattering of the brain cortex, *Journal of Biophotonics*, 2(10):588-595 (2009).

[18] Blanc JL, Schmidt N, Bonnier L, Pezard L, Quantifying neural correlations using Lempel-Ziv complexity, *Deuxime confrence franaise de Neurosciences Computationnelles, "Neurocomp08"*, Marseille, France (2008).

[19] Blatt M, Wiseman S, Domany E, Superparamagnetic Clustering of Data. *Physical Reviews Letter* 76:3251-3254 (1996).

[20] Boley DL, Principal Direction Divisive Partitioning, *Data Mining and Knowledge Discovery*, 2:325-344 (1998).

[21] Bullmore E, Sporns O, Complex brain networks: graph theoretical analysis of structural and functional systems, *Nature Neuroscience Review*, 10:186-198 (2009).

[22] Bushnell MC et al, Pain Perception: is there a role for primary somatosensory cortex?, *Proceedings of Natonal Academy of Science USA* 96:7705-9 (1999).

[23] Camproux AC, Saunier F, Chouvet G, Thalabard JC, Thomas G, A hidden Markov model approach to neuron firing patterns, *Biophysical Journal*, 71:2404-2412, (1996).

[24] Catani M, Mesulam M, What is a disconnection syndrome?, *Cortex*, 44:911-913 (2008).

[25] Cebrián M, Alfonseca M, Ortega A, Common pitfalls using the normalized compression distance: what to watch out for in a compressor, *Communications in Informations and Systems*, International Press, 5:367-384 (2005).

[26] Christen M, Kohn A, Ott T, Stoop R, Measuring spike pattern reliability with the Lempel-Ziv distance, *Journal of Neuroscience Methods* 156:342-350 (2006).

[27] Chu KL, Faltynek CR, Jarvis MF, McGaraughty S, Increased WDR spontaneous activity and receptive field size in rats following a neuropathic or inflammatory injury: implications for mechanical sensitivity, *Neuroscience Letters* 372:123-126 (2004).

[28] Cilibrasi R, Vitányi P, Clustering by Compression, *IEEE Transactions on Information Theory*, 51:1523-1545 (2005).

[29] Cilibrasi R, Statistical Inference through Data Compression, PhD Thesis at Institute for Logic, Language and Computation Universiteit van Amsterdam, *ILLC Dissertation Series* DS-2007-01.

[30] Cleary J, Witten I, Data Compression Using Adaptive Coding and Partial String Matching, *IEEE Transactions on Communications*, 32(4):396-402 (1984).

[31] Cleary J, Teahan W, Experiments on the Zero Frequency Problem, *Proceedings of the IEEE Data Compression Conference*, Snowbird, Utah, pp. 480-491, (1995).

[32] Cossart R, Aronov D, Yuste R, Attractor Dynamics of Network UP States in the Neocortex, *Nature*, 423:283-288 (2003).

[33] Diamond ME, von Heimendahl M,Knutsen PM,Kleinfeld D, Ahissar E, "Where" and "What" in the Whisker Sensory System, Nature Review Neuroscience 9:601-612 (2008).

[34] Drdla R, Sandkühler J, Long-term potentiation at C-fibre synapses by low-level presynaptic activity in vivo, *Molecular Pain*, 4:18 (2008).

[35] Ebeling W, Nicolis G, Word Frequency and Entropy of Symbolic Sequences: a Dynamical Perspective, *Chaos, Solitons & Fractals*, 2(6):635-650 (1992).

[36] Eide PK, Wind-up and the NMDA receptor complex from a clinical perspective, *European Journal of Pain*, 4:5-15 (2000).

[37] Endo T et al, Functional MRI of the brain detects neuropathic pain in experimental spinal cord injury, *Pain*, 138:292-300 (2008).

[38] Fox B in *Pain Management A Practical Guide for Clinicians sixth Edition*, Pain and Its Magnitude ed Richard S. Weiner (CRC Press Boca Raton London New York Washington, D.C.) pp 3-8 (2002).

[39] Gerstner W, Kistler WK, Spiking Neuron Models, *Cambridge University Press* (2002).

[40] Grahek N, *Feeling Pain and Being in Pain* Dissociation Phenomena in Human Pain Experience (A Bradford Book The MIT Press Cambridge, Massachusetts London, Englands) pp 31-41 (2001).

[41] Green AL et al, Neural signatures in patients with neuropathic pain, *Neurology*, 72:569-571 (2009).

[42] Greicius MD, Krasnow B, Reiss AL, Menon V, Functional connectivity in the resting brain: A network analysis of the default mode hypothesis, *Proceedings of the National Academy of Science USA*, 100:253-258 (2003).

[43] Gutnisky DA, Josic K, Generation of Spatio-Temporally Correlated Spike-Trains and Local Field Potentials Using a Multivariate Autoregressive Process, *Journal of Neurophysiology*, pp. 2912-2930 (2009).

[44] Gubellini P, Salin P, Kerkerian-Le Goff L, Baunez C, Deep brain stimulation in neurological diseases and experimental models: from molecule to complex behavior, *Progress in Neurobiology*, 89:79-123 (2009).

[45] Guyonneau R, van Rullen R, Thorpe S: Neurons Tune to the Earliest Spikes Through STDP. *Neural Computation* 17(4): 859-879 (2005).

[46] Hall P, On some simple estimates of an exponent of regular variation, *Journal of the Royal Statistical Society*, Series B (1982).

[47] Hao JX, Kupers R-C, Xu XJ, Response characteristics of spinal cord dorsal horn neurons in chronic allodynic rats after spinal cord injury, *Journal of Neurophysiology* 92:1391-1399 (2004).

[48] Harris KD, Henze DA, Csicsvari J, Hirase H, Buzsaki G, Accuracy of Tetrode Spike Separation as Determined by Simultaneous Intracellular and Extracellular Measurements.*Journal of Neurophysiology* 84:401-414 (2000).

[49] Hebb DO, The organization of behaviour, *Wiley*, New York (1949).

[50] Hjornevik T et al, Metabolic plasticity in the supraspinal pain modulating circuitry after noxious stimulus-induced spinal cord LTP, *Pain*, 140:456-64 (2008).

[51] Hodgkin A, Huxley A, A quantitative description of membrane current and its application to conduction and excitation in nerve, *Journal of Physiology* 117:500544 (1952).

[52] Hu J, Gao J, Principe JC, Analysis of biomedical signals by the Lempel-Ziv complexity: the effect of finite data size, *IEEE Transactions in biomedical engineering*, 53:2606-2609 (2006).

[53] Iadarola MJ et al, Unilateral decrease in thalamic activity observed with positron emission tomography in patients with chronic neuropathic pain, *Pain*, 63:55-64 (1995).

[54] Ikegay Y, Gloster A, Cossart R, Aronov D, Lampl I, Ferster D and Yuste R, Synfire Chains and Cortical Songs: Temporal Modules of Cortical Activity, *Science*, 304:559-564 (2004).

[55] Izhikevich E, Simple Model of Spiking Neurons, *IEEE Transactions on Neural Networks*, 14:1569- 1572 (2003).

[56] Izhikevich EM, Dynamical Systems in Neuroscience: The Geometry of Excitability and Bursting. *MIT press* (2007).

[57] Jones EG, The thalamic matrix and thalamocortical synchrony, *Trends in Neuroscience*, 24:595-601 (2001).

[58] Kawabe T, Kondo Y, Intermittent Chaos Generated by Logaritmic Map, *Progress of Theoretical Physics*, 86(3):581-586 (1991).

[59] Keogh E, Lonardi S, Ratanamahatana CA, Towards Parameter-Free Data Mining, *Proceedings of the* 10*th ACM SIGKDD International Conference on Knowledge Discovery and Data Mining*, pp. 206-215 (2004).

[60] Keogh E, Lonardi S, Ratanamahatana CA, Wei L, Lee SH, Handley J, Compression-based data mining of sequential data, *Data Mining and Knowledge Discovery*, Springer Netherlands, Vol 14 (2007).

[61] Klein T et al, Effects of the NMDA-receptor antagonist ketamine on perceptual correlates of long-term potentiation within the nociceptive system, *Neuropharmacology*, 52:655-661 (2007).

[62] Krichevsky RE, Trofimov VK, The Performance of Universal Encoding, *IEEE Trans. Information Theory*, 27:(2)199-207 (1981).

[63] Lefaucheur JP et al, The use of repetitive transcranial magnetic stimulation (rTMS) and transcranial direct current stimulation (tDCS) to relieve pain, *Brain Stimulation*, 1:337-44 (2008).

[64] Lempel A, Ziv J, On the Complexity of Finite Sequences, *IEEE Transactions on Information Theory*, 1:75-81 (1976).

[65] Letelier JC and Weber PP, Spike sorting based on discrete wavelet transform coefficients, *Journal of Neuroscience Methods*, 101:93-106, (2000).

[66] Levy R, Deer TR, Henderson J, Intracranial neurostimulation for pain control: a review *Pain Physician* 13:157-165 (2010).

[67] Lima MC, Fregni F, Motor cortex stimulation for chronic pain: systematic review and meta-analysis of the literature, *Neurology*, 70:2329-2337 (2008).

[68] Llinás RR, Ribary U, Jeanmonod D, Kronberg E, Mitra PP, Thalamocortical dysrhythmia: A neurological and neuropsychiatric syndrome characterized by magnetoencephalography, *Proceedings of the National Academy of Science USA*, 96:15222-15227 (1999).

[69] Logothetis NK, The ins and outs of fMRI signals, Nature Neuroscience, 10:1230-1232 (2007).

[70] London M, Schreibman A, Häusser M, Larkum ME, Segev I, The information efficacy of a synapse, *Nature Neuroscience*, 5:332-340 (2002).

[71] MacLean JN, Watson BO, Aaron GB, Yuste R, Internal Dynamics Determine the Cortical Response to Thalamic Stimulation, *Neuron*, 48:811-823 (2005).

[72] Mao J, Mayer DJ, Price DD, Patterns of increased brain activity indicative of pain in a rat model of peripheral mononeuropathy, *Journal of Neuroscience*, 13:2689-2702 (1993).

[73] Melzack R, From the gate to the neuromatrix *Pain* Suppl 6:S121-126 (1999).

[74] Melzack R, Coderre TJ, Katz J, Vaccarino AL, Central neuroplasticity and pathological pain, *Annals of the New York Academy of Science USA*, 933:157-174 (2001).

[75] Merskey H and Bogduk N in *Classification of Chronic Pain*, Pain in Part III eds H. Merskey and N. Bogduk (IASP Press, Seattle), pp 209-214 (1994).

[76] Mesulam MM, From sensation to cognition, *Brain*, 121:1013-52 (1998).

[77] Monconduit L, Lopez-Avila A, Molat J, Chalus M, Villanueva L, Corticofugal Output from the Primary Somatosensory Cortex Selectively Modulates Innocuous and Noxious Inputs in the Rat Spinothalamic System, *Journal of Neuroscience*, 26(33):8441-8450 (2006).

[78] Oshiro Y, Quevedo AS, McHaffie JG, Kraft RA, Coghill RC, Brain mechanisms supporting discrimination of sensory features of pain: a new model *Journal of Neuroscience* 29:14924-1431 (2009).

[79] Ott E, Chaos in Dynamical Systems. New York, *Cambridge University Press*, 2nd edition, 2002

[80] Panzeri S, Senatore R, Montemurro MA, Petersen RS, Correcting for the Sampling Bias Problem in Spike Train Information Measures, *Journal of Neurophysiology*, 98:1064-1072 (2007).

[81] Panzeri S, Pola G, Petersen RS, Coding of sensory signals by neuronal populations: the role of correlated activity, *The Neuroscientist : a review journal bringing neurobiology, neurology and psychiatry*, 9:175-180 (2003).

[82] Panzeri S, Petersen RS, Schultz SR, Lebedev M, Diamond ME, The role of spike timing in the coding of stimulus location in rat somatosensory cortex. *Neuron*, 29:769-777 (2001).

[83] Parthimos D, Edwards DH, Griffith TM, Universal scaling properties of type-I intermittent chaos in isolated resistance arteries are unaffected by endogenous nitric oxide synthesis, *Physical Review E*, 64:1-5 (2001).

[84] Petersen R, Panzeri S, Maravall M, Neural Coding and Contextual Influences in the Whisker System, *Biological Cybernetics*, 100(6):427-446 (2009).

[85] Petersen RS, Brambilla M, Bale MR, Alenda A, Panzeri S, Montemurro MA, Maravall M, Diverse and temporally precise kinetic feature selectivity in the VPm thalamic nucleus, *Neuron*, 60:890-903 (2008).

[86] Petersen RS, Panzeri S, Diamond ME, The role of individual spikes and spike patterns in population coding of stimulus location in rat somatosensory cortex, *Bio Systems*, 67:187-93 (2002).

[87] Pomeau Y, Manneville P, Intermittent Transition to Turbolence in Dissipative Dynamical Systems, *Communications In Mathematical Physics*, 74:189-197 (1980).

[88] Porro CA, Cettolo V, Francescato MP, Baraldi P, Temporal and intensity coding of pain in human cortex, *Journal of Neurophysiology* 80:3312-3320 (1998).

[89] Porro C, Functional imaging and pain: behavior, perception, and modulation, *Neuroscientist*, 354-369 (2003).

[90] Portnoy RK, Hagen NA, Breakthrough pain: Definition, prevalence, and characteristics, *Pain*, 41:273-281 (1990).

[91] Quiroga QR, Unsupervised Spike Detection and Sorting with Wavelets and Superparamagnetic Clustering, *Neural Computation*, 16:1661-1687 (2004).

[92] Raichle ME et al, A default mode of brain function, *Proceedings of National Academy of Science USA*, 98:676-682 (2001).

[93] Raichle ME, Snyder AZ, A default mode of brain function: a brief history of an evolving idea, *NeuroImage*, 37:1083-1090 (2007).

[94] Rieke F, Warland D, Ruyter van Steveninck RR, Bialek W, Spikes: Exploring the Neural Code. Cambridge, MA, *MIT Press*, June 1999.

[95] Ries CR, Puil E, Mechanism of Anesthesia Revealed by Shunting Actions of Isoflurane on Thalamocortical Neurons *Journal of Neurophysiology*, 81:1795-1801 (1999).

[96] Rissanen J, A Universal Data Compression System, *IEEE Transactions on Information Theory*, Vol IT-29, No. 5, (1983).

[97] Rissanen J, Universal coding, information, prediction, and estimation, *IEEE Transactions on Information Theory*, 30:629-636 (1984).

[98] Ron D, Singer Y, Tishby N, The power of amnesia: learning probabilistic automata with variable memory length, *Machine Learning*, 25:117-149 (1996).

[99] Roza C, Laird JM, Cervero F, Spinal mechanisms underlying persistent pain and referred hyperalgesia in rats with an experimental ureteric stone, *Journal of Neurophysiology*, 79:1603-12 (1998).

[100] Sarnthein J, Jeanmonod D, High thalamocortical theta coherence in patients with neurogenic pain, *Neuroimage*, 39:1910-1917 (2007).

[101] Sandkühler J, Understanding LTP in pain pathways, *Molecular Pain* 3:9 (2007).

[102] Sasaki T, Matsuki N, Ikegaya Y, Metastability of Active CA3 Networks, *The Journal of Neuroscience*, 27(3):517-528 (2007).

[103] Schiff ND, Giacino JT, Kalmar K, Victor JD, Baker K, Gerber M, Fritz B, Eisenberg B, O'Connor J, Kobylarz EJ, Farris S, Machado A, McCagg C, Plum F, Fins JJ, Rezai AR, Behavioural improvements with thalamic stimulation after severe traumatic brain injury, *Nature*, 448:600-603 (2007).

[104] Schneidman E, Berry MJ, Segev R, Bialek W, Weak pairwise correlations imply strongly correlated network states in a neural population, *Nature* 440:1007-1012 (20 April 2006).

[105] Sculley D, Brodley CE, Compression and Machine Learning: A New Perspective on Feature Space Vectors, *Proceedings of Data Compression Conference (DCC'06)* (2006).

[106] Segev R, Benveniste M, Hulata E, Cohen N, Palevsky A, Kapon E, Shapira Y, Ben-Jacob E, Long Term Behavior of Lithohgrafically Prepared In Vitro Neural Networks *Physical Review Letters*, 88:1-4 (2002).

[107] Seltzer Z, Dubnerb R, Shirc Y, A novel behavioral model of neuropathic pain disorders produced in rats by partial sciatic nerve injury, 43(2):205-218 (1990).

[108] Sherman SM, Guillery RW, The role of the thalamus in the flow of information to the cortex, *Philosophical Transactions of the Royal Society B*, 1428:1695-1708 (2002).

[109] Sherman SM, Guillery RW, Exploring the Thalamus and its Role in Cortical Function *MIT Press* Cambridge, MA (2006).

[110] So BC, Mori H, Power Spectra on Intermittent Chaos Generated by quadratic Tangent Bifurcation, *Progress of Theoretical Physics*, 72(6):1258-1261 (1984).

[111] Sporns O, Tononi G, Edelman GM, Theoretical neuroanatomy and the connectivity of the cerebral cortex, *Behavioral Brain Research*, 135:69-74 (2002).

[112] Sotgiu ML, Lacerenza M, Marchettini P, Effect of Systemic Lidocaine on Dorsal Horn Neuron Hyperactivity Following Chronic Peripheral Nerve Injury in Rats, *Somatosensory and Motor Research*, 9:227-233 (1992).

[113] Sotgiu ML, Biella G, Riva L, A study of early ongoing activity in dorsal horn units following sciatic nerve constriction, *Neuroreport*, 5:2609-12 (1994).

[114] Stills HF, Bailey MQ, The use of Freund's Complete Adjuvant, *Laboratory Animals*, 20:25-31 (1991).

[115] Storchi R, Biella GE, Liberati D, Baselli G, Extraction and characterization of essential discharge patterns from multisite recordings of spiking ongoing activity. *PLoSONE* 4:4299 (2009).

[116] Storchi R, Zippo AG, Valente M, Caramenti G, Biella GEM, Neural signature of chronic pain in the thalamocortical circuit, Submitted to *Neuron*, November 2010.

[117] Storchi R, Zippo AG, Caramenti GC, Valente M, Lin J, Biella GEM, Modeling Neural Ensemble Firing Activity Through Intermittent Chaos, *IEEE Natural Computing*, In the press, September 2010.

[118] Strong SP, Koberle R, Ruyter van Steveninck R, Bialek W, "Entropy and Information in Neural Spike Trains, *Physical Review Letter*, 86:197-200 (1998).

[119] Staud R, Craggs JG, Robinson M-E, Perlstein W-M, Price D-D (2007) Brain activity related to temporal summation of C-fiber evoked pain *Pain*, 129:130-42.

[120] Suzuki R, Dickenson A, Spinal and supraspinal contributions to central sensitization in peripheral neuropathy, *Neurosignals*, 14:175-81 (2005).

[121] Szekely JI, Torok K, Mate G, The role of ionotropic glutamate receptors in nociception with special regard to the AMPA binding sites, *Current Pharmaceutical Design*, 8:887-912 (2002).

[122] Teahan W, Probability estimation for PPM, *Proceedings of the New Zealand Computer Science Research Students' Conference*, University of Waikato, Hamilton, New Zealand, (1995).

[123] Tennigkeit F, Ries CR, Schwarz DW, Puil E, Isoflurane Attenuates Resonant Responses of Auditory Thalamic Neurons, *Journal of Neurophysiology*, 78:591-596 (1997).

[124] Thienhaus O, Cole BE *The Classification of Pain Management, A Practical Guide for Clinicians sixth Edition* ed Richard S. Weiner (CRC PRESS Boca Raton London New York Washington, D.C.) pp 27-36 (2002).

[125] Tjalkens TJ, Volf PAJ, Frans M, Willems J, Context-Tree Weighting Method for Text Generating Sources, *Data Compression Conference (DCC '97)* (1997).

[126] Tononi G, Sporns O, Measuring information integration, *BMC Neuroscience*, 4:31 (2003).

[127] Tracey I, Functional connectivity and pain: how effectively connected is your brain?, *Pain*, (Editorial) (2005).

[128] Tracey I, Mantyh PW The Cerebral Signature for Pain Perception and Its Modulation *Neuron* 55:377-391 (2007).

[129] Tracey I, Imaging pain, *British Journal of Anaesthesia*, 101:32-39 (2008).

[130] Villanueva L, Diffuse Noxious Inhibitory Control (DNIC) as a tool for exploring dysfunction of endogenous pain modulatory systems, *Pain* 143:161-162 (2009).

[131] Viswanathan A Freeman RD, Neurometabolic coupling in cerebral cortex reflects synaptic more than spiking activity, *Nature Neuroscience*, 10:1308-1312 (2007).

[132] Wang LX, Wang ZJ, Animal and cellular models of chronic pain, *Advanced Drug Delivery Reviews*, 55:949-965 (2003).

[133] Wanga Kun et al, Temporal scaling properties and spatial synchronization of spontaneous blood oxygenation level-dependent (BOLD) signal fluctuations in rat sensorimotor network at different levels of isoflurane anesthesia, *NMR Biomed* (2010), in the press (2010).

[134] Watts DJ, Strogatz SH, Collective dynamics of 'small-world' networks, *Nature*, 393:409-10 (1998).

[135] Weinberger MJ, Lempel A, Ziv J, A sequential algorithm for the universal coding of finite-memory sources, *IEEE Transactions Information Theory*, 38:10021014 (1982).

[136] Wenjuan C, Xiangning L, Jiangbo P, and Qingming L, Spatial-temporal dynamics of chaotic behavior in cultured hippocampal networks, *Physical Review E* 81:061903 (2010).

[137] Willems F, Shtarkov Y, Tjalkens T, The Context Tree Weighting Method : Basic Properties, *IEEE Transactions on Information Theory*, 41(3):653-664, (1995).

[138] Willems F, The Context-Tree Weighting Method: Extensions, *IEEE Transactions on Information Theory*, 44(2):792-798, 1998.

[139] Williams AC, Facial expression of pain: An evolutionary account *Behavioral and Brain Sciences* 25:439-488 (2002).

[140] Wu S, Amari S, Nakahara H, Population Coding and Decoding in a Neural Field: A Computational Study, *Neural Computation* 14:999-1026 (2002)

[141] Yelle MD, Oshiro Y, Kraft RA, Coghill RC, Temporal filtering of nociceptive information by dynamic activation of endogenous pain modulatory systems *Journal of Neuroscience* 29:10264-10271 (2009).

[142] Yu S, Huang D, Singer W, Nikolic D, A small world of neuronal synchrony, *Cerebral Cortex*, 18:2891-2901 (2008).

[143] Zaki MJ, Parallel Sequence Mining on Shared-Memory Machines, *Journal of Parallel and Distributed Computing*, 61:401-426 (2001).

[144] Zaki MJ, Carothers DC, Szymanski BK,VOGUE: A Variable Order Hidden Markov Model with Duration based on Frequent Sequence Mining,*ACM Transactions on Knowledge Discovery in Data*, 4(1):5 (2010).

[145] Zebrowski JJ, Baranowski R, Type I intermittency in nonstationary systemsmodels and human heart rate variability, *Physica A*, 336:7483 (2004).

[146] Zippo AG, Storchi R, Caramenti G, Valente M, Lin J, Biella GEM, Higher order Synchrony Predictability in Somatosensory Cortex during Spontaneous Activity, *Natural Computing, Frontiers in Neuroscience*, in the press, September 2010.

[147] Ziv J, Lempel A, Compression of individual sequences via variable-rate coding *IEEE Transactions Information Theory*, 24:530-53 (1978).